Decoupling Coefficients and the Lightest CP-Even Higgs Boson Mass in the Minimal Supersymmetric Standard Model

Zur Erlangung des akademischen Grades eines
DOKTORS DER NATURWISSENSCHAFTEN
an der Fakultät für Physik des
Karlsruher Instituts für Technologie (KIT)

genehmigte

Dissertation

von

Dipl.-Phys. David Alexander Kunz

aus Karlsruhe

Tag der mündlichen Prüfung: 10. Juli 2015
Referent: Prof. Dr. M. Steinhauser
Korreferentin: Priv.-Doz. Dr. L. Mihaila

Contents

Contents

1. Introduction

With the Large Hadron Collider (LHC), a new era for particle physics has started. In 2012, physicists of the CERN collaboration discovered the Higgs boson whose existence is postulated by a mechanism which explains how mass could arise in local gauge theories, proposed in three scientific papers, written in 1964. Its authors are Robert Brout and Francois Englert [1, 2], Peter Higgs [3] and Gerald Guralni, C. Richard Hagen and Tom Kibble [4, 5]. In 2013, Francois Englert and Peter Higgs were awarded with the Nobel Prize in Physics »for the theoretical discovery of a mechanism that contributes to our understanding of the origin of mass of subatomic particles, and which recently was confirmed through the discovery of the predicted fundamental particle, by the ATLAS and CMS experiments at CERN's Large Hadron Collider« [6]. Indeed the discovery of the Higgs boson was a huge success for the current Standard Model of particle physics (SM) since its properties are in agreement with SM predictions [7]. However, there are some deficiencies in the SM regarding neutrino oscillations, the nature of dark matter and dark energy, the matter-antimatter asymmetry and the hierarchy problem [8–12]. There are many theoretical developments to resolve some of these issues, e.g. string theory, extra dimensions or supersymmetric extensions of the SM [13].

One of the best studied candidates for physics beyond the SM is the Minimal Supersymmetric Standard Model (MSSM) which realizes supersymmetry with the minimum number of new particle states and new interactions, consistent with phenomenology, see e.g. [12]. Supersymmetry relates bosons which have an integer-valued spin with fermions which have a half-integer-valued spin, i.e. each boson is associated with a fermionic superpartner and *vice versa*. In a theory with unbroken supersymmetry, each pair of partner and superpartner share the same mass and internal quantum numbers except the spin. However, no superpartner has been found yet and therefore, supersymmetry must be broken to allow for heavy supersymmetric particles. To avoid a gauge anomaly[1], an additional Higgs doublet is introduced in the MSSM, see e.g. [12]. To give an overview of the MSSM field content, the chiral fields are shown in Table 1.1 and the gauge fields in Table 1.2 including their associated transformation properties under the SM gauge group $SU(3)_C \times SU(2)_L \times U(1)_Y$. A supersymmetric partner of a SM state is denoted by a tilde.

---

[1]The conditions for cancellation of gauge anomalies include $\mathrm{Tr}(T_3^2 Y) = \mathrm{Tr}(Y^3) = 0$ where T_3 and Y are the third component of the weak isospin and the weak hypercharge, respectively and the traces run over all left-handed Weyl fermionic degrees of freedom. A fermionic partner of a Higgs chiral supermultiplet would make a non-zero contribution.

1. Introduction

Names		spin 0	spin 1/2	$SU(3)_C, SU(2)_L, U(1)_Y$
squarks, quarks	Q	$(\tilde{u}_L \ \tilde{d}_L)$	$(u_L \ d_L)$	$(\mathbf{3}, \mathbf{2}, \frac{1}{6})$
($\times$3 families)	$\bar{u}$	$\tilde{u}_R^*$	$u_R^\dagger$	$(\overline{\mathbf{3}}, \mathbf{1}, -\frac{2}{3})$
	$\bar{d}$	$\tilde{d}_R^*$	$d_R^\dagger$	$(\overline{\mathbf{3}}, \mathbf{1}, \frac{1}{3})$
sleptons, leptons	L	$(\tilde{\nu} \ \tilde{e}_L)$	$(\nu \ e_L)$	$(\mathbf{1}, \mathbf{2}, -\frac{1}{2})$
($\times$3 families)	$\bar{e}$	$\tilde{e}_R^*$	$e_R^\dagger$	$(\mathbf{1}, \mathbf{1}, 1)$
Higgs, Higgsinos	H_1	$(H_1^0 \ H_1^-)$	$(\tilde{H}_1^0 \ \tilde{H}_1^-)$	$(\mathbf{1}, \mathbf{2}, -\frac{1}{2})$
	H_2	$(H_2^+ \ H_2^0)$	$(\tilde{H}_2^+ \ \tilde{H}_2^0)$	$(\mathbf{1}, \mathbf{2}, +\frac{1}{2})$

Table 1.1.: Chiral fields in the MSSM. The spin-0 fields are complex scalars and the spin-1/2 fields are left-handed two-component Weyl fermions [12].

Names	spin 1/2	spin 1	$SU(3)_C, SU(2)_L, U(1)_Y$
gluino, gluon	$\tilde{g}$	g	$(\mathbf{8}, \mathbf{1}, 0)$
winos, W bosons	$\tilde{W}^\pm \ \tilde{W}^0$	$W^\pm \ W^0$	$(\mathbf{1}, \mathbf{3}, 0)$
bino, B boson	$\tilde{B}^0$	B^0	$(\mathbf{1}, \mathbf{1}, 0)$

Table 1.2.: Gauge fields in the MSSM [12].

There are two possibilities to search for supersymmetry, indirect and direct searches.

In the latter, one uses simplified models for parameter constraints. Since many assumptions are employed, these constraints cannot be applied to general supersymmetry models. So far, no supersymmetric particle was discovered, see e.g. [14].

In indirect searches, one precisely measures observables which are sensitive to quantum effects due to supersymmetric particles and compares experimental results with precise theoretical predictions.

With the discovery of the Higgs boson, a careful study of its properties in combination with precise theoretical predictions could be very valuable for finding hints of supersymmetry.

For example, the mass of the SM-Higgs boson is a free parameter whereas in the MSSM the lightest CP-even Higgs boson mass can be predicted by theory. Therefore, by assuming the lightest CP-even Higgs boson to be the measured spin-zero particle, one can predict its mass and exclude those MSSM scenarios for which the theoretical value is not in agreement with experimental data.

The calculation of the lightest CP-even Higgs boson mass in the MSSM is very sensitive to the value of the running top-quark mass. Therefore, a precise determination of the latter is of great importance to reach experimental precision in theoretical predictions.

In addition, great interest is devoted to the study of Higgs boson couplings, especially to the top and bottom quarks. They are very sensitive to new physics at the multi-TeV scale [15, 16]. Deviations in the Higgs boson couplings from SM predictions can be an indirect evidence of the existence of additional Higgs bosons [17].

In this thesis, a new method for the computation of the running top-quark mass and top Yukawa coupling in the MSSM is presented, taking into account strong-coupling and the dominant electroweak radiative corrections.

The outline of this thesis is the following.

In Chapter 2, the basic principles of an effective field theory are discussed and all steps are described to relate the relevant SM parameters to their counterparts in the MSSM. In Chapter 3, details on the actual computation and some analytical results are given. A numerical analysis of these results is presented in Chapter 4 for selected MSSM scenarios. In Chapter 5, the effects of the running top-quark mass on the determination of the lightest CP-even Higgs boson mass in the MSSM are discussed.

2. Decoupling Coefficients

In order to describe physical phenomena in an efficient way, it is advisable to have a theory with the minimum number of dynamical degrees of freedom. The energy scale is a good classifier to rank those degrees of freedom. Effects of physical processes which only play a role at very small energy scales can be quite important but in many cases the knowledge of the exact dynamics is redundant.

In particle physics one can observe many different effects depending on the energy at which the experiments take place. Therefore a reduction of a 'full' theory to an effective theory, which is valid in a certain energy range, seems desirable. In this way one can isolate the most important phenomena.

For example, in the context of a Grand Unifying Theory (GUT) one assumes that gauge or Yukawa couplings are unified at some scale which is higher than the GUT scale. With the help of Renormalization Group Equations (RGEs) one can run those couplings to low energy scales at which one can compare them to experimental results. When using an on-shell renormalization scheme, gigantic logarithms appear which spoil perturbation theory to a degree where predictions are not valid anymore. To avoid such logarithms, one can use a mass independent renormalization scheme, e.g. the $\overline{\text{MS}}$ scheme [18–20]. But then a mechanism is needed to take into account mass threshold effects since the RGEs do not depend on masses and therefore the theory remains unbroken regarding the evolution of gauge couplings.

2.1. Decoupling Theorem

In Quantum Field Theory (QFT) it is possible to construct an effective theory which has the same predictions of low energy processes as the full theory but contains only the light degrees of freedom. This reduces the amount of dynamical particles which have to be taken into account. The decoupling theorem by Appelquist and Carazzone [21] states that effects of heavy particles can be neglected below a certain energy scale. However, this statement is not valid for mass independent renormalization schemes. The reason for this is that the β functions and anomalous dimensions do not depend on any mass but on the number of active particles. To circumvent this problem one has to rescale the parameters of the effective field theory by so-called decoupling coefficients [22] which depend on heavy particle masses and on the underlying theory.

Let $\mathcal{L}$ be a Lagrange density which contains fields of light particles φ as well as fields of heavy particles ϕ:

$$\mathcal{L} = \mathcal{L}(\varphi, \phi) \tag{2.1}$$

One can isolate terms $\mathcal{L}_{light}$ which contain only fields of light particles:

$$\mathcal{L}(\varphi, \phi) = \mathcal{L}_{light}(\varphi) + \mathcal{L}_{rest}(\varphi, \phi) \tag{2.2}$$

Now one can construct an effective theory whose Lagrange density $\mathcal{L}'(\varphi')$[1] has the same structure as $\mathcal{L}_{light}(\varphi)$[2]. Its predictions are the same as in the full theory up to a correction of the order of the inverse of the heavy masses. The fields φ' and parameters in the effective theory are related to the original fields φ and parameters by multiplicative factors called decoupling coefficients which are calculated by matching the effective and full theory [23].

2.2. Decoupling Limit

Throughout this thesis, the MSSM is regarded as the full and the SM as the effective field theory. In the MSSM, an additional Higgs doublet has to be introduced since otherwise the electroweak gauge symmetry would suffer a gauge anomaly. Therefore, the Higgs sector is changed compared to the SM. On the other hand, all current data by the CMS and ATLAS collaboration suggest, that the observed scalar state is a SM-like Higgs boson [24, 25]. Fortunately, there exists a so-called decoupling limit of the MSSM [26] where the low-energy Higgs spectrum is identical to that of the SM. In short, it is defined by considering the CP-odd Higgs mass M_A to be much larger than the electroweak scale:

$$M_A \gg M_Z \tag{2.3}$$

In this limit the tree level Higgs masses are

$$M_{H^0} \simeq M_{H^\pm} \simeq M_A \gg M_Z \tag{2.4}$$

and

$$M_{h^0} \simeq M_Z |c_{2\beta}|. \tag{2.5}$$

The trigonometric functions are abbreviated as

$$\tan(x) \equiv t_x, \tag{2.6}$$
$$\sin(x) \equiv s_x \tag{2.7}$$
$$\tag{2.8}$$

and

$$\cos(x) \equiv c_x. \tag{2.9}$$

It should be noted that quantum corrections can easily shift the mass M_{h^0} to its experimental value at about $125\,\text{GeV}$. In Table 2.1, the tree-level couplings of the Higgs boson H in the SM and h^0 in the MSSM to top and bottom quarks and vector bosons, normalized to the corresponding SM values are shown. Expanding in inverse powers of M_A, one gets

$$\frac{c_\alpha}{s_\beta} = 1 + \mathcal{O}\left(\frac{M_Z^2}{M_A^2}\right), \tag{2.10}$$

$$-\frac{s_\alpha}{c_\beta} = 1 + \mathcal{O}\left(\frac{M_Z^2}{M_A^2}\right) \tag{2.11}$$

---

[1]Fields and parameters of effective theories are denoted by a prime throughout this thesis, except stated otherwise.

[2]In addition, new interactions in the Lagrange density can potentially occur.

	ϕ	$g_{\phi \bar{t}t}$	$g_{\phi \bar{b}b}$	$g_{\phi VV}$
SM	H	1	1	1
MSSM	h^0	c_α/s_β	$-s_\alpha/c_\beta$	$s_{\beta-\alpha}$

Table 2.1.: Tree level Higgs couplings in the MSSM, normalized to the SM couplings

and

$$s_{\beta-\alpha} = 1 + \mathcal{O}\left(\frac{M_Z^4}{M_A^4}\right). \tag{2.12}$$

Therefore, in the decoupling limit the tree-level couplings of the MSSM Higgs boson h^0 are identical to the couplings of the SM Higgs boson H. In addition, similar results have been observed at the one-loop level, see e.g. [27]. It has been shown that for both large SUSY mass parameters and a large CP-odd Higgs mass the $\Gamma(h^0 \to b\bar{b})$ decay width approaches its SM value. Also the Higgs masses keep a similar pattern as the tree level ones [28].

However, it should be noted that in some cases an apparent SM-like Higgs signal can also arise in a region that may not be governed by the decoupling limit [27, 29]. However, this possibility will not be considered in this thesis.

2.3. Gauge-less Limit

To simplify the calculations, the so-called gauge-less limit is used. In this limit, the electroweak gauge couplings $g_{1,2}$ are neglected which leads to vanishing masses for the W and Z bosons. One can write

$$M_W^2 = \frac{g_2^2 v^2}{2} \to 0, \tag{2.13}$$

$$M_Z^2 = \frac{(g_1^2 + g_2^2)v^2}{2} \to 0 \tag{2.14}$$

while keeping the ratio

$$c_W = \frac{M_W}{M_Z} \tag{2.15}$$

and the vacuum expectation value v fixed. It is a reasonable limit since effects of the strong and Yukawa couplings are dominant at the TeV scale where calculations in this thesis are performed. The effects of the gauge-less limit on the sectors of the MSSM are reviewed in the following. The notation is mainly based on [30, 31].

2.3.1. Squark Sector

The tree-level mass terms for the squarks $\tilde{q}_{L,R}$ are given by

$$\mathcal{L}_{mass}^{\tilde{q}} = \begin{pmatrix} \tilde{q}_L^* & \tilde{q}_R^* \end{pmatrix} \mathcal{M}_{\tilde{q}}^2 \begin{pmatrix} \tilde{q}_L \\ \tilde{q}_R \end{pmatrix} \tag{2.16}$$

with the non-diagonal mass matrix

$$\mathcal{M}_{\tilde{q}}^2 = \begin{pmatrix} M_{\tilde{q}LL}^2 & M_{\tilde{q}LR}^2 \\ M_{\tilde{q}LR}^2 & M_{\tilde{q}RR}^2 \end{pmatrix} \tag{2.17}$$

and

$$M_{\tilde{q}LL}^2 = M_{\tilde{Q}_L}^2 + m_q^2 + c_{2\beta}(T_q^3 - Q_q s_W^2)M_Z^2, \tag{2.18}$$

$$M_{\tilde{q}LR}^2 = m_q(A_q - \mu t_\beta^{-2T_q^3}), \tag{2.19}$$

$$M_{\tilde{q}RR}^2 = M_{\tilde{q}_R}^2 + m_q^2 + c_{2\beta}Q_q s_W^2 M_Z^2. \tag{2.20}$$

$M_{\tilde{Q}_L}^2$ is the parameter of the soft supersymmetry-breaking term of the left-handed doublet. $M_{\tilde{q}_R}^2$ is the parameter of the soft supersymmetry-breaking term of the right-handed singlet. m_q is the mass of the corresponding quark. The third component of the isospin is T_q^3 and the charge is denoted by Q_q. A_q is the parameter of the trilinear supersymmetry-breaking term and μ is the Higgsino mass parameter. The electroweak angle is denoted by W and t_β is the ratio of the Higgs vacuum expectation values.

If one assumes zero quark masses the mass matrix becomes diagonal. Additionally imposing the gauge-less limit yields $M_{\tilde{q}LL}^2 = M_{\tilde{Q}_L}^2$ which is identical for squarks of the same generation. Therefore, the tree-level masses of squarks which correspond to left-handed quarks are identical in the same generation, e.g.

$$m_{\tilde{t}_1} = m_{\tilde{b}_1}. \tag{2.21}$$

2.3.2. Slepton Sector

The slepton sector is analog to the squark sector and is shown for completion. The mass terms of the superpartner of a lepton e are given by

$$\mathcal{L}_{mass}^{\tilde{e}} = \begin{pmatrix} \tilde{e}_L^* & \tilde{e}_R^* \end{pmatrix} \mathcal{M}_{\tilde{e}}^2 \begin{pmatrix} \tilde{e}_L \\ \tilde{e}_R \end{pmatrix} \tag{2.22}$$

with the mass matrix

$$\mathcal{M}_{\tilde{e}}^2 = \begin{pmatrix} M_{\tilde{e}LL}^2 & M_{\tilde{e}LR}^2 \\ M_{\tilde{e}LR}^2 & M_{\tilde{e}RR}^2 \end{pmatrix} \tag{2.23}$$

and

$$M_{\tilde{e}LL}^2 = M_{\tilde{L}_L}^2 + m_e^2 + c_{2\beta}(-\frac{1}{2} + s_W^2)M_Z^2, \tag{2.24}$$

$$M_{\tilde{e}LR}^2 = m_e(A_e - \mu t_\beta), \tag{2.25}$$

$$M_{\tilde{e}RR}^2 = M_{\tilde{e}_R}^2 + m_e^2 - c_{2\beta}s_W^2 M_Z^2. \tag{2.26}$$

$M_{\tilde{L}_L}^2$ is the soft supersymmetry-breaking parameter of the left-handed doublet and $M_{\tilde{e}_R}$ of the right-handed singlet. m_e is the mass of the corresponding lepton. A_e is the parameter of the trilinear supersymmetry-breaking term.

2.3.3. Higgs Sector

One can express the two Higgs doublets H_1 and H_2 with vacuum expectation values v_1 and v_2 through fields $\phi_{1,2}^0$, $\varphi_{1,2}^0$, ϕ_1^- and ϕ_2^+ whose vacuum expectation values vanish by writing

$$H_1 = \begin{pmatrix} H_1^0 \\ H_1^- \end{pmatrix} = \begin{pmatrix} \frac{1}{\sqrt{2}}(v_1 + \phi_1^0 - i\varphi_1^0) \\ -\phi_1^- \end{pmatrix} \tag{2.27}$$

and

$$H_2 = \begin{pmatrix} H_2^+ \\ H_2^0 \end{pmatrix} = \begin{pmatrix} \phi_2^+ \\ \frac{1}{\sqrt{2}}(v_2 + \phi_2^0 + i\varphi_2^0) \end{pmatrix}. \tag{2.28}$$

The mass terms are

$$\mathcal{L}_{mass}^{\varphi^0} = -\frac{1}{2} \begin{pmatrix} \varphi_1^0 & \varphi_2^0 \end{pmatrix} \mathcal{M}_{\varphi^0}^2 \begin{pmatrix} \varphi_1^0 \\ \varphi_2^0 \end{pmatrix}, \tag{2.29}$$

$$\mathcal{L}_{mass}^{\phi^0} = -\frac{1}{2} \begin{pmatrix} \phi_1^0 & \phi_2^0 \end{pmatrix} \mathcal{M}_{\phi^0}^2 \begin{pmatrix} \phi_1^0 \\ \phi_2^0 \end{pmatrix} \tag{2.30}$$

and

$$\mathcal{L}_{mass}^{\phi^\pm} = -\begin{pmatrix} \phi_1^- & \phi_2^- \end{pmatrix} \mathcal{M}_{\phi^\pm}^2 \begin{pmatrix} \phi_1^+ \\ \phi_2^+ \end{pmatrix} \tag{2.31}$$

with

$$\mathcal{M}_{\varphi^0}^2 = \begin{pmatrix} m_1^2 + \frac{g^2 + g'^2}{8}(v_1^2 - v_2^2) & m_{12}^2 \\ m_{12}^2 & m_2^2 - \frac{g^2 + g'^2}{8}(v_1^2 - v_2^2) \end{pmatrix}, \tag{2.32}$$

$$\mathcal{M}_{\phi^0}^2 = \mathcal{M}_{\varphi^0}^2 + \frac{g^2 + g'^2}{4} \begin{pmatrix} v_1^2 & -v_1 v_2 \\ -v_1 v_2 & v_2^2 \end{pmatrix} \tag{2.33}$$

and

$$\mathcal{M}_{\phi^\pm}^2 = \mathcal{M}_{\varphi^0}^2 + \frac{g^2}{4} \begin{pmatrix} v_2^2 & -v_1 v_2 \\ -v_1 v_2 & v_1^2 \end{pmatrix}. \tag{2.34}$$

Here, m_1 and m_2 are the soft supersymmetry-breaking mass parameters and m_{12} the mixing parameter of the Higgs doublets H_1 and H_2. The gauge couplings of the $SU(2)_L$ and $U(1)_Y$ symmetry are denoted by g and g'.

The diagonalization of the Higgs mass matrices is performed via orthogonal transformations with the angle α for the $\mathcal{CP}$-even part and β for the charged and $\mathcal{CP}$-odd part, i.e. the mass Eigenstates (G^0, A^0), (H^0, h^0) and $(G^\pm, H^\pm)$ can be written as

$$\begin{pmatrix} G^0 \\ A^0 \end{pmatrix} = U(\beta) \begin{pmatrix} \varphi_1^0 \\ \varphi_2^0 \end{pmatrix}, \tag{2.35}$$

2. Decoupling Coefficients

$$\begin{pmatrix} H^0 \\ h^0 \end{pmatrix} = U(\alpha) \begin{pmatrix} \phi_1^0 \\ \phi_2^0 \end{pmatrix} \tag{2.36}$$

and

$$\begin{pmatrix} G^\pm \\ H^\pm \end{pmatrix} = U(\beta) \begin{pmatrix} \phi_1^\pm \\ \phi_2^\pm \end{pmatrix} \tag{2.37}$$

with

$$U(x) = \begin{pmatrix} c_x & s_x \\ -s_x & c_x \end{pmatrix}. \tag{2.38}$$

The mixing angles are determined by diagonalizing the mass mixing matrices, e.g.

$$U(\alpha) \mathcal{M}_{\phi^0}^2 U(-\alpha) = \mathrm{diag}(M_{H^0}^2, M_{h^0}^2). \tag{2.39}$$

The mixing angle α can be written as

$$t_{2\alpha} = t_{2\beta} \frac{M_A^2 + M_Z^2}{M_A^2 - M_Z^2}. \tag{2.40}$$

The tree-level masses are

$$M_h^2 = \frac{1}{2} \left\{ M_A^2 + M_Z^2 - \sqrt{(M_A^2 + M_Z^2)^2 - 4M_A^2 M_Z^2 c_{2\beta}^2} \right\}, \tag{2.41}$$

$$M_H^2 = \frac{1}{2} \left\{ M_A^2 + M_Z^2 + \sqrt{(M_A^2 + M_Z^2)^2 - 4M_A^2 M_Z^2 c_{2\beta}^2} \right\} \tag{2.42}$$

and

$$M_{H^\pm}^2 = M_A^2 + M_W^2. \tag{2.43}$$

In the gauge-less limit, the tree-level masses simplify to[3]

$$M_h = 0 \tag{2.44}$$

and

$$M_{H^\pm}^2 = M_H^2 = M_A^2. \tag{2.45}$$

One gets for the mixing angles

$$s_\alpha = -c_\beta \tag{2.46}$$

and

$$c_\alpha = s_\beta \tag{2.47}$$

which is compatible with the decoupling limit, see equations (2.10)-(2.12).

---

[3]The formal requirement $M_h = 0$ seems a bit strong, e.g. in the context of calculating the lightest CP-even Higgs boson mass. However, it is a common practice for higher-order correction to use this limit, see e.g. [32]. A consistent treatment of the gauge-less limit without imposing $M_h = 0$ is shown in [33].

2.3.4. Chargino and Neutralino Sector

The Higgsinos $\tilde{H}_{1,2}$, which are the superpartners of the Higgs bosons, can be expressed through left-handed Weyl spinors

$$\tilde{H}_1 = \begin{pmatrix} \tilde{H}_1^0 \\ \tilde{H}_1^- \end{pmatrix} \tag{2.48}$$

and

$$\tilde{H}_2 = \begin{pmatrix} \tilde{H}_2^+ \\ \tilde{H}_2^0 \end{pmatrix}. \tag{2.49}$$

Let $\tilde{B}^0$ be the gaugino of the $U(1)_Y$ and $\tilde{W}^i$ ($i = 0, 1, 2$) the gauginos of the $SU(2)_L$ gauge group. By setting $\tilde{W}^\pm = \frac{1}{2}(\tilde{W}^1 \mp \tilde{W}^2)$, one can define the chargino fields $\Psi_{R,L}^c$ as

$$\Psi_R^c = \begin{pmatrix} \tilde{W}^- \\ \tilde{H}_1^- \end{pmatrix} \tag{2.50}$$

and

$$\Psi_L^c = \begin{pmatrix} \tilde{W}^+ \\ \tilde{H}_2^+ \end{pmatrix}. \tag{2.51}$$

The chargino mass terms can be written as

$$\mathcal{L}_{mass}^c = -i(\Psi_R^{c^T} X \Psi_L^c + \bar{\Psi}_L^{c^T} X^\dagger \bar{\Psi}_R^c) \tag{2.52}$$

with $\sigma^\mu = (1, \tau^i)$ and $\bar{\sigma}^\mu = (1, -\tau^i)$ expressed through Pauli matrices τ^i ($i = 1, 2, 3$). The chargino mass mixing matrix X is given by

$$X = \begin{pmatrix} M_2 & \sqrt{2}M_W s_\beta \\ \sqrt{2}M_W c_\beta & \mu \end{pmatrix}. \tag{2.53}$$

M_2 is the soft supersymmetry-breaking parameter of the wino $\tilde{W}^i$ ($i = 0, 1, 2$).

In the gauge-less limit, X becomes diagonal with the resulting tree-level masses as M_2 and μ.

One can define the neutralino fields as

$$\Psi^n = \begin{pmatrix} \tilde{B}^0 \\ \tilde{W}^0 \\ \tilde{H}_1^0 \\ \tilde{H}_2^0 \end{pmatrix} \tag{2.54}$$

with the mass terms

$$\mathcal{L}_{mass}^n = -\frac{1}{2}(\Psi^{n^T} Y \Psi^n + \bar{\Psi}^{n^T} Y^\dagger \bar{\Psi}^n). \tag{2.55}$$

Here, the mixing matrix of the neutralinos is

$$Y = \begin{pmatrix} M_1 & 0 & -M_Z s_W c_\beta & M_Z s_W s_\beta \\ 0 & M_2 & M_Z c_W c_\beta & -M_Z c_W s_\beta \\ -M_Z s_W c_\beta & M_Z c_W c_\beta & 0 & -\mu \\ M_Z s_W s_\beta & -M_Z c_W s_\beta & -\mu & 0 \end{pmatrix}. \tag{2.56}$$

M_1 is the soft supersymmetry-breaking parameter of the bino $\tilde{B}^0$. Applying the gauge-less limit yields

$$Y = \begin{pmatrix} M_1 & 0 & 0 & 0 \\ 0 & M_2 & 0 & 0 \\ 0 & 0 & 0 & -\mu \\ 0 & 0 & -\mu & 0 \end{pmatrix} \tag{2.57}$$

which can be diagonalized by

$$\tilde{Y} = N^* Y N^\dagger = \mathrm{diag}(m_{\tilde{\chi}_1^0}, m_{\tilde{\chi}_2^0}, m_{\tilde{\chi}_3^0}, m_{\tilde{\chi}_4^0})$$
$$= \mathrm{diag}(M_1, M_2, \mu, \mu) \tag{2.58}$$

with

$$N = \begin{pmatrix} 1 & 0 & 0 & 0 \\ 0 & 1 & 0 & 0 \\ 0 & 0 & \frac{i}{\sqrt{2}} & \frac{i}{\sqrt{2}} \\ 0 & 0 & \frac{-1}{\sqrt{2}} & \frac{1}{\sqrt{2}} \end{pmatrix}. \tag{2.59}$$

N is chosen complex to ensure the masses to be non-negative. Alternatively, as done in [33] and which is a common practice, one can drop the factors i in equation (2.59) and formally use a negative value for $m_{\tilde{\chi}_4^0}$.

Without applying the gauge-less limit, it is a non-trivial task to make use of unitarity relations in calculations where diagonalization matrices of the neutralino sector are present. In the gauge-less limit N can just be expressed by equations (2.59) which simplifies the calculations.

2.4. Renormalization Constants and Decoupling Coefficients of the Bottom- and Top-Quark Mass

Within the framework of supersymmetry, the decoupling coefficients of the bottom- [34] and top-quark mass [35] have been computed in SQCD up to $\mathcal{O}(\alpha_s^2)$. In this thesis, also electroweak effects are taken into account and therefore a short review on how to calculate decoupling coefficients is given. In addition, explicit formulas for the corresponding renormalization constants are derived.

One possibility is to calculate Green's functions both in the effective and in the full theory. Then the decoupling coefficients can be derived by demanding equality of both Green's functions. However, the calculation of decoupling coefficients can be reduced to the solution of vacuum integrals as shown in [22]. The explicit formulas for decoupling
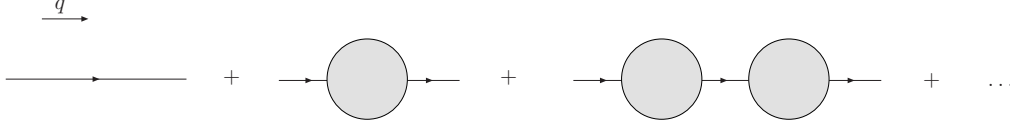
Figure 2.1.: Corrections to the fermionic propagator, drawn with `Jaxodraw` [37]. One-particle-irreducible diagrams are denoted by a gray circle.

coefficients of the top- and bottom-quark mass can be derived through the requirement that on-shell parameters are identical in both the effective and full theory. This was done in [34] and the explicit calculation is presented in the following.

In the full theory, the on-shell top-quark mass M_t can be related to the bare mass $m_t^{(0)}$ by the on-shell renormalization constant $Z_{m_t}^{\mathrm{OS}}$:

$$m_t^{(0)} = Z_{m_t}^{\mathrm{OS}} M_t \tag{2.60}$$

In the effective theory, the analog relation is

$$m_t'^{(0)} = Z_{m_t}'^{\mathrm{OS}} M_t \tag{2.61}$$

with the on-shell renormalization constant $Z_{m_t}'^{\mathrm{OS}}$ and the bare top-quark mass $m_t'^{(0)}$ of the effective theory. The on-shell top-quark mass is identical in both theories. To connect the bare mass of the full and effective theory one can introduce the decoupling coefficient $\zeta_{m_t}^{(0)}$ by writing

$$m_t'^{(0)} = \zeta_{m_t}^{(0)} m_t^{(0)}. \tag{2.62}$$

Combining equations (2.60) to (2.62) yields

$$\zeta_{m_t}^{(0)} = \frac{Z_{m_t}'^{\mathrm{OS}}}{Z_{m_t}^{\mathrm{OS}}}. \tag{2.63}$$

The on-shell mass M_t is defined by demanding the top-quark propagator to have a pole at $q^2 = M_t^2$, where q is the external momentum. In the MSSM the self-energy $i\Sigma_F$ consists of a vector, an axial, a scalar and a pseudoscalar part as defined in equation (A.3). If the parameters of the MSSM are chosen to be real the pseudoscalar part vanishes because of hermiticity, see e.g. [30, 36]. For simplicity, the color structure will be suppressed in the following discussion.

To compute corrections to the fermionic propagator one can sum up one-particle-irreducible diagrams[4] $i\Sigma_F$. Graphically, this is illustrated in Figure 2.1 where $i\Sigma_F$ is denoted by a gray circle.

Using the Feynman rule for fermionic propagators $\frac{i}{\not{q}-m}$, one can sum up the diagrams

---

[4]i.e. diagrams which cannot be split into two parts by removing a single line

shown in Figure 2.1:

$$iS_F = \frac{i}{\slashed{q}-m} + \frac{i}{\slashed{q}-m}i\Sigma_F(q)\frac{i}{\slashed{q}-m} + \frac{i}{\slashed{q}-m}i\Sigma_F(q)\frac{i}{\slashed{q}-m}i\Sigma_F(q)\frac{i}{\slashed{q}-m} + \dots \quad (2.64)$$

$$= \frac{i}{\slashed{q}-m}\sum_{k=0}^{\infty}\left(i\Sigma_F(q)\frac{i}{\slashed{q}-m}\right)^k$$

$$= \frac{i}{\slashed{q}-m}\left(1 + \Sigma_F(q)(\slashed{q}-m)\right)^{-1}$$

$$= i\left(\slashed{q}-m+\Sigma_F(q)\right)^{-1}$$

By exploiting the Lorentz structure one can calculate the inverse of $\slashed{q}-m+\Sigma_F(q)$. The result reads

$$iS_F = i\,\frac{m\left[\Sigma_F^S(q^2)-\gamma_5\Sigma_F^P(q^2)-1\right]-\slashed{q}\left[\Sigma_F^V(q^2)-\gamma_5\Sigma_F^A(q^2)+1\right]}{m^2\left[\left(1-\Sigma_F^S(q^2)\right)^2-\left(\Sigma_F^P(q^2)\right)^2\right]-q^2\left[\left(1+\Sigma_F^V(q^2)\right)^2-\left(\Sigma_F^A(q^2)\right)^2\right]}.$$

If the bare mass m is renormalized with the on-shell renormalization constant Z_m^{OS}, the loop-corrected inverse propagator has to vanish for $q^2 = M^2$ with M being the on-shell mass. This leads to the equation

$$0 = \left(Z_m^{OS}M\right)^2\left[\left(1-\Sigma_F^S(M^2)\right)^2-\left(\Sigma_F^P(M^2)\right)^2\right] \quad (2.65)$$

$$- M^2\left[\left(1+\Sigma_F^V(M^2)\right)^2-\left(\Sigma_F^A(M^2)\right)^2\right]. \quad (2.66)$$

Solving for Z_m^{OS} gives

$$Z_m^{OS} = \sqrt{\frac{\left(1+\Sigma_F^V(M^2)\right)^2-\left(\Sigma_F^A(M^2)\right)^2}{\left(1-\Sigma_F^S(M^2)\right)^2-\left(\Sigma_F^P(M^2)\right)^2}}. \quad (2.67)$$

To extract $\zeta_{m_t}^{(0)}$ from equation (2.62) one has to calculate $Z_{m_t}^{OS}$ both in the effective and full theory. Since all masses in the effective theory are much smaller than the heavy ones of the full theory one can approximate them to be zero. Since $q^2 = M^2$, this leads to a vanishing external momentum and consequently, one has to calculate only tadpole diagrams. In the effective theory, the integrals appearing in the self-energies become dimensionless and disappear in dimensional regularization or dimensional reduction[5] [38, 39]. This approximation leads to

$$\zeta_{m_t}^{(0)} = \frac{1}{Z_{m_t}^{OS}} = \sqrt{\frac{\left(1-\Sigma_t^S(0)\right)^2-\left(\Sigma_t^P(0)\right)^2}{\left(1+\Sigma_t^V(0)\right)^2-\left(\Sigma_t^A(0)\right)^2}}. \quad (2.68)$$

---

[5]Dimensional reduction will be briefly discussed in Section 3.3.

Therefore, the calculation of $\zeta_{m_t}^{(0)}$ is reduced to the calculation of self-energies of the full theory with vanishing external momenta. Only diagrams with at least one heavy particle in loop integrals have to be considered. For $\Sigma_t^P = \Sigma_t^A = 0$, which is valid in the SM, equation (2.68) is identical to equation (12) in [22].

$\zeta_{m_t}^{(0)}$ relates bare masses of the full and effective theory. Additionally one can define an analog relation for $\overline{\text{DR}}$[6] renormalized masses with ζ_{m_t} through

$$m_t'^{\overline{\text{DR}}} = \zeta_{m_t} m_t^{\overline{\text{DR}}}. \tag{2.69}$$

Since both $m_t'^{\overline{\text{DR}}}$ and $m_t^{\overline{\text{DR}}}$ are finite, ζ_{m_t} must be finite.

In order to connect ζ_{m_t} to $\zeta_{m_t}^{(0)}$ one can use the relations

$$m_t^{(0)} = Z_{m_t}^{\overline{\text{DR}}} m_t^{\overline{\text{DR}}} \tag{2.70}$$

in the full theory and

$$m_t'^{(0)} = Z_{m_t}'^{\overline{\text{DR}}} m_t'^{\overline{\text{DR}}} \tag{2.71}$$

in the effective theory. With equations (2.62), (2.69), (2.70) and (2.71) one gets

$$\zeta_{m_t} = \frac{Z_{m_t}^{\overline{\text{DR}}}}{Z_{m_t}'^{\overline{\text{DR}}}} \zeta_{m_t}^{(0)}. \tag{2.72}$$

The calculation of the renormalization constant of the top-quark mass in the $\overline{\text{DR}}$ scheme is described in [40]. For convenience, the main steps are discussed in the following.

The renormalization constants for the left- and right-handed fields of the top quark are defined as

$$\psi_t^{L(0)} = \sqrt{Z_{2t}^{L\overline{\text{DR}}}} \psi_t^L \tag{2.73}$$

$$\psi_t^{R(0)} = \sqrt{Z_{2t}^{R\overline{\text{DR}}}} \psi_t^R. \tag{2.74}$$

By introducing the left- and right-handed self-energies Σ_t^L and Σ_t^R via

$$\Sigma_t^L = \Sigma_t^V - \Sigma_t^A \tag{2.75}$$

and

$$\Sigma_t^R = \Sigma_t^V + \Sigma_t^A \tag{2.76}$$

the inverse of the top-quark propagator can be written as

$$(iS_t)^{-1}(q) = -i\slashed{q}\left(P_L Z_{2t}^{L\overline{\text{DR}}}(1 + \Sigma_t^L(q^2)) + P_R Z_{2t}^{R\overline{\text{DR}}}(1 + \Sigma_t^R(q^2)) \right) \tag{2.77}$$

$$+ im_t \sqrt{Z_{2t}^{L\overline{\text{DR}}} Z_{2t}^{R\overline{\text{DR}}}} Z_{m_t}^{\overline{\text{DR}}}(1 - \Sigma_t^S(q^2))$$

---

[6]The $\overline{\text{DR}}$ renormalization scheme is analog to the $\overline{\text{MS}}$ scheme but within the framework of dimensional reduction.

2. Decoupling Coefficients

where the pseudoscalar part is set to zero. The $\overline{\text{DR}}$ renormalization constant is defined by the requirement that the propagator is finite. This leads to the recursive relations

$$Z_{2t}^{L\overline{\text{DR}}} = 1 - K_\epsilon\left(\Sigma_t^L(q^2) Z_{2t}^{L\overline{\text{DR}}}\right), \tag{2.78}$$

$$Z_{2t}^{R\overline{\text{DR}}} = 1 - K_\epsilon\left(\Sigma_t^R(q^2) Z_{2t}^{R\overline{\text{DR}}}\right) \tag{2.79}$$

and

$$\sqrt{Z_{2t}^{L\overline{\text{DR}}} Z_{2t}^{R\overline{\text{DR}}}} Z_{m_t}^{\overline{\text{DR}}} = 1 + K_\epsilon\left(\Sigma_t^S(q^2)\sqrt{Z_{2t}^{L\overline{\text{DR}}} Z_{2t}^{R\overline{\text{DR}}}} Z_{m_t}^{\overline{\text{DR}}}\right) \tag{2.80}$$

which have to be solved iteratively. The operator $K_\epsilon(x)$ is defined by only taking terms of x proportional to some positive power of $1/\epsilon$. To retrieve explicit formulas for the renormalization constants one can make a perturbative expansion in the appearing couplings and separate the different loop orders by writing

$$Z = 1 + Z^{(1)} + Z^{(2)} + \dots \tag{2.81}$$

and

$$\Sigma = 1 + \Sigma^{(1)} + \Sigma^{(2)} + \dots. \tag{2.82}$$

Up to two loops one gets

$$Z_{2t}^{L\overline{\text{DR}}(1)} = -K_\epsilon\left(\Sigma_t^{L(1)}\right), \tag{2.83}$$

$$Z_{2t}^{R\overline{\text{DR}}(1)} = -K_\epsilon\left(\Sigma_t^{R(1)}\right), \tag{2.84}$$

$$Z_{2t}^{L\overline{\text{DR}}(2)} = K_\epsilon\left(\Sigma_t^{L(1)} K_\epsilon\left(\Sigma_t^{L(1)}\right)\right) - K_\epsilon\left(\Sigma_t^{L(2)}\right) \tag{2.85}$$

and

$$Z_{2t}^{R\overline{\text{DR}}(2)} = K_\epsilon\left(\Sigma_t^{R(1)} K_\epsilon\left(\Sigma_t^{R(1)}\right)\right) - K_\epsilon\left(\Sigma_t^{R(2)}\right). \tag{2.86}$$

The renormalization constant for the top-quark mass is

$$Z_{m_t}^{\overline{\text{DR}}(1)} = -\frac{1}{2}\left(Z_{2t}^{L\overline{\text{DR}}(1)} + Z_{2t}^{R\overline{\text{DR}}(1)}\right) + K_\epsilon\left(\Sigma_t^{S(1)}\right) \tag{2.87}$$

$$
\begin{aligned}
Z_{m_t}^{\overline{\text{DR}}(2)} = \frac{1}{8}\Bigg\{ & 3\left(Z_{2t}^{L\overline{\text{DR}}(1)}\right)^2 + 3\left(Z_{2t}^{R\overline{\text{DR}}(1)}\right)^2 - 4Z_{2t}^{L\overline{\text{DR}}(2)} - 4Z_{2t}^{R\overline{\text{DR}}(2)} \\
& + 2Z_{2t}^{L\overline{\text{DR}}(1)} Z_{2t}^{R\overline{\text{DR}}(1)} - 4K_\epsilon\left(\Sigma_t^{S(1)}\right)\left(Z_{2t}^{L\overline{\text{DR}}(1)} + Z_{2t}^{R\overline{\text{DR}}(1)}\right) \\
& + 8K_\epsilon\left(\Sigma_t^{S(1)} K_\epsilon\left(\Sigma_t^{S(1)}\right)\right) + 8K_\epsilon\left(\Sigma_t^{S(2)}\right) \Bigg\}.
\end{aligned}
$$

2.5. Decoupling Coefficient of the Strong Coupling Constant

Within the framework of QCD, the decoupling coefficient of the strong coupling constant is known to two- [22, 41, 42], three- [22] and even four-loop order [43, 44] and the simultaneous decoupling of two heavy quarks has been computed at three-loop order [45].

In the context of supersymmetry, SQCD corrections at two-loop order were calculated for a degenerate supersymmetric mass spectrum [46, 47] and for the general case [34]. For certain mass hierarchies even the $\mathcal{O}(\alpha_s^3)$ corrections were computed [48]. In the scope of this thesis, also electroweak effects on the decoupling coefficient are calculated, hence the main steps of the computation are reviewed here.

To calculate the decoupling coefficient of the strong coupling constant g_s, one has to consider a physical quantity that includes g_s. To simplify the calculation one can for example use the $g\bar{c}c$ vertex. Analog to equation (2.62), the definition of $\zeta_{g_s}^{(0)}$ reads

$$g_s'^{(0)} = \zeta_{g_s}^{(0)} g_s^{(0)}. \tag{2.88}$$

Matching the full and the effective theory [22] leads to

$$\zeta_{g_s}^{(0)} = \frac{\tilde{\zeta}_1^{(0)}}{\tilde{\zeta}_3^{(0)} \sqrt{\zeta_3^{(0)}}} \tag{2.89}$$

with the decoupling coefficient $\tilde{\zeta}_1^{(0)}$ of the one-particle-irreducible $g\bar{c}c$ vertex, the decoupling coefficient $\tilde{\zeta}_3^{(0)}$ of the ghost wave function and $\zeta_3^{(0)}$ of the gluon wave function. They can be computed according to

$$\zeta_3^{(0)} = 1 + \Pi_g^{(0),h}(0),$$
$$\tilde{\zeta}_3^{(0)} = 1 + \Pi_c^{(0),h}(0),$$
$$\tilde{\zeta}_1^{(0)} = 1 + \Gamma_{g\bar{c}c}^{(0),h}(0,0) \tag{2.90}$$

where $\Gamma_{g\bar{c}c}^{(0)}(q,k)$ is the one-particle-irreducible part of the amputated $g\bar{c}c$ Green's function with outgoing four-momenta q and k and $\Pi_g^{(0)}(q^2)$ and $\Pi_c^{(0)}(q^2)$ are the gluon and ghost vacuum polarizations, respectively. The superscript h indicates that only the hard part of the respective quantities needs to be computed.

In general, equation (2.89) can be written as

$$\zeta_{\text{coupling}}^{(0)} = \frac{\zeta_{\text{vertex}}^{(0)}}{\prod_i \sqrt{\zeta_{\Phi_i}^{(0)}}} \tag{2.91}$$

where the product goes over all external particles i with the corresponding decoupling coefficients of the wave function $\zeta_{\Phi_i}^{(0)}$.

It has been shown that $\tilde{\zeta}_1^{(0)}$ is equal to one up to two-loop order. To compute the decoupling coefficient of the ghost wave function, the self-energy of the ghost propagator

2. Decoupling Coefficients

has to be considered where only the color structure is projected out. For the decoupling coefficient of the gluon wave function, the self-energy of the gluon propagator has to be separated into a longitudinal and a transversal part, see equation (A.2). Because of the generalized Ward-Takahashi identity [49] only the transversal part contributes. The renormalized decoupling coefficient ζ_{g_s} can be computed analog to equation (2.72) by

$$\zeta_{g_s} = \frac{Z_{g_s}^{\overline{\mathrm{DR}}}}{Z_{g_s}^{\prime\overline{\mathrm{DR}}}} \zeta_{g_s}^{(0)}. \tag{2.92}$$

To compute the renormalization constants $Z_{g_s}^{\overline{\mathrm{DR}}}$ and $Z_{g_s}^{\prime\overline{\mathrm{DR}}}$ one can proceed in an analog way. This gives

$$Z_{g_s}^{\overline{\mathrm{DR}}} = \frac{Z_{g\bar{c}c}^{\overline{\mathrm{DR}}}}{\tilde{Z}_3^{\overline{\mathrm{DR}}} \sqrt{Z_3^{\overline{\mathrm{DR}}}}} \tag{2.93}$$

with $Z_{g\bar{c}c}^{\overline{\mathrm{DR}}}$ as the renormalization constant for the $g\bar{c}c$ vertex, $\tilde{Z}_3^{\overline{\mathrm{DR}}}$ for the ghost wave function and $Z_3^{\overline{\mathrm{DR}}}$ for the gluon wave function. The analog relation holds for the effective theory. The renormalization of the decoupling coefficient $\zeta_{g_s}^{(0)}$ in equation (2.92) can also be written as

$$\zeta_{g_s} = \frac{\dfrac{Z_{g\bar{c}c}^{\overline{\mathrm{DR}}}}{Z_{g\bar{c}c}^{\prime\overline{\mathrm{DR}}}} \tilde{\zeta}_1^{(0)}}{\dfrac{\tilde{Z}_3^{\overline{\mathrm{DR}}}}{\tilde{Z}_3^{\prime\overline{\mathrm{DR}}}} \tilde{\zeta}_3^{(0)} \sqrt{\dfrac{Z_3^{\overline{\mathrm{DR}}}}{Z_3^{\prime\overline{\mathrm{DR}}}} \zeta_3^{(0)}}}, \tag{2.94}$$

emphasizing independent renormalization of the vertex and the wave function decoupling coefficients. This has the advantage that all individual pieces

$$\tilde{\zeta}_1 \equiv \frac{Z_{g\bar{c}c}^{\overline{\mathrm{DR}}}}{Z_{g\bar{c}c}^{\prime\overline{\mathrm{DR}}}} \tilde{\zeta}_1^{(0)}, \tag{2.95}$$

$$\tilde{\zeta}_3 \equiv \frac{\tilde{Z}_3^{\overline{\mathrm{DR}}}}{\tilde{Z}_3^{\prime\overline{\mathrm{DR}}}} \tilde{\zeta}_3^{(0)} \tag{2.96}$$

and

$$\zeta_3 \equiv \frac{Z_3^{\overline{\mathrm{DR}}}}{Z_3^{\prime\overline{\mathrm{DR}}}} \zeta_3^{(0)} \tag{2.97}$$

are finite which enables additional checks for the calculation. In order to calculate the renormalization constants one proceeds in a similar way to the previous section, i.e. decomposing the renormalization constants to different loop orders and solving the recursive relations.

2.6. Decoupling Coefficient of the Top Yukawa Coupling

As explained in the previous section, the calculation of the decoupling coefficient of the top Yukawa coupling is done by considering a physical quantity where this coupling appears. One can use the $h^0 \bar{t} t$ vertex where h^0 is the light SM-like Higgs boson. By considering the decoupling limit, the tree-level couplings to the top quarks are identical in the MSSM and the SM, as can bee seen in table 2.1. In this way, one can compute $\zeta_{y_t}^{(0)}$, which relates the bare SM top Yukawa coupling $y_t^{\prime(0)}$ to its analogon in the MSSM $\tilde{y}_t^{(0)}$ through the relation

$$y_t^{\prime(0)} = \zeta_{y_t}^{(0)} \tilde{y}_t^{(0)}.$$
(2.98)

In contrast to the definition in the SM, the MSSM definition of the top Yukawa coupling $y_t^{(0)}$ contains an additional factor of $1/s_\beta^{(0)}$. The tree-level coupling of the top quark to the lightest CP-even Higgs boson in the decoupling limit can be written as

$$g_{h^0 \bar{t} t} \sim y_t^{(0)} c_\alpha^{(0)} = y_t^{(0)} s_\beta^{(0)}$$
$$= \tilde{y}_t^{(0)}.$$
(2.99)

This leads to

$$y_t^{\prime(0)} = \zeta_{y_t}^{(0)} s_\beta^{(0)} y_t^{(0)}.$$
(2.100)

$\zeta_{y_t}^{(0)}$ can be derived according to equation (2.91). The result is

$$\zeta_{y_t}^{(0)} = \frac{\zeta_{h^0 \bar{t} t}^{(0)}}{\sqrt{\zeta_{2t}^{(0),L} \zeta_{2t}^{(0),R} \zeta_{h^0}^{(0)}}}$$
(2.101)

where $\zeta_{2t}^{(0),L/R}$ are the decoupling coefficients of the left/right handed top-quark wave functions and ζ_{h^0} for the Higgs wave function. They are computed according to

$$\zeta_{h^0}^{(0)} = 1 + \Pi_{h^0}^{(0),h}(0),$$
$$\zeta_{2t}^{(0),L} = 1 + \Pi_t^{(0),L,h}(0),$$
$$\zeta_{2t}^{(0),R} = 1 + \Pi_t^{(0),R,h}(0),$$
$$\zeta_{h^0 \bar{t} t}^{(0)} = 1 + \Gamma_{h^0 \bar{t} t}^{(0),h}(0,0)$$
(2.102)

with $\Gamma_{h^0 \bar{t} t}^{(0),h}(q,k)$ being the one-particle-irreducible part of the amputated $h^0 \bar{t} t$ Green's function and $\Pi_{h^0}^{(0),h}(q^2)$ and $\Pi_t^{(0),L/R,h}(q^2)$ being the self-energy of the Higgs boson and the left-/right-handed vector part of the self-energy of the top quark, respectively. The latter is defined in equation (A.4). Again, one can define the renormalized decoupling coefficient ζ_{y_t} through the relation

$$y_t' = \zeta_{y_t} s_\beta y_t = \zeta_{y_t} \tilde{y}_t$$
(2.103)

2. Decoupling Coefficients

with

$$\zeta_{y_t} = \frac{Z_{\tilde{y}_t}^{\overline{\text{DR}}}}{Z_{y_t'}^{\overline{\text{DR}}}} \zeta_{y_t}^{(0)} \tag{2.104}$$

where the renormalization constant $Z_{\tilde{y}_t}^{\overline{\text{DR}}}$ is calculated with the equation

$$Z_{\tilde{y}_t}^{\overline{\text{DR}}} = \frac{Z_{h^0 \bar{t}t}^{\overline{\text{DR}}}}{\sqrt{Z_{2t}^{L\overline{\text{DR}}} Z_{2t}^{R\overline{\text{DR}}} Z_{h^0}^{\overline{\text{DR}}}}} \tag{2.105}$$

in the full theory and in an analog way in the effective theory. As discussed in the previous section, it is advisable to decompose equations (2.104) and (2.105) into individual finite pieces. One gets

$$\zeta_{h^0 \bar{t}t} \equiv \frac{Z_{h^0 \bar{t}t}^{\overline{\text{DR}}}}{Z_{h^0 \bar{t}t}^{\prime \overline{\text{DR}}}} \zeta_{h^0 \bar{t}t}^{(0)}, \tag{2.106}$$

$$\zeta_{2t}^{L/R} \equiv \frac{Z_{2t}^{L/R\overline{\text{DR}}}}{Z_{2t}^{\prime L/R\overline{\text{DR}}}} \zeta_{2t}^{L/R(0)} \tag{2.107}$$

and

$$\zeta_{h^0} \equiv \frac{Z_{h^0}^{\overline{\text{DR}}}}{Z_{h^0}^{\prime \overline{\text{DR}}}} \zeta_{h^0}^{(0)}. \tag{2.108}$$

Since $Z_{\tilde{y}_t}^{\overline{\text{DR}}}$ is not the renormalization constant of the top Yukawa coupling, see equation (2.100), a comparison to literature is not directly possible. However, one can calculate $Z_{y_t}^{\overline{\text{DR}}}$ by considering the $\phi_2^0 t\bar{t}$ vertex[7] which is at tree level proportional to y_t without a factor of c_α[8].

ϕ_1 and ϕ_2 can be retrieved by rotating the mass Eigenstates h^0 and H^0 with the orthogonal matrix $U(\alpha)$, as can be seen by equations (2.36) and (2.38).

One can relate the renormalization constants $\tilde{Z}_{\phi_1^0 \phi_2^0}^{1/2}$ for the fields $\phi_{1,2}^0$ which can be written in the diagonal form

$$\tilde{Z}_{\phi_1^0 \phi_2^0}^{1/2} = \begin{pmatrix} Z_{\phi_1^0}^{1/2} & 0 \\ 0 & Z_{\phi_2^0}^{1/2} \end{pmatrix} \tag{2.109}$$

with $\tilde{Z}_{H^0 h^0}^{1/2}$ for the wave functions of the physical fields

$$\tilde{Z}_{H^0 h^0}^{1/2} = \begin{pmatrix} Z_{H^0}^{1/2} & Z_{H^0 h^0}^{1/2} \\ Z_{H^0 h^0}^{1/2} & Z_{h^0}^{1/2} \end{pmatrix} \tag{2.110}$$

---

[7]The Higgs field ϕ_2^0 is defined through equations (2.27) and (2.28).
[8]$= s_\beta$ in the decoupling limit

by rotating the basis with equations (2.36). Since these $\overline{\text{DR}}$ renormalization constants do not depend on masses, one can calculate them in a massless theory for which the pole part of the corresponding renormalized Lagrange density has to vanish. This leads to the equations

$$K_\epsilon\left((\tilde{Z}^{1/2}_{H^0h^0})^T(q^2 + \hat{\Sigma}_{H^0h^0})(\tilde{Z}^{1/2}_{H^0h^0})\right) = 0. \tag{2.111}$$

where q is the external momentum and $\hat{\Sigma}_{H^0h^0}$ the self-energies in the basis of H^0 and h^0. One can calculate the renormalization constants of the physical fields in equations (2.111) order by order in perturbation theory and consequently $Z_{\phi_2^0}$ by switching to the $\phi_1^0\phi_2^0$ basis . The result is

$$Z_{\phi_2^0} = 1 + Z^{(1)}_{\phi_2^0} + Z^{(2)}_{\phi_2^0} \tag{2.112}$$

with

$$Z^{(1)}_{\phi_2^0} = c_\alpha^2 Z^{(1)}_{h^0} + 2c_\alpha s_\alpha Z^{(1)}_{H^0h^0} + s_\alpha^2 Z^{(1)}_{H^0} \tag{2.113}$$

and

$$Z^{(2)}_{\phi_2^0} = \frac{1}{4}\left\{c_\alpha^2\left((Z^{(1)}_{H^0h^0})^2 + 4Z^{(2)}_{h^0}\right) + s_\alpha^2\left((Z^{(1)}_{H^0h^0})^2 + 4Z^{(2)}_{H^0}\right)\right.$$
$$\left. + 2c_\alpha s_\alpha\left(Z^{(1)}_{h^0}Z^{(1)}_{H^0h^0} - (Z^{(1)}_{H^0h^0})^2 + Z^{(1)}_{H^0h^0}Z^{(1)}_{H^0} + 4Z^{(2)}_{H^0h^0}\right)\right\}. \tag{2.114}$$

Now one can use the analog equation of (2.105) for the $\phi_2\bar{t}t$ vertex to compute $Z^{\overline{\text{DR}}}_{y_t}$. The result was checked with the literature [50] and full agreement was obtained. The result of $Z^{\overline{\text{DR}}}_{y_t}$ to $\mathcal{O}(\alpha_s^2, \alpha_s\alpha_{t,b,\tau})$ reads

$$Z^{\overline{\text{DR}}}_{y_t} = \frac{a_s}{2\epsilon}(-C_F) + \frac{3a_t}{4\epsilon} + \frac{a_b}{8\epsilon}$$
$$+ \frac{1}{\epsilon}\left\{a_s^2\left(\frac{1}{8}C_F^2 + \frac{3}{4}TC_F - \frac{3}{16}C_FC_A\right) + \frac{1}{4}a_sa_t\right\}$$
$$+ \frac{1}{\epsilon^2}\left\{a_s^2\left(\frac{-3}{4}TC_F + \frac{1}{8}C_F^2 + \frac{3}{16}C_FC_A\right) - a_sa_t - \frac{1}{6}a_sa_b\right\} \tag{2.115}$$

with $a_x \equiv \alpha_x/\pi$ where $\alpha_s = g_s^2/4\pi$ and $\alpha_{t,b,\tau} = y_{t,b,\tau}^2/4\pi$. The quadratic Casimir invariants for the adjoint and fundamental representations are expressed as C_A and C_F and the Dynkin index is $T = 1/2$. In the Yukawa sector, these symbols are substituted by their numerical values.

2.7. Decoupling Coefficient of the Bottom Yukawa Coupling

The calculation of the bottom is analog to the top Yukawa coupling. The corresponding vertex is the $h^0\bar{b}b$ vertex. In the decoupling limit, the lightest CP-even Higgs boson in the MSSM has the same tree-level couplings to bottom quarks as the SM Higgs boson, see

2. Decoupling Coefficients

table 2.1. One can introduce the decoupling coefficient for the bottom Yukawa coupling by writing

$$y_b^{\prime(0)} = \zeta_{y_b}^{(0)} \tilde{y}_b^{(0)}. \tag{2.116}$$

As for the top Yukawa coupling, the definition of the bottom Yukawa coupling in the MSSM $y_b^{(0)}$ differs from the one in the SM by a factor. For down-type quarks this factor is $1/c_\beta^{(0)}$ which leads to

$$y_b^{\prime(0)} = \zeta_{y_b}^{(0)} c_\beta^{(0)} y_b^{(0)}. \tag{2.117}$$

One can compute ζ_{y_b} through

$$\zeta_{y_b}^{(0)} = \frac{\zeta_{h^0\bar{b}b}^{(0)}}{\sqrt{\zeta_{2b}^L \zeta_{2b}^R \zeta_{h^0}}}, \tag{2.118}$$

with the decoupling coefficient of the left/right handed bottom-quark wave function.

The renormalized decoupling coefficient ζ_{y_b} is

$$\zeta_{y_b} = \frac{Z_{\tilde{y}_b}^{\overline{\text{DR}}}}{Z_{y_b'}^{\overline{\text{DR}}}} \zeta_{y_b}^{(0)} \tag{2.119}$$

where $Z_{\tilde{y}_b}^{\overline{\text{DR}}}$ can be calculated according to

$$Z_{\tilde{y}_b}^{\overline{\text{DR}}} = \frac{Z_{h^0\bar{b}b}^{\overline{\text{DR}}}}{\sqrt{Z_{2b}^{L\overline{\text{DR}}} Z_{2b}^{R\overline{\text{DR}}} Z_{h^0}^{\overline{\text{DR}}}}} \tag{2.120}$$

in the full theory theory and in an analog way in the effective theory.

Decomposing equations (2.119) and (2.120) into individual finite pieces leads to the finite quantities

$$\zeta_{h^0\bar{b}b} \equiv \frac{Z_{h^0\bar{b}b}^{\overline{\text{DR}}}}{Z_{h^0\bar{b}b}^{\prime\overline{\text{DR}}}} \zeta_{h^0\bar{b}b}^{(0)}, \tag{2.121}$$

$$\zeta_{2b}^{L/R} \equiv \frac{Z_{2b}^{L/R\overline{\text{DR}}}}{Z_{2b}^{\prime L/R\overline{\text{DR}}}} \zeta_{2b}^{L/R(0)} \tag{2.122}$$

and

$$\zeta_{h^0} \equiv \frac{Z_{h^0}^{\overline{\text{DR}}}}{Z_{h^0}^{\prime\overline{\text{DR}}}} \zeta_{h^0}^{(0)}. \tag{2.123}$$

3. Calculating the Decoupling Coefficients

In the following, the details of the calculation of the decoupling coefficients and renormalization constants, mentioned in the previous chapter, are discussed. The calculation is quite extensive, therefore several computer programs are needed to perform the computation.

3.1. Used Computer Programs

To generate Feynman diagrams, the program QGRAF [51] is used. In the configuration file one can define fermionic and bosonic propagators and vertices of the desired model. After specifying external particles, the loop order, options and constraints, QGRAF generates all corresponding Feynman diagrams. Symmetry factors and factors regarding Dirac fermions are computed correctly but the treatment of Majorana fermions has to be corrected according to [52] with the help of the additional program majoranas.pl [53, 54]. In order for exp [55, 56] to read the output of QGRAF, the program q2e [55, 56] is used. In this step the Feynman rules of the MSSM are taken into account.

Since the number of Feynman rules for the MSSM is large, it is advisable to make use of a well tested implementation and transfer it to QGRAF and q2e. Fortunately, the program FeynArts [57] has already implemented the MSSM Feynman rules, among other models. The transformation to a format which can be read by QGRAF and q2e is done with the program FeynArtsToQ2E [58, 59]. exp can now be used to create amplitudes out of Feynman diagrams and perform naive and asymptotic expansions in masses and momenta, see Section 3.2. The mapping to master integrals is done with MATAD [60] for diagrams with vanishing external momenta and with MINCER [61] for massless diagrams. Both MATAD and MINCER are based on FORM [62–65], a program for symbolic manipulation of mathematical terms. In the case of one-loop on-shell integrals, the diagrams are expressed in terms of B_0 functions [66].

Since many different physical quantities have to be calculated, an automation of the procedure described above is useful. For this purpose, the Python program Project.py was written. It reads a global configuration file which contains all the relevant information (e.g. external particles, loop order, projectors) and sequentially runs QGRAF, majoranas.pl, q2e, exp and MATAD/MINCER and presents the result in a FORM file.

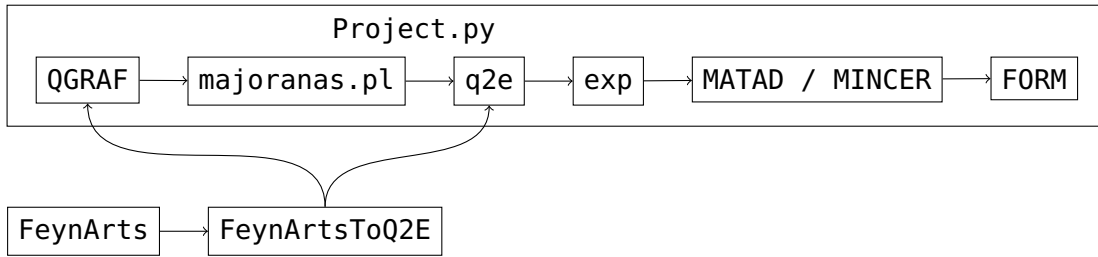Figure 3.1 gives a schematic overview of the used programs.

Figure 3.1.: Schematic overview of the used programs, the upper ones are managed by the program code `Project.py`

3.2. Asymptotic Expansion

Analytic expressions for higher order corrections are in most cases too complex to compute since the appearing integrals contain several different mass scales. In order to solve this problem, one can make use of the so-called asymptotic expansion technique [67], a mathematical prescription to consistently expand Feynman diagrams in large scales. In this way, occurrent hierarchies between different mass scales can be exploited to expand the given diagram with respect to a small quantity. The result of a certain diagram is obtained in four steps:

- Shrink the lines of the hard subgraph[1] to a point, the remaining diagram is called co-subgraph.

- Expand the propagators and evaluate the integrals in the hard subgraph for which the result is inserted into the co-subgraph.

- Evaluate the remaining integrals in the co-subgraph.

- Sum over all terms.

3.3. Dimensional Reduction and Epsilon Scalars

To preserve gauge invariance, unitarity and global supersymmetry, a modified form of dimensional regularization is used, called dimensional reduction [38, 39]. Unlike in dimensional regularization, the dimension of the gauge boson fields is held fixed. In dimensional reduction to $D = 4 - 2\epsilon$ dimensions, the remaining 2ϵ components of the gauge field behave under gauge transformations as a multiplet of scalar fields which are called epsilon scalars.

3.4. Assumptions and Simplifications

Even though the top Yukawa coupling is the most dominant one in the Yukawa sector, the bottom and tau Yukawa couplings are not approximated to be zero since they can

---

[1]In the case of expansions w.r.t. a large mass one has to find all subgraphs which contain all lines carrying the large mass and are one-particle-irreducible w.r.t. light lines in their connected parts.

get enhanced by large values of t_β. At tree level, one can write $y_b/y_t = (m_b/m_t)t_\beta$ and $y_\tau/y_t = (m_\tau/m_t)t_\beta$ so that their ratios become large for large values of t_β.

Since the measured particles of the SM are assumed to be much lighter than their supersymmetric counterparts, their masses are approximated to be zero. However, care has to be taken regarding the masses of the top and bottom quark and the τ lepton. Their masses cannot be set to zero from the beginning since they may also appear in projectors which are used to extract left- and right-handed scalar contributions from self-energy diagrams, see Appendix A. In addition, they can contribute to Yukawa couplings since these are proportional to their masses. Therefore a naive expansion[2] in $m_{t,b,\tau}$ is performed.

In order to be as flexible as possible regarding different MSSM scenarios, masses of occurring heavy particles should be distinct. However, computations become more extensive and results are more lengthy if one chooses each particle to have a distinct mass, especially in the Yukawa sector at two-loop order.

In the SQCD and one-loop electroweak sector, each mass of the heavy particles is chosen to be distinct except the heavy Higgs masses which are equal due to the decoupling limit. The couplings $g_{1,2}$ are not set to zero at one-loop order except for $\zeta_{m_{t,b}}$. In the two-loop electroweak sector, the gauge-less limit is applied and every particle is approximated to have the same mass M_S[3] except $\tilde{t}_2$ and $\tilde{b}_2$, whose masses are $M_{\tilde{t}_2}$ and $M_{\tilde{b}_2}$, respectively. The latter ensures that renormalization of the mixing angles θ_t and θ_b as well as the transitions

$$s_{2\theta_t}(M_S^2 - m_{\tilde{t}_2}^2) \to 2X_t m_t, \tag{3.1}$$

$$s_{2\theta_b}(M_S^2 - m_{\tilde{b}_2}^2) \to 2X_b m_b \tag{3.2}$$

can be performed without any additional complications, e.g. see Section 3.6. The effect of mass degeneracy at one-loop order will be discussed in Chapter 4.

Some MSSM scenarios predict neutralinos which are lighter than some SM particles. In this case, light neutralinos must be present in the effective theory. One example mass spectrum of such a scenario will be discussed Chapter 4 and is given in Section C.1 in the appendix. A consistent treatment of light neutralinos is postponed to future analysis.

The masses of epsilon scalars are free parameters and are chosen to be M_S. In this way, they can be integrated out with the rest of the supersymmetric particles. This corresponds to dimensional regularization in the effective theory and dimensional reduction in the full theory, as was shown in [34, 68]. The diagonalization matrices of the neutralinos and charginos in the two-loop Yukawa sector are set according to the gauge-less limit, see Section 2.3. The full dependence on all gauge parameters was kept to ensure gauge independence of the final results.

3.5. Tadpole Diagrams

The so-called tadpole diagram [69] denotes a subdiagram which is connected to the rest of a Feynman diagram only through a single line, e.g. see Figure 3.2.

---

[2]That means purely performing an expansion in small quantities of the integrand, in contrast to asymptotic expansion.

[3]M_S is chosen to be the arithmetic mean of the corresponding masses.

In the SM, electroweak corrections to the relationships between the Yukawa couplings and the pole masses are free of tadpole contributions [70, 71]. However, tadpole contributions are indispensable to ensure gauge-independence in the electroweak sector for $\overline{\text{MS}}$ quark masses. Since a $\overline{\text{MS}}$ mass is not a physical quantity nor a Lagrangian parameter the requirement of gauge-invariance is not mandatory. An alternative definition, without the inclusion of tadpole contributions, was used in [72,73] and can also be established for the $\overline{\text{DR}}$ top-quark mass in supersymmetry. In Chapter 5, the running top-quark mass will be used in the self-energies of the CP-even Higgs boson in the MSSM which are calculated without the inclusion of tadpole diagrams, see Figure 1 of [32]. In the context of this thesis, tadpole diagrams are therefore omitted.
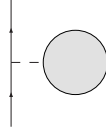
Figure 3.2.: Tadpole contribution to a fermionic propagator: One-particle-irreducible diagrams are represented as a gray circle.

3.6. Mixing in the $\tilde{\tau}$ Sector

The limit of equal masses can cause complications for mixing particles, if not done correctly. To give an example, the mixing in the $\tilde{\tau}$ sector in the computation of $\zeta_{h^0 \bar{b} b}$ is discussed.

To simplify calculations, one can suppose that the masses of $\tilde{\tau}_{1,2}$ are equal to an arbitrary mass M_{S}. It turns out, that this assumption has to be carefully applied in practice. For example in the calculation of $\zeta_{h^0 \bar{b} b}$, see equation (2.121), there are diagrams at two-loop order where tau sleptons occur. One example diagram is shown in Figure 3.3.

Figure 3.3.: Sample two-loop diagram needed for the calculation of $\zeta_{h^0 \bar{b} b}$ involving tau sleptons

In the case of $M_{\tilde{\tau}_1} \neq M_{\tilde{\tau}_2}$, there are terms

$$\sim s_{2\theta_\tau}(M_{\tilde{\tau}_1}^2 - M_{\tilde{\tau}_2}^2) \tag{3.3}$$

which can be written as

$$\sim 2X_\tau m_\tau. \tag{3.4}$$

Throughout the calculation a naive expansion in the top, bottom and τ masses is performed. However, m_τ of equation (3.4) can be absorbed into y_τ through the relation

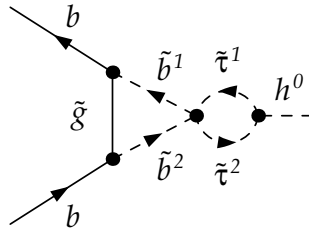$$y_\tau = \frac{m_\tau e}{\sqrt{2} M_W c_B s_w}, \tag{3.5}$$

while M_W is canceled by prefactors coming from Feynman rules. Finally one ends up with terms

$$\sim X_\tau y_\tau \tag{3.6}$$

which are non-zero. By putting $M_{\tilde{\tau}_1} = M_{\tilde{\tau}_2}$ in the beginning, those terms would not occur in $\zeta_{h^0 \bar{b} b}$. Therefore, the approximation $M_{\tilde{\tau}_1} = M_{\tilde{\tau}_2} = M_S$ can only be applied after the substitution

$$s_{2\theta_\tau}(M_{\tilde{\tau}_1}^2 - M_{\tilde{\tau}_2}^2) \to 2X_\tau m_\tau. \tag{3.7}$$

3.7. Diagrams

In the following, the counting of contributing diagrams is based on taking into account all one-particle-irreducible diagrams of $\mathcal{O}(\alpha_s^2, \alpha_s \alpha)$ with $\alpha = e^2/4\pi$ and discarding all diagrams which are proportional to $M_{W,Z}$ since they vanish in the gauge-less limit and discarding all diagrams which only contain light particles since they are scaleless and vanish in dimensional reduction. An example file for QGRAF is given in Appendix B. The number of diagrams of the corresponding vertices are listed in Table 3.1. Some sample diagrams are shown in Figures 3.4-3.8.

External Particles	# Diagrams
$\bar{t}t$	$3 + 9 + 134 + 256 = 402$
$\bar{b}b$	$3 + 9 + 134 + 264 = 410$
$h^0 h^0$	$0 + 18 + 0 + 218 = 236$
$h^0 \bar{t}t$	$5 + 27 + 403 + 1324 = 1759$
$h^0 \bar{b}b$	$5 + 15 + 403 + 1372 = 1795$

Table 3.1.: Number of contributing diagrams, displayed as:
one-loop SQCD + one-loop Yukawa + two-loop SQCD + two-loop mixed

3. Calculating the Decoupling Coefficients

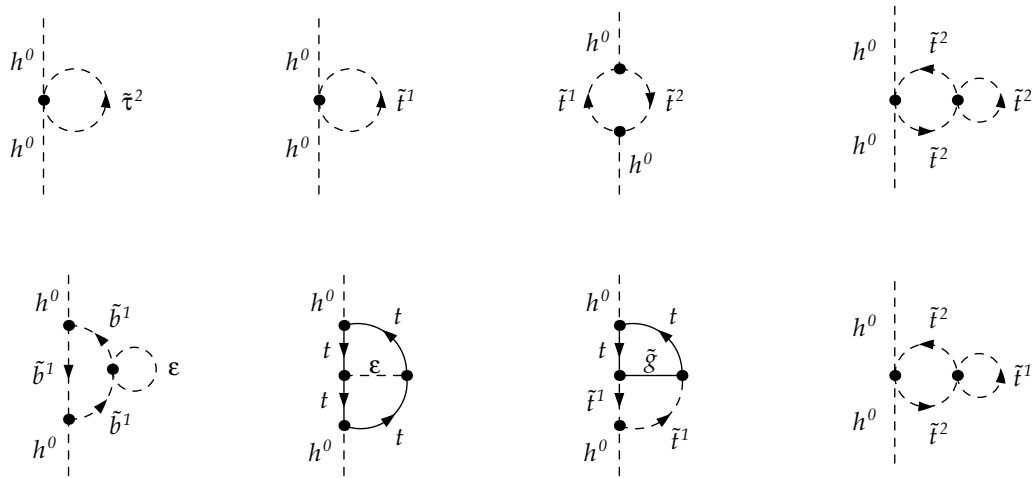Figure 3.4.: Sample diagrams needed for the calculation of ζ_{h^0}
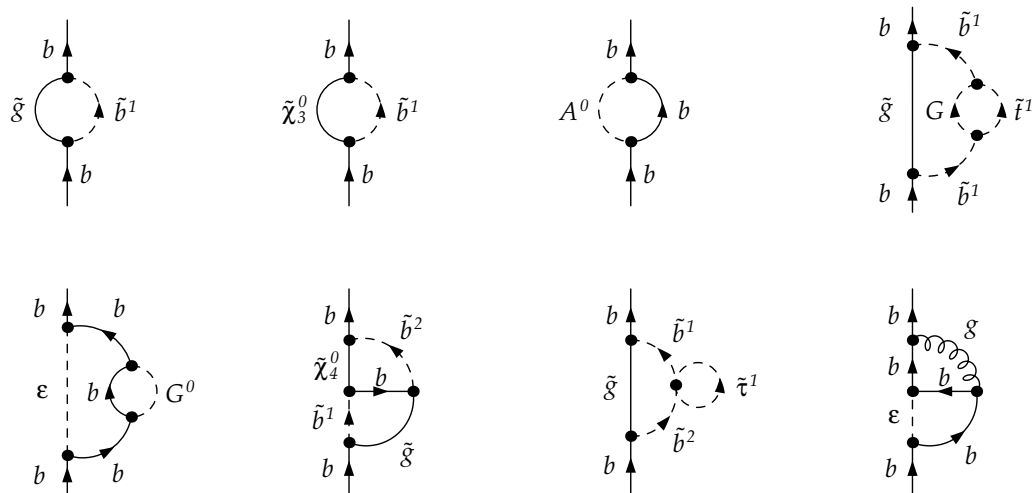

Figure 3.5.: Sample diagrams needed for the calculation of $\zeta_{2b}^{L/R}$

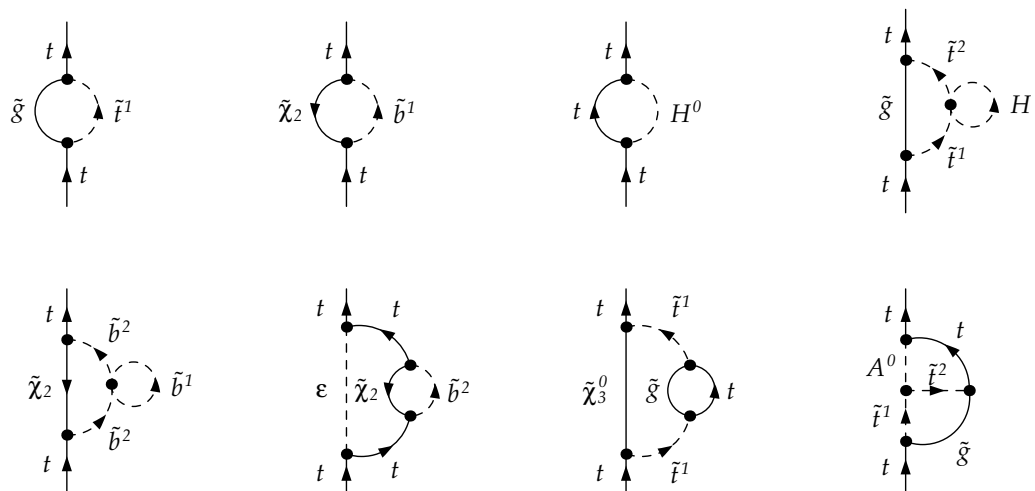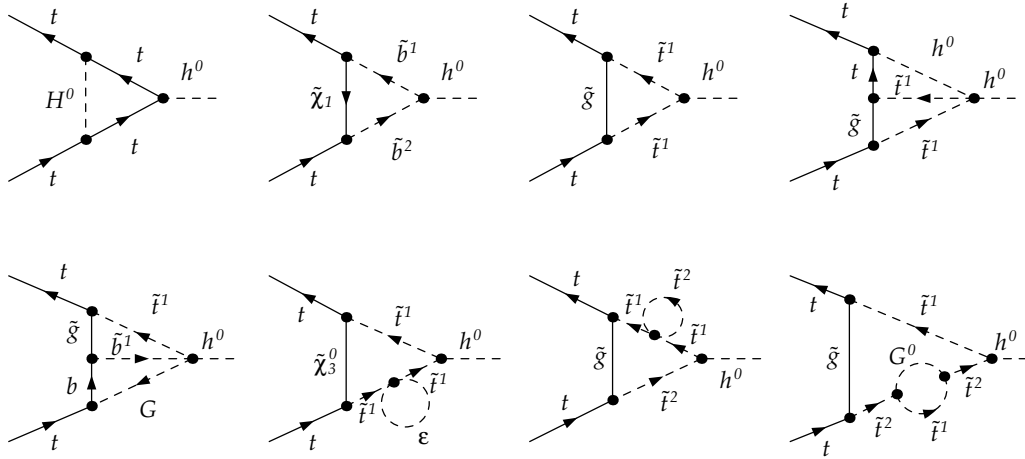Figure 3.6.: Sample diagrams needed for the calculation of $\zeta_{2t}^{L/R}$

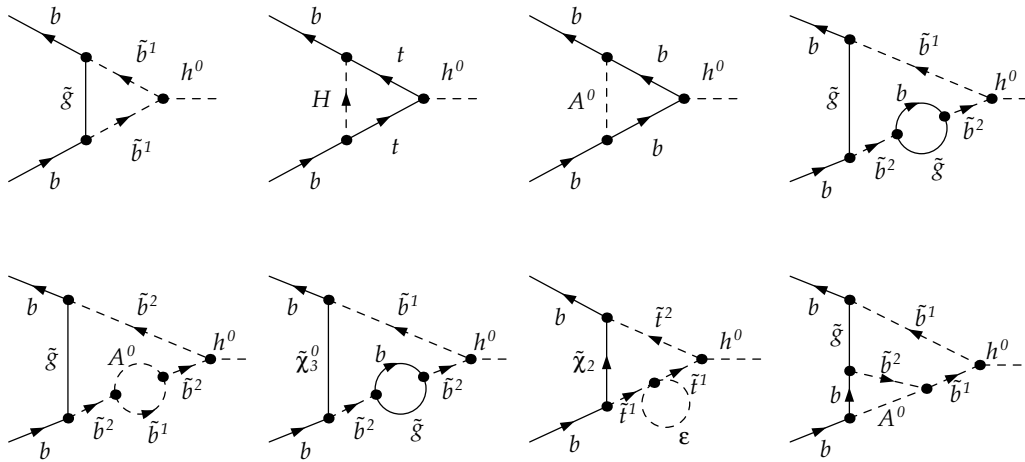Figure 3.7.: Sample diagrams needed for the calculation of $\zeta_{h^0 \bar{t} t}$

Figure 3.8.: Sample diagrams needed for the calculation of $\zeta_{h^0 \bar{b} b}$

3.8. Renormalization Scheme

Each parameter is renormalized in the on-shell scheme, except $m_{t,b,\tau}$ and the couplings for which the $\overline{\text{DR}}$ scheme is used. To simplify the renormalization procedure, the Yukawa couplings $y_{t,b,\tau}$ are expressed in terms of $m_{t,b,\tau}$ using

$$y_t = \frac{em_t}{\sqrt{2}M_W s_\beta s_W},\tag{3.8}$$

$$y_b = \frac{em_b}{\sqrt{2}M_W c_\beta s_W}\tag{3.9}$$

and

$$y_\tau = \frac{em_\tau}{\sqrt{2}M_W c_\beta s_W}.\tag{3.10}$$

Since only $\mathcal{O}(\alpha_s^2, \alpha_s\alpha)$ corrections are taken into account, only few counterterms are needed:

$$
\begin{aligned}
g_s &\to g_s + \delta g_s, & \xi &\to \xi + \delta\xi, & M_\epsilon &\to M_\epsilon + \delta M_\epsilon, \\
m_{t,b} &\to m_{t,b} + \delta m_{t,b}, & M_{\tilde{g}} &\to M_{\tilde{g}} + \delta M_{\tilde{g}}, & M_{\tilde{q}} &\to M_{\tilde{q}} + \delta M_{\tilde{q}}, \\
\theta_{t,b} &\to \theta_{t,b} + \delta\theta_{t,b}
\end{aligned}
\tag{3.11}
$$

Here, ξ denotes the gauge parameter of the gluon and ϵ the corresponding ϵ scalar.

The renormalization of the mixing angles $\theta_{t,b}$ is performed using the common prescription

$$\delta\theta_x = \frac{1}{2} \frac{\Sigma_{\tilde{x}_1 \tilde{x}_2}(M_{\tilde{t}_1}^2) + \Sigma_{\tilde{x}_1 \tilde{x}_2}(M_{\tilde{t}_2}^2)}{M_{\tilde{x}_1}^2 - M_{\tilde{x}_2}^2} \qquad (x = t, b),\tag{3.12}$$

introduced in [74]. For more details, see [30].

By imposing the relation

$$s_{2\theta_x} = \frac{2X_x m_x}{M_{\tilde{x}_1}^2 - M_{\tilde{x}_2}^2} \qquad (x = t, b, \tau)\tag{3.13}$$

to hold to all orders in perturbation theory, it is clear that $X_{t,b,\tau}$ is given in a mixed scheme.

The computation of the renormalization constants was done according to [30, 31].

For some counterterms, $m_{t,b}$ cannot be assumed to be zero in the beginning and a naive expansion up to $\mathcal{O}(m_{t,b})$ must be performed. The limit $m_{t,b} \to 0$ can only be applied in the final result since the counterterms will be inserted into the one-loop expression which can potentially contain factors of the inverse of the masses due to projectors, see

Appendix A. An expansion of the counterterms up to $\mathcal{O}(\epsilon^0)$ is sufficient since the pole part of the one-loop result is mass independent.

Care has to be taken regarding the on-shell renormalization of the squark masses since the soft-breaking parameters for the left-handed up- and down-type squarks are identical due to $SU(2)$-invariance. Therefore, the counterterms of the squark masses within a generation are not fully independent, as described in [75] and one gets

$$
\delta M^2_{\tilde{b}_1} = \frac{1}{c^2_{\theta_b}}\Big(c^2_{\theta_t}\delta M^2_{\tilde{t}_1} + s^2_{\theta_t}\delta M^2_{\tilde{t}_2} - s^2_{\theta_b}\delta M^2_{\tilde{b}_2} - s_{2\theta_t}(M^2_{\tilde{t}_1} - M^2_{\tilde{t}_2})\delta\theta_t
$$
$$
+ s_{2\theta_b}(M^2_{\tilde{b}_1} - M^2_{\tilde{b}_2})\delta\theta_b - 2m_t\delta m_t + 2m_b\delta m_b \Big) \tag{3.14}
$$

and for the remaining two generations

$$
\delta M^2_{\tilde{d}_1} = \delta M^2_{\tilde{u}_1} \tag{3.15}
$$

and

$$
\delta M^2_{\tilde{s}_1} = \delta M^2_{\tilde{c}_1} \tag{3.16}
$$

since the quark masses and mixing angles are assumed to be zero.

3.9. One-Loop Decoupling Coefficients

The renormalization of bare decoupling coefficients $\zeta_x^{(0)}$ is done with the general relation

$$
\zeta_x = \frac{Z_x^{\overline{\text{DR}}}}{Z_x'^{\overline{\text{DR}}}}\zeta_x^{(0)}. \tag{3.17}
$$

The parameters appearing in $Z_x'^{\overline{\text{DR}}}$ are parameters of the effective theory and have to be decoupled in order to express the final result in terms of parameters of the full theory. Again, the Yukawa couplings $y_{t,b}$ are expressed in terms of $m_{t,b}$. Therefore, the following decoupling relations have to be applied in the one-loop result of $Z'^{\overline{\text{DR}}}$:

$$
m'_{t,b} = \zeta_{m_{t,b}}m_{t,b}, \qquad\qquad \xi' = \zeta_\xi\xi, \qquad\qquad g'_s = \zeta_{g_s}g_s \tag{3.18}
$$

The needed renormalized one-loop decoupling coefficients up to $\mathcal{O}(\epsilon)$ are given in Appendix E.

3.10. Results

In the following, the results of the decoupling coefficients are presented. Since the complete expressions up to $\mathcal{O}(\alpha_s^2, \alpha_s\alpha_{t,b,\tau}, \alpha_s, \alpha_{t,b,\tau,1,2})$ are very lengthy, they are only given as an attachment in an electronic format. To get a first impression, the results are shown in certain limits.

3. Calculating the Decoupling Coefficients

3.10.1. ζ_{g_s}

The two-loop SQCD result for ζ_{g_s} is very compact and reads

$$
\begin{aligned}
\zeta_{g_s}^{(\text{SQCD})} = {}& -\frac{a_s}{8}\frac{1}{3}\left[C_A\left(1+2L_{M_{\tilde{g}}}\right) + T\sum_{\tilde{q}}\sum_{i=1,2} L_{M_{\tilde{q}_i}} \right] \\
& -\frac{1}{8}\left(\frac{a_s}{4}\right)^2\frac{1}{9}\left[C_A\left(1+2L_{M_{\tilde{g}}}\right) + T\sum_{\tilde{q}}\sum_{i=1,2} L_{M_{\tilde{q}_i}} \right]^2 \\
& +\frac{1}{2}\left(\frac{a_s}{4}\right)^2\Bigg\{ C_A^2\left(-\frac{125}{18}-\frac{44}{9}L_{M_{\tilde{g}}}+\frac{4}{9}L_{M_{\tilde{g}}}^2\right) \\
& + C_A T\frac{2}{9}\Bigg[30 + \sum_{\tilde{q}}\sum_{i=1,2}\Bigg(6\frac{M_{\tilde{q}_i}^2}{M_{\tilde{g}}^2} + 6\frac{M_{\tilde{g}}^2-M_{\tilde{q}_i}^2}{M_{\tilde{g}}^2}B_{0,\text{fin}}(M_{\tilde{g}}^2,M_{\tilde{q}_i},0) \\
& + 2L_{M_{\tilde{q}_i}}L_{M_{\tilde{g}}} - \frac{2M_{\tilde{g}}^4-5M_{\tilde{g}}^2 M_{\tilde{q}_i}^2+6M_{\tilde{q}_i}^4}{M_{\tilde{g}}^2(M_{\tilde{g}}^2-M_{\tilde{q}_i}^2)}L_{M_{\tilde{q}_i}} + 3\frac{M_{\tilde{g}}^2}{M_{\tilde{g}}^2-M_{\tilde{q}_i}^2}L_{M_{\tilde{g}}} \Bigg) \Bigg] \\
& + T^2\left(\frac{1}{3}\sum_{\tilde{q}}\sum_{i=1,2}L_{M_{\tilde{q}_i}}\right)^2 + C_F T\frac{2}{3}\Bigg[+ \sum_{\tilde{q}}\sum_{i=1,2}\Bigg(1+\frac{M_{\tilde{g}}^2}{M_{\tilde{q}_i}^2} \\
& -\frac{M_{\tilde{g}}^2-M_{\tilde{q}_i}^2}{M_{\tilde{q}_i}^2}B_{0,\text{fin}}(M_{\tilde{q}_i}^2,M_{\tilde{g}},0) - 2\frac{3M_{\tilde{g}}^2-2M_{\tilde{q}_i}^2}{M_{\tilde{g}}^2-M_{\tilde{q}_i}^2}L_{M_{\tilde{q}_i}} \\
& +\left(4+\frac{M_{\tilde{g}}^2}{M_{\tilde{q}_i}^2}+\frac{2M_{\tilde{q}_i}^2}{M_{\tilde{g}}^2-M_{\tilde{q}_i}^2}\right)L_{M_{\tilde{g}}}\Bigg) \\
& +\sum_{\text{gen}}\Bigg(-3\frac{M_{\tilde{q}_{u1}}^2}{M_{\tilde{q}_{d1}}^2} - \frac{M_{\tilde{g}}^2-M_{\tilde{q}_{u1}}^2}{M_{\tilde{q}_{d1}}^2}B_{0,\text{fin}}(M_{\tilde{q}_{u1}}^2,M_{\tilde{g}},0) \\
& +\frac{M_{\tilde{g}}^2-M_{\tilde{q}_{d1}}^2}{M_{\tilde{q}_{d1}}^2}B_{0,\text{fin}}(M_{\tilde{q}_{d1}}^2,M_{\tilde{g}},0) + L_{M_{\tilde{q}_{d1}}} - \frac{M_{\tilde{q}_{u1}}^2}{M_{\tilde{q}_{d1}}^2}L_{M_{\tilde{q}_{u1}}} \\
& +\frac{1}{2}\frac{M_{\tilde{q}_{d1}}^2}{M_{\tilde{g}}^2-M_{\tilde{q}_i}^2}L_{M_{\tilde{g}}} \Bigg) \Bigg] \Bigg\}.
\end{aligned}
\tag{3.19}
$$

The abbreviations $L_{M_x}\equiv\ln(\frac{\mu^2}{M_x^2})$ and $a_x\equiv\alpha_x/\pi$ are used where α_x are the coupling constants of the full theory. The sum $\sum_{\tilde{q}}$ runs over all quark flavors and $\sum_{\text{gen}}$ over all generations. $B_{0,\text{fin}}$ denotes the finite part of the B_0 function [76]. Equation (3.19) is in full agreement with the results in the literature [48].

3.10.2. ζ_{m_t} and ζ_{m_b}

Even at one-loop order, the full electroweak results for ζ_{m_t} and ζ_{m_b} are too lengthy to be displayed. To give an impression on the results, the gauge-less limit is applied. Also,

all masses appearing in the Yukawa sector are chosen to have the same value M_S except $M_{\tilde{t}_2}$ and $M_{\tilde{b}_2}$. The result reads

$$
\begin{aligned}
\zeta_{m_t} =\; & 1 + 4a_s C_F \Bigg\{ \frac{M_{\tilde{t}_1}^2}{32(M_{\tilde{t}_1}^2 - M_{\tilde{g}}^2)} + \frac{M_{\tilde{g}}^2}{32(M_{\tilde{t}_2}^2 - M_{\tilde{g}}^2)} \\
& + L_{M_{\tilde{g}}} \Bigg(- \frac{M_{\tilde{g}}^4 (2M_{\tilde{g}}^4 - 2M_{\tilde{g}}^2 M_{\tilde{t}_1}^2 + M_{\tilde{t}_1}^4 - 2M_{\tilde{g}}^2 M_{\tilde{t}_2}^2 + M_{\tilde{t}_2}^4)}{32(M_{\tilde{t}_1}^2 - M_{\tilde{g}}^2)^2 (M_{\tilde{g}}^2 - M_{\tilde{t}_2}^2)^2} \\
& \qquad + \frac{M_{\tilde{g}}^3 X_t}{8(M_{\tilde{g}}^2 - M_{\tilde{t}_1}^2)(M_{\tilde{g}}^2 - M_{\tilde{t}_2}^2)} \Bigg) \\
& + \Bigg[L_{M_{\tilde{t}_1}} \Bigg(- \frac{M_{\tilde{t}_1}^2 (-2M_{\tilde{g}}^2 + M_{\tilde{t}_1}^2)}{32(M_{\tilde{t}_1}^2 - M_{\tilde{g}}^2)^2} + \frac{M_{\tilde{g}} M_{\tilde{t}_1}^2 X_t}{8(M_{\tilde{t}_1}^2 - M_{\tilde{g}}^2)(M_{\tilde{t}_1}^2 - M_{\tilde{t}_2}^2)} \Bigg) + \tilde{t}_1 \leftrightarrow \tilde{t}_2 \Bigg] \Bigg\} \\
& + a_t \Bigg\{ \frac{L_{M_S}}{16} \Bigg(-2 - 3c_\beta^2 - \frac{M_S^4}{(M_S^2 - M_{\tilde{t}_2}^2)^2} \Bigg) \\
& \qquad + \frac{L_{M_{\tilde{t}_2}}}{16} \Bigg(-1 + \frac{M_S^4}{(M_S^2 - M_{\tilde{t}_2}^2)^2} \Bigg) \\
& \qquad + \frac{1}{32} \Bigg(-1 - 3c_\beta^2 - \frac{2M_S^2}{M_S^2 - M_{\tilde{t}_2}^2} \Bigg) \Bigg\} \\
& + \frac{a_b}{32(M_S^2 - M_{\tilde{b}_2}^2)^2 s_\beta} \Bigg\{ - \Big(4(1 + L_{M_S}) + c_\beta^2(7 + 6L_{M_S}) \Big) M_S^4 s_\beta \\
& \qquad + 2 \Big(3 + 2L_{M_S} + c_\beta^2(7 + 6L_{M_S}) + 2L_{M_{\tilde{b}_2}} \Big) M_S^2 M_{\tilde{b}_2}^2 s_\beta \\
& \qquad - \Big(c_\beta^2(7 + 6L_{M_S}) + 2(1 + L_{M_S} + L_{M_{\tilde{b}_2}}) \Big) M_{\tilde{b}_2}^4 s_\beta \\
& \qquad + 8c_\beta M_S^3 X_b + 8c_\beta(-1 + L_{M_S} - L_{M_{\tilde{b}_2}}) M_S M_{\tilde{b}_2}^2 X_b \Bigg\}.
\end{aligned}
\tag{3.20}
$$

The indication $\tilde{t}_1 \leftrightarrow \tilde{t}_2$ means that the expression inside the bracket is repeated whereas $\tilde{t}_1$ is interchanged with $\tilde{t}_2$.

The expression for ζ_{m_b} can be derived from ζ_{m_t} by interchanging

$$
\begin{aligned}
a_t &\leftrightarrow a_b, \\
X_t &\leftrightarrow X_b, \\
M_{\tilde{t}_2} &\leftrightarrow M_{\tilde{b}_2}
\end{aligned}
\tag{3.21}
$$

and for terms which are proportional to a_t and a_b one has to additionally interchange

$$
c_\beta \leftrightarrow s_\beta.
\tag{3.22}
$$

This was verified analytically at one- and two-loop order. The decoupling coefficient ζ_{m_b} was compared to the literature [34] up to $\mathcal{O}(\alpha_s^2)$ and full agreement was obtained. The terms of $\mathcal{O}(\alpha_s, \alpha_t)$ in ζ_{m_t} are in full agreement with [77].

To give an impression for the two-loop results of the SQCD part, the following special mass hierarchies are chosen.

3. Calculating the Decoupling Coefficients

- Scenario A: The squark masses are chosen to be M_S and much heavier than the gluino mass $M_{\tilde{g}}$ (known as split supersymmetry [78–80]).

- Scenario B: All supersymmetric particles have the same mass M_S.

In Scenario A, the result is

$$
\zeta_{m_t}^{M_S \gg M_{\tilde{g}}, \text{SQCD}} = \frac{a_s}{4} C_F \left\{ \frac{1}{2} - L_{M_S} + \frac{1}{M_S^2}(M_{\tilde{g}}^2 - 2M_{\tilde{g}} X_t) \right.
$$

$$
\left. + \frac{1}{M_S^4}\left[M_{\tilde{g}}^4(1 + L_{M_S} - L_{M_{\tilde{g}}}) + 2X_t M_{\tilde{g}}^3(-1 + L_{M_{\tilde{g}}} - L_{M_S}) \right] \right\}
$$

$$
+ \left(\frac{a_s}{4}\right)^2 C_F \left\{ -\frac{C_A}{72 M_S^4}\left[M_S^4\left(-481 + 432 L_{M_S} + 108 L_{M_S}^2 \right. \right. \right.
$$

$$
+ 120 L_{M_{\tilde{g}}} - 72 L_{M_{\tilde{g}}}^2 + 576\zeta(2)\big) - 36 M_{\tilde{g}}^3\big(M_{\tilde{g}}(38 + 4L_{M_S}
$$

$$
+ 13 L_{M_S}^2 + 2L_{M_{\tilde{g}}} - 20 L_{M_S} L_{M_{\tilde{g}}} + 7L_{M_{\tilde{g}}}^2 - 20\zeta(2))
$$

$$
- 4X_t(5 + 19L_{M_S} + 3L_{M_S}^2 - 16 L_{M_{\tilde{g}}} - 3L_{M_S} L_{M_{\tilde{g}}} + 2\zeta(2)))
$$

$$
+ 72 M_S^2 M_{\tilde{g}}\big(2X_t(7 + 6L_{M_S} - 3L_{M_{\tilde{g}}} + 2\zeta(2))
$$

$$
\left. + M_{\tilde{g}}(-15 + 3L_{M_S} - 6L_{M_{\tilde{g}}} + 10\zeta(2)))\right]
$$

$$
+ \frac{C_F}{8M_S^4}\left[-8M_S^2 M_{\tilde{g}}\big(M_{\tilde{g}}(21 + L_{M_S} - 20\zeta(2)) \right.
$$

$$
+ X_t(5 - 6L_{M_S} - 8\zeta(2))\big) - 2M_{\tilde{g}}^3\big(M_{\tilde{g}}(175 + 60L_{M_S}^2
$$

$$
+ 90 L_{M_{\tilde{g}}} + 56 L_{M_{\tilde{g}}}^2 - 2L_{M_S}(43 + 58L_{M_{\tilde{g}}}) - 104\zeta(2))
$$

$$
+ 4X_t(15 - 6L_{M_S}^2 + 11L_{M_{\tilde{g}}} + L_{M_S}(-17 + 6L_{M_{\tilde{g}}}) - 8\zeta(2)))
$$

$$
\left. + M_S^4\big(-189 - 48L_{M_S} + 4L_{M_S}^2 + 120\zeta(2)\big)\right]
$$

$$
+ \frac{T}{3M_S^4}\left[-36 M_S^2 M_{\tilde{g}}\big((-1 + L_{M_S})M_{\tilde{g}} + X_t - 2L_{M_S} X_t\big) \right.
$$

$$
+ 3M_{\tilde{g}}^3\big((-13 - 12L_{M_S}^2 + 6L_{M_{\tilde{g}}} + 6L_{M_S}(-3 + 2L_{M_{\tilde{g}}}))M_{\tilde{g}}
$$

$$
+ 4(7 + 6L_{M_S}^2 + L_{M_S}(9 - 6L_{M_{\tilde{g}}}) - 3L_{M_{\tilde{g}}})X_t\big)
$$

$$
\left.\left. + M_S^4\big(127 - 30L_{M_S} + 36L_{M_S}^2 - 36\zeta(2)\big)\right]\right\} \tag{3.23}
$$

and for Scenario B one gets

$$
\zeta_{m_t}^{M_S, \text{SQCD}} = -\frac{a_s}{4} C_F \left(-1 + \frac{X_t}{M_S} + L_{M_S}\right)
$$

$$
+ \left(\frac{a_s}{4}\right)^2 \left\{ C_F^2\left[-\frac{71}{8} - \frac{13}{2} L_{M_S} + \frac{1}{2} L_{M_S}^2 + \frac{X_t}{M_S}(-5 + 3L_{M_S}) \right] \right.
$$

$$
+ C_F T\left[\frac{109}{3} - 16 L_{M_S} + 12 L_{M_S}^2 + 12 \frac{X_t}{M_S}(-1 + L_{M_S}) \right]
$$

$$
\left. + C_F C_A\left[-\frac{23}{72} - \frac{37}{6} L_{M_S} - \frac{1}{2} L_{M_S}^2 - \frac{X_t}{M_S}(1 + 3L_{M_S}) \right] \right\} \tag{3.24}
$$

where $\zeta(x)$ is the Riemann zeta function. For both scenarios, the asymptotic expansion method was used which is available in the code `q2e/exp` [55, 56]. The results were verified analytically and numerically against the exact calculation. For Scenario A, the verification for the first three terms of the expansion in the mass ratio $M_{\tilde{g}}^2/M_S^2$ was performed. In addition, the direct numerical comparison of the exact and asymptotically expanded results gives good agreement. For Scenario B, agreement is obtained by neglecting corrections proportional to the mass differences between supersymmetric particles.

3.10.3. ζ_{y_t} and ζ_{y_b}

For ζ_{y_t}, applying the same assumptions as for ζ_{m_t}, one gets at one-loop order

$$
\begin{aligned}
\zeta_{y_t} =\,& 1 + \zeta_{m_t}^{\text{SQCD},(1)} \\
& + \frac{a_t}{32(M_S^2 - M_{\tilde{t}_2}^2)^3}\Big\{ (M_S^2 - M_{\tilde{t}_2}^2)\Big(-6(1 + 2L_{M_S})M_S^4 \\
& \quad + 2(5 + 10L_{M_S} + 2L_{M_{\tilde{t}_2}})M_S^2 M_{\tilde{t}_2}^2 \\
& \quad - 2(2 + 5L_{M_S} + L_{M_{\tilde{t}_2}})M_{\tilde{t}_2}^4 + 3(1 + 2L_{M_S})(M_S^2 - M_{\tilde{t}_2}^2)^2 s_\beta^2 \Big) \\
& \quad + 6\Big(-M_S^4 + 2(-L_{M_S} + L_{M_{\tilde{t}_2}})M_S^2 M_{\tilde{t}_2}^2 + M_{\tilde{t}_2}^4 \Big)s_\beta^2 X_t^2 \Big\} \\
& + \frac{a_b}{128(M_S^2 - M_{\tilde{b}_2}^2)^3}\Big\{ 24c_\beta^2\Big(-M_S^4 + 2(-L_{M_S} + L_{M_{\tilde{b}_2}})M_S^2 M_{\tilde{b}_2}^2 + M_{\tilde{b}_2}^4 \Big)X_b^2 \\
& \quad + (M_S^2 - M_{\tilde{b}_2}^2)\Big(-2\big((15 + 14L_{M_S})M_S^4 - 2(13 + 10L_{M_S} + 4L_{M_{\tilde{b}_2}})M_S^2 M_{\tilde{b}_2}^2 \\
& \quad + (11 + 10L_{M_S} + 4L_{M_{\tilde{b}_2}})M_{\tilde{b}_2}^4 + c_{2\beta}(7 + 6L_{M_S})(M_S^2 - M_{\tilde{b}_2}^2)^2 \big) \\
& \quad + \frac{32c_\beta M_S(M_S^2 + (-1 + \ln M_S - \ln M_{\tilde{b}_2})M_{\tilde{b}_2}^2)X_b}{s_\beta} \Big) \Big\} \\
& - \frac{a_\tau}{48M_S^2}c_\beta^2 X_\tau^2.
\end{aligned}
\tag{3.25}
$$

The abbreviation $\zeta_{m_t}^{\text{SQCD},(1)}$ denotes the one-loop SQCD part of ζ_{m_t}. It is not accidental, that the SQCD parts of ζ_{y_t} and ζ_{m_t} coincide, since the decoupling coefficients of the parameters e, M_W, s_β and s_W in equation (3.8) only get electroweak contributions.

In addition, ζ_{y_t} was calculated in the mass hierarchy[4] $M_S \gg M_{\tilde{t}_2} \gg M_{\tilde{b}_2}$ by making use of the asymptotic expansion method using the code `q2e/exp`. An analytical comparison against the expanded exact result was performed and agreement for the first few terms in the mass ratios $M_{\tilde{t}_2}/M_S$, $M_{\tilde{b}_2}/M_S$ and $M_{\tilde{b}_2}/M_{\tilde{t}_2}$ was obtained.

ζ_{y_b} can be retrieved from ζ_{y_t} by applying the substitutions (3.21) and (3.22). This was verified analytically up to two-loop order.

Up to $\mathcal{O}(\alpha_s, \alpha_t)$, ζ_{y_t} was compared to the literature [77] and full agreement was obtained.

---

[4]This mass hierarchy is only used for internal checks.

4. Running and Decoupling of α_s, α_t and m_t

In this chapter, a method is presented to compute the strong coupling, top Yukawa coupling and running top-quark mass in the MSSM.

In a straightforward way, one can calculate the conversion relation between the running and pole mass for the top quark in the MSSM. At two-loop order, the fermion self-energies and pole masses for a general renormalizable theory with massless gauge bosons are known [81] and can be evaluated numerically using the program code `TSIL` [82]. However, if supersymmetric particles are assumed to be at the TeV scale, the radiative corrections of the top-quark pole mass are large. This is caused by the occurrence of logarithms of the form $\ln(M_t/M_{\mathrm{SUSY}})$ in the self-energy of the top quark, with M_{SUSY} being the typical mass scale of supersymmetric particles. For $M_t \ll M_{\mathrm{SUSY}}$, these logarithms are large and spoil perturbation theory resulting in radiative corrections that can be one magnitude larger than the experimental uncertainties. Unfortunately, the needed on-shell self-energy diagrams at three-loop order with several mass scales are currently not feasible[1].

In the following, an alternative method is presented where large logarithms are automatically resummed by the use of Renormalization Group Equations (RGEs). It can be applied as long as $M_t \ll M_{\mathrm{SUSY}}$. In the following, details on this procedure as well as a numerical analysis is presented.

4.1. Running-And-Decoupling in SQCD

In this section, the two-loop SQCD threshold corrections for the prediction of the running top-quark mass at some high scale is discussed. The results are published in [83]. Since RGEs are used to evolve the running top-quark mass from one scale to another and decoupling coefficients to decouple heavy particles, this approach will be named running-and-decoupling. The running-and-decoupling approach can be written as

$$M_t \overset{(i)}{\to} m'_t(M_t) \overset{(ii)}{\to} m'_t(\mu_{\mathrm{dec}}) \overset{(iii)}{\to} m_t(\mu_{\mathrm{dec}}) \overset{(iv)}{\to} m_t(\mu) \tag{4.1}$$

with the following steps:

- (i) The transition between the top-quark pole mass M_t and the running mass m'_t in the SM is done using the three-loop relation from [84–87], which is also available at four-loop order [88].

---

[1]without using asymptotic expansion techniques

- (*ii*) The evolution of $m_t'(M_t)$ to an arbitrary scale μ_{dec} is done using the RGE at three-loop order from [89–93], which is also calculated to four- [94] and even five-loop order [95]. μ_{dec} is the scale at which the decoupling is performed. To ensure smallness of the appearing logarithms μ_{dec} should be chosen around the SUSY scale M_{SUSY}. In this work, the arithmetic average over the squark masses and the gluino mass is chosen:

$$M_{\text{SUSY}} = \frac{1}{13}\left(M_{\tilde{g}} + \sum_{\tilde{q}} \sum_{i=1,2} M_{\tilde{q}_i}\right) \tag{4.2}$$

- (*iii*) For a consistent analysis, n-loop RGEs are combined with $(n-1)$-loop threshold corrections, see e.g. [96]. Therefore, the threshold corrections are evaluated at two-loop order. Since the ϵ scalars are decoupled with the rest of the SUSY particles, there is also a change in the renormalization scheme from $\overline{\text{MS}}$ to $\overline{\text{DR}}$.

- (*iv*) The evolution of $m_t(\mu_{\text{dec}})$ to some renormalization scale μ is done using the RGEs at three-loop order from [97] and [54].

4.2. Analyzed Scenarios

For the numerical evaluation, the SM values of M_Z and the strong coupling in five-flavor QCD $\alpha_s(M_Z)$ are taken from [98] and the top-quark pole mass from [99]:

$$M_Z = 91.1876 \pm 0.0021 \text{ GeV}$$
$$\alpha_s(M_Z) = 0.1184 \pm 0.0007$$
$$M_t = 173.34 \pm 0.27 \pm 0.71 \text{ GeV} \tag{4.3}$$

Regarding the parameters of the MSSM, two scenarios where chosen, which are motivated in [100]. In the following, they are denoted by the Heavy Higgs and the Heavy Sfermions scenario. For simplicity, the Supersymmetry Les Houches Accord (SLHA) [101, 102] is followed which specifies generic file structures for supersymmetric model specification and input parameters. The explicit values are taken from the spectrum generator SOFTSUSY v. 3.6.1 [103] for which the following input parameters are chosen:

- Heavy Sfermions: All $\overline{\text{DR}}$ breaking parameters are defined at the input scale Q_{in}. The defining parameters are listed in Table 4.1. This scenario results in very weakly mixing top squarks which are about 1 TeV lighter than the other sfermions. One can increase the squark mass spectrum by increasing the value of $\tilde{m}_t$. For $\tilde{m}_t \approx 3$ TeV the mass of the lightest Higgs boson is compatible with the currently measured value.

- Heavy Higgs: The defining parameters of this scenario are listed in Table 4.2. Here, light Higgs masses are possible for sub-TeV values of $\tilde{m}_t$ which is due to stop mixing. Also, one can get light stop masses of order 300 GeV for $\tilde{m}_t$ values of the same size.

Block: EXTPAR	Value	Comment
0	$\tilde{m}_t$	Input scale Q_{in}
46	$\tilde{m}_t$	$M_{\tilde{t}_R}$
43	$\tilde{m}_t$	$M_{\tilde{Q}_L}$ (third generation)
31-42,44,45,47-49	$\tilde{m}_t + 1$ TeV	Sfermion mass breaking parameters
11	20 GeV	A_t
12	4 TeV	A_b
13	4 TeV	A_τ
1	1.5 TeV	M_1
2	1.5 TeV	M_2
3	1.5 TeV	M_3
23	200 GeV	μ_{SUSY}
26	1 TeV	M_A
Block: MINPAR	Value	Comment
3	20	t_β

Table 4.1.: Input parameters of the Heavy Sfermions scenario, $\tilde{m}_t$ is held as a free parameter

So far, in the Heavy Higgs and Heavy Sfermions scenario t_β is chosen to be 20. To give an impression on how the running-and-decoupling procedure works for scenarios with higher values of t_β, the following cMSSM parameter point is chosen, taken from [104]:

$$
\begin{aligned}
t_\beta &= 50, \\
m_0 &= 7240 \text{ GeV}, \\
M_{1/2} &= 800 \text{ GeV}, \\
A_0 &= -6000 \text{ GeV}, \\
\mu &> 0
\end{aligned}
\tag{4.4}
$$

In the following, it will be called the cMSSM scenario. It has attractive dark matter properties and the mass of the lightest CP even Higgs boson agrees with the experimental central value, see Chapter 5. Also the gluino and squark masses are heavy enough not to be ruled out by current LHC data. Since t_β is quite large, the bottom and tau Yukawa corrections have a higher impact on the running-and-decoupling procedure which enables more extensive studies, as will be discussed in Section 4.5.

The explicit mass spectra of the chosen scenarios are given in Appendix C.

Block: EXTPAR	Value	Comment
0	1014.91 GeV	Input scale Q_{in}
46	$\tilde{m}_t$	$M_{\tilde{t}_R}$
31-45,47-49	1000 GeV	Sfermion mass breaking parameters
11	1500 GeV	A_t
12	2469.45 GeV	A_b
13	2469.45 GeV	A_τ
1	$5s_W^2/(3c_W^2)M_2$	M_1
2	200 GeV	M_2
3	800 GeV	M_3
23	200 GeV	μ_{SUSY}
26	1 TeV	M_A
Block: MINPAR	Value	Comment
3	20	t_β

Table 4.2.: Input parameters of the Heavy Higgs scenario, $\tilde{m}_t$ is chosen as a free parameter

4.3. Numerical Results in SQCD

The running-and-decoupling approach is now discussed and numerical results for the Heavy Higgs, Heavy Sfermions and cMSSM scenario are presented. In the following, the running-and-decoupling method is denoted by nl with n being the loop order of the RGEs and $(n-1)$ being the loop order of the threshold corrections. The decoupling-scale dependence of the running top-quark mass is unphysical and therefore a measure of the theoretical uncertainty due to the truncation of the perturbative expansion. Hence, it is expected that the decoupling-scale dependence will decline when taking into account radiative corrections at higher orders in the analysis as will be discussed in the following.

In Figure 4.1, the dependence of the running top-quark mass on the decoupling scale in the Heavy Higgs, Heavy Sfermions and cMSSM scenario is shown. The arithmetic average over all squark masses and the gluino mass is denoted by M_{SUSY} as defined in equation (4.2). The vertical lines corresponds to $\mu_{\text{dec}} = M_t$. The decoupling scale is varied in the range from M_Z to $10M_{\text{SUSY}}$ while the renormalization scale is fixed to $\mu_{\text{ren}} = \sqrt{M_{\tilde{t}_1} M_{\tilde{t}_2}}$. At one-loop level, one observes a huge decoupling-scale dependence in all investigated scenarios and a precise determination of the running top-quark mass is not possible. By including more loop corrections to the analysis, the dependence declines until at three-loop order the variation of the running top-quark mass in all three scenarios is below 100 MeV for $\mu_{\text{dec}} \gtrsim 0.5M_{\text{SUSY}}$. This precision is sufficient since the current experimental error on the top-quark pole mass is about 1 GeV and is expected to be of $\mathcal{O}(100\,\text{MeV})$ at future experiments at the ILC [105]. For small decoupling scales $\mu_{\text{dec}} \lesssim 0.1M_{\text{SUSY}}$, the convergence regarding the inclusion of higher order corrections is worse than for higher values of μ_{dec} since the logarithms $\log(M_{\text{SUSY}}/\mu_{\text{dec}})$ appearing in the decoupling coefficients are large and spoil the perturbative expansion. In the Heavy Higgs scenario, setting $\tilde{m}_t = 350$ GeV will result in a light stop mass at an intermediate scale of about the same size while the rest of the SUSY spectrum has masses of about 1 TeV. This could in principle lead to complications since in this analysis all SUSY particles are decoupled simultaneously at a certain decoupling scale, where not all logarithms

(a) Heavy Higgs, $\tilde{m}_t = 350$ GeV

(b) Heavy Sfermions, $\tilde{m}_t = 3$ TeV

(c) cMSSM

Figure 4.1.: Dependence of the running top-quark mass on the decoupling scale in the Heavy Higgs, Heavy Sfermions and cMSSM scenario. The renormalization scale is kept fixed. The result of the one-, two- and three-loop running-and-decoupling analysis in SQCD is shown as dotted, dashed and solid curves, respectively.

are small if the particle spectrum contains both heavy and light masses. However, Figure 4.1 (a) demonstrates that at least the decoupling-scale dependence is small for this dangerous scenario.

In order to do a comparison with the result of the running-and-decoupling approach, an alternative method for the determination of the running top-quark mass is used, namely to calculate the ratio between the running and the pole top-quark mass through a direct numerical evaluation of one- and two-loop on-shell integrals within SQCD using the computer program TSIL. This method is denoted by TSIL *nl* where *n* is the loop order of the on-shell integrals. Three-loop on-shell integrals are not implemented in TSIL.

(a) Heavy Higgs, $\tilde{m}_t = 350$ GeV
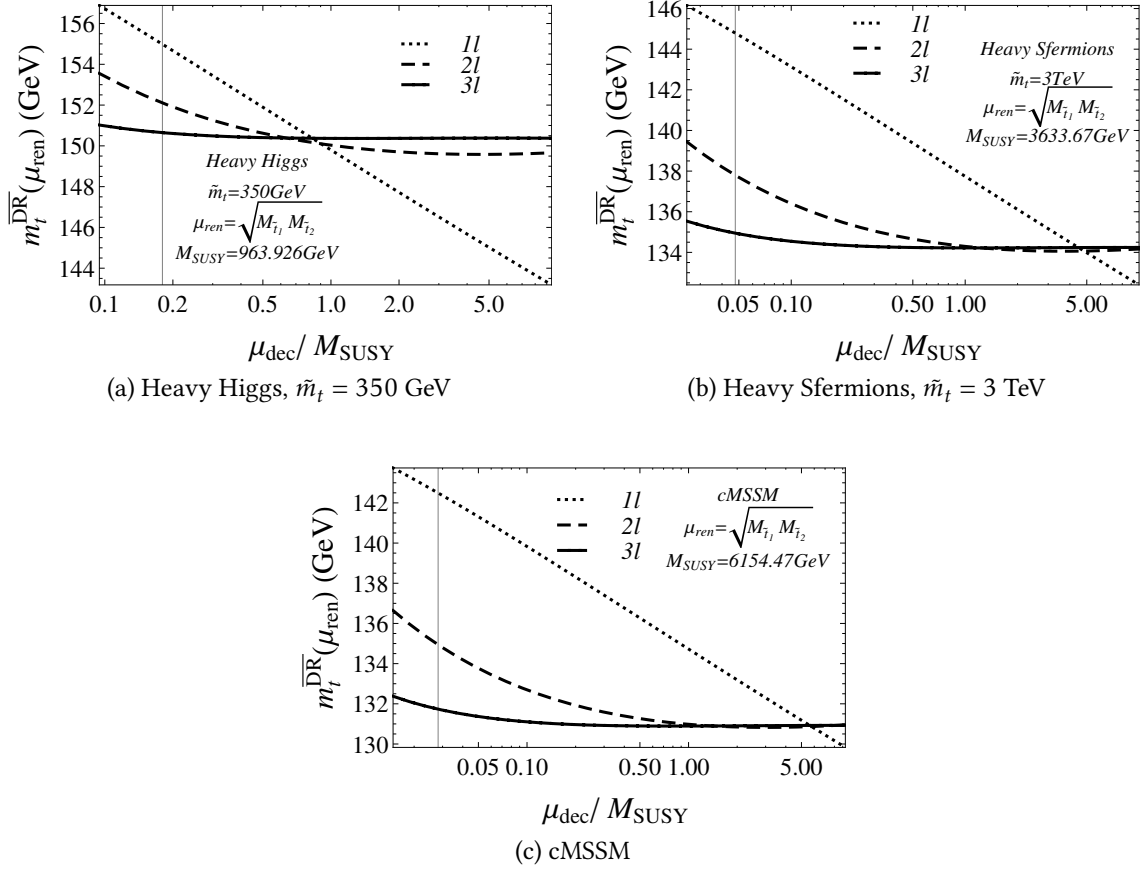
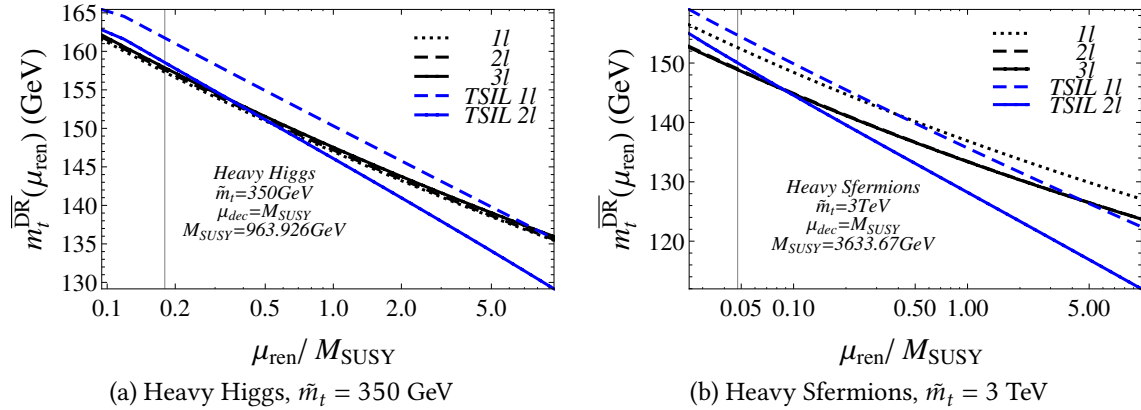(b) Heavy Sfermions, $\tilde{m}_t = 3$ TeV

Figure 4.2.: Dependence of the running top-quark mass on the renormalization scale in the Heavy Higgs and Heavy Sfermions scenario. The decoupling scale is kept fixed at M_{SUSY}. The result of the one-, two- and three-loop running-and-decoupling analysis in SQCD is shown as dotted, dashed and solid black curves, respectively. The result obtained with `TSIL` at one- and two-loop order in SQCD is shown as dashed and solid blue curves, respectively.

In Figure 4.2, the running top-quark mass of both approaches as a function of the renormalization scale is shown in the Heavy Higgs and Heavy Sfermions scenario. In the running-and-decoupling approach, the predictions for the running top-quark mass at every renormalization scale quickly converge for both investigated scenarios by including higher loop corrections in the analysis and thus reaching experimental precision. In Figure 4.2 (b), the two-loop curve is almost indistinguishable from the three-loop curve. However, radiative corrections from one- to two-loop order of the direct numerical computation with `TSIL` are much larger than the experimental uncertainty. They amount to approximately 3 GeV in the Heavy Higgs and 5 GeV in the Heavy Sfermions scenario for $\mu_{\text{ren}} = M_t$ and increase for higher values of the renormalization scale. For small renormalization scales at about $\mu_{\text{ren}} = M_t$, the running-and-decoupling approach and the direct computation have compatible predictions for the running top-quark mass. This is expected, since a resummation of logarithms of the form $\log(\mu_{\text{ren}}/M_t)$ is not needed for small renormalization scales. However, this is not the case for higher values of μ_{ren}. Such logarithms are only resummed in the running-and-decoupling approach but are present in the direct computation. Therefore, the direct computation is not reliable for high renormalization scales since perturbation theory is spoiled.

In Figure 4.3, the running top-quark mass is shown as a function of the SUSY scale $\tilde{m}_t$ in the Heavy Sfermions scenario. The renormalization scale is set to the geometric mean of both stop-quark masses. One can see that in the running-and-decoupling approach radiative corrections are small for all values of $\tilde{m}_t$, compared to the direct computation. Since there are no large logarithms for small values of $\tilde{m}_t$, the predictions of both approaches coincide. However, by increasing the SUSY scale $\tilde{m}_t$ the direct computation becomes unreliable since the radiative corrections from one- to two-loop order are of $\mathcal{O}(10 \text{ GeV})$ which spoils perturbation theory.
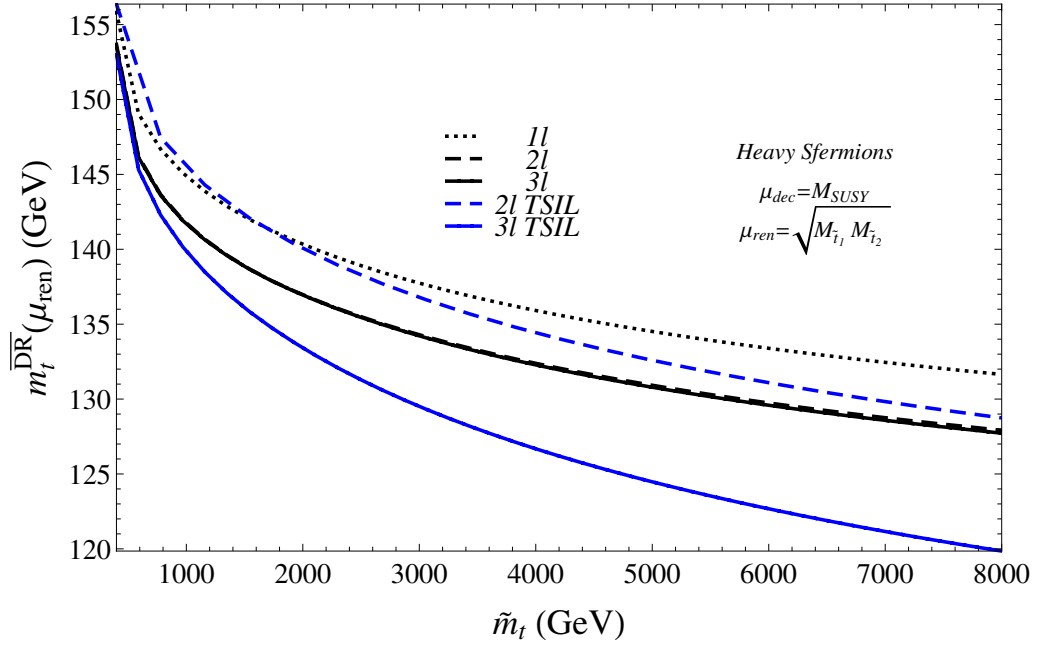
Figure 4.3.: Dependence of the running top-quark mass on the SUSY scale $\tilde{m}_t$ in the Heavy Sfermions scenario. The decoupling scale is kept fixed at M_{SUSY}. The renormalization scale is set to $\sqrt{M_{\tilde{t}_1} M_{\tilde{t}_2}}$. The result of the one-, two- and three-loop running-and-decoupling analysis in SQCD is shown as dotted, dashed and solid black curves, respectively. The result obtained with TSIL at one- and two-loop order in SQCD is shown as dashed and solid blue curves, respectively.

In summary, both methods provide results in good agreement for small renormalization scales or low SUSY mass scales. However, both results differ significantly when SUSY particles have masses in the multi-TeV regime. These discrepancies can have important phenomenological implications. The radiative corrections from one to two loops and from two to three loops in the running-and-decoupling approach show good convergence behavior which leads to small theoretical uncertainties due to unknown higher order corrections which are well below the present experimental error on the top-quark pole mass.

4.4. Running-And-Decoupling including Electroweak Interactions

In addition to the pure SQCD analysis, effects of electroweak interactions on the running-and-decoupling procedure are discussed in this section.

The SM gauge couplings $\alpha_{1,2} = g_{1,2}^2/4\pi$ in the $\overline{\mathrm{MS}}$ scheme with six flavors evaluated at $\mu_{\mathrm{ren}} = M_Z$ can be computed according to [106] using the equations

4. Running and Decoupling of α_s, α_t and m_t

$$\alpha_1^{(6),\overline{\text{MS}}} = \frac{5}{3} \frac{\alpha^{(6),\overline{\text{MS}}}}{\left(c_\theta^{(6),\overline{\text{MS}}}\right)^2} \tag{4.5}$$

and

$$\alpha_2^{(6),\overline{\text{MS}}} = \frac{\alpha^{(6),\overline{\text{MS}}}}{\left(s_\theta^{(6),\overline{\text{MS}}}\right)^2} \tag{4.6}$$

with $\alpha^{(6),\overline{\text{MS}}}$ being the QED coupling constant. They can be derived from the experimental measured fine-structure constant and the weak-mixing angle, taken from [98]:

$$\alpha = 1/137.035999074(44),$$

$$\left(s_\theta^{(5),\overline{\text{MS}}}(M_Z)\right)^2 = 0.23116(12) \tag{4.7}$$

The strong coupling $\alpha_s^{(6),\overline{\text{MS}}}(M_Z)$ is derived from the experimental input $\alpha_s^{(5),\overline{\text{MS}}}(M_Z)$ using the computer program RunDec [107]. With the experimental input from equations (4.3) and (4.7) one gets

$$\alpha_1^{(6),\overline{\text{MS}}}(M_Z) = 0.016925,$$

$$\alpha_2^{(6),\overline{\text{MS}}}(M_Z) = 0.0337207,$$

$$\alpha_s^{(6),\overline{\text{MS}}}(M_Z) = 0.117329. \tag{4.8}$$

For the computation of the Yukawa couplings, the relations

$$\alpha_{t,b,\tau}^{(6),\overline{\text{MS}}}(M_Z) = \frac{\left(m_{t,b,\tau}^{(6),\overline{\text{MS}}}(M_Z)\right)^2}{2\pi\left(v^{(6),\overline{\text{MS}}}(M_Z)\right)^2} \tag{4.9}$$

can be used. The vacuum expectation value can be computed according to formula (D.17) of [108] which reads

$$\left(v^{(6),\overline{\text{MS}}}(M_Z)\right)^2 = \frac{1}{\pi} \frac{(M_Z)^2 + \text{Re}\Pi_{ZZ}^{T,(6)}(M_Z)}{\frac{3}{5}\alpha_1^{(6),\overline{\text{MS}}}(M_Z) + \alpha_2^{(6),\overline{\text{MS}}}(M_Z)} \tag{4.10}$$

with the transversal part of the self-energy of the Z boson $\Pi_{ZZ}^{T,(6)}$. The latter can be derived from the self-energy of the Z boson in 't Hooft-Feynman gauge in the MSSM, see equation (D.4) of [108], by only taking into account the SM contributions and neglecting tadpole diagrams. For the top Yukawa coupling a precise determination is necessary since it is the most dominant one. The relation between M_t and the $\overline{\text{MS}}$ top Yukawa coupling at M_t is given in a numerical format [109]:

$$\alpha_t^{(6),\overline{\text{MS}}}(M_t) = \frac{\left(y_t^{(6),\overline{\text{MS}}}(M_t)\right)^2}{4\pi} \tag{4.11}$$

with

$$y_t^{(6),\overline{MS}}(M_t) = 0.93690 + 0.00556\left(\frac{M_t}{\text{GeV}} - 173.34\right) - 0.00042\frac{\alpha_s^{(5),\overline{MS}}(M_Z) - 0.1184}{0.0007}$$

(4.12)

To give an insight on the computation at the two-loop level, equation (4.12) was obtained according to

$$y_t^{(6),\overline{MS}}(M_t) = 2\left(\frac{G_\mu}{\sqrt{2}}M_t^2\right)^{1/2} + y_t^{(1)}(M_t) + y_t^{(2)}(M_t)$$

(4.13)

with

$$y_t^{(1)}(M_t) = -\delta^{(1)}y_t^{OS}\big|_{\text{fin}},$$
$$y_t^{(2)}(M_t) = -\delta^{(2)}y_t^{OS}\big|_{\text{fin}} + \Delta_{y_t}$$

(4.14)

and

$$\delta^{(1)}y_t^{OS} = 2\left(\frac{G_\mu}{\sqrt{2}}M_t^2\right)^2\left(\frac{\delta^{(1)}M_t}{M_t} + \frac{\Delta r_0^{(1)}}{2}\right),$$

$$\delta^{(2)}y_t^{OS} = 2\left(\frac{G_\mu}{\sqrt{2}}M_t^2\right)^2\left(\frac{\delta^{(2)}M_t}{M_t} + \frac{\Delta r_0^{(2)}}{2} - \frac{\Delta r_0^{(1)}}{2}\left[\frac{\delta^{(1)}M_t}{M_t} + \frac{3\Delta r_0^{(1)}}{4}\right]\right).$$

(4.15)

Here, $\big|_{\text{fin}}$ denotes the finite part[2] of the corresponding quantity and Δ_{y_t} is the two-loop finite contribution to y_t that is obtained when the OS parameters entering the $1/\epsilon$ pole in the OS counterterm are expressed in terms of $\overline{MS}$ quantities. $\Delta r_0^{(1)}$ and $\Delta r_0^{(2)}$ are the one- and two-loop corrections, coming from the relation between the Fermi constant G_μ and the bare vacuum v_0:

$$\frac{G_\mu}{\sqrt{2}} = \frac{1}{2v_0^2}(1 + \Delta r_0^{(1)} + \Delta r_0^{(2)})$$

(4.16)

The one- and two-loop top-quark mass counterterms $\delta^{(1)}M_t$ and $\delta^{(2)}M_t$ do not include tadpole contributions, see Section 3.5. To be consistent, the renormalized vacuum is chosen to be the minimum of the radiatively corrected potential.

In [109], the full NNLO electroweak and the NNNLO QCD effects for $y_t^{(6),\overline{MS}}$ are taken into account which leads to a theoretical uncertainty in $y_t^{(6),\overline{MS}}$ of ± 0.00050.

The bottom Yukawa coupling can be computed according to equations (4.9). The value of the bottom-quark mass in the five-flavor $\overline{MS}$ scheme can be taken[3] from [98]:

$$m_b(m_b) = 4.18 \pm 0.03 \text{ GeV}$$

(4.17)

---

[2] w.r.t. the regularization parameter ϵ

[3] A more precise value for the bottom-quark mass is given in [110]. However, the numerical effects of small deviations of the bottom-quark mass are small for the discussed running-and-decoupling procedure and the conservative value from [98] is sufficiently precise.

4. Running and Decoupling of α_s, α_t and m_t

The transition to the six-flavor $\overline{\text{MS}}$ scheme can be done using `RunDec`, taking into account three-loop QCD corrections to ζ_{m_b}. Since the tau Yukawa coupling is very small for most MSSM scenarios, a precise determination is not necessary. The $\overline{\text{MS}}$ tau mass can therefore be approximated by the value of the tau pole mass from [98]:

$$M_\tau = 1776.82 \pm 0.16 \text{ MeV} \tag{4.18}$$

The transition to the tau Yukawa coupling is then done according to equations (4.9). The running of the couplings is done using a system of RGEs taking into account strong and electroweak interactions and of the top-quark mass strong and Yukawa interactions.

For the SM, the RGEs for $y_{t,b,\tau}, g_{1,2,s}$ can be taken from the literature [111], [112], [113], [114], [115]. The QCD and Yukawa part of the anomalous dimension of the top-quark mass can be extracted from the renormalization constant Z_{m_t} by writing

$$\gamma_t = \sum_{x=t,b,\tau,s} \frac{\partial Z_{m_t}^{1/\epsilon}}{\partial \alpha_x} \alpha_x, \tag{4.19}$$

with $Z_{m_t}^{1/\epsilon}$ being the $\frac{1}{\epsilon}$ part of Z_{m_t}. The latter can be retrieved by taking the product of the renormalization constants of the vacuum expectation value and the top-Yukawa coupling, as can be seen by the relation

$$m_t = \frac{1}{\sqrt{2}} y_t v. \tag{4.20}$$

The renormalization constants Z_{y_t} and Z_v are available in an electronic format on the `arXiv` pages of [93] and [116].

For the MSSM, the RGEs for the couplings can be taken from [97], [117]. However, care has to be taken regarding the anomalous dimension of the top-quark mass. The SQCD part is identical to the anomalous dimension of the chiral superfield γ_t, see equations (7),(8a) and (9a) of [97]. The Yukawa part of the anomalous dimension of the top-quark mass can be extracted from its renormalization constant, see equation (4.19), which was already needed at two-loop order for the renormalization of $\zeta_{m_t}^{(0)}$.

So far, the couplings $\alpha_{1,2,s,b,\tau}^{(6),\overline{\text{MS}}}(M_Z)$ and $\alpha_t^{(6),\overline{\text{MS}}}(M_t)$ are determined. Since the differential equations are coupled, one has to proceed in an iterative way to evaluate $\alpha_t^{(6),\overline{\text{MS}}}(M_Z)$. As a starting value for $\alpha_t^{(6),\overline{\text{MS}}}(M_Z)$, the QCD value for the $\overline{\text{MS}}$ top-quark mass, obtained from the on-shell top-quark mass using `RunDec`, is used as an input in equation (4.10). Then, one evolves the couplings from $\mu_{\text{ren}} = M_Z$ to $\mu_{\text{ren}} = M_t$. At this scale, the value for $\alpha_t^{(6),\overline{\text{MS}}}(M_t)$ from equations (4.11) and (4.12) is used. Running down to $\mu_{\text{ren}} = M_Z$ will give a new value for $\alpha_t^{(6),\overline{\text{MS}}}(M_Z)$ which is used for the next iteration step. Practically, only one iteration is sufficient to have a stable result up to more than seven digits.

In order to have a precise starting value for the mass of the top quark, one uses the value of $\alpha_t^{(6),\overline{\text{MS}}}(M_Z)$ together with equation (4.9) to retrieve $m_t^{(6),\overline{\text{MS}}}(M_Z)$.

Alternatively, one can directly compute the running top-quark mass by using the relation between the pole and $\overline{\text{MS}}$ mass up to $\mathcal{O}(\alpha_s^3, \alpha_s\alpha)$ [84–87, 118, 119]. However, care has to be taken regarding tadpole diagrams which give the largest contribution of $\mathcal{O}(10\,\text{GeV})$. The relationship between the pole and $\overline{\text{MS}}$ mass is gauge independent only if tadpole contributions are retained, see Section 3.5. However, using a definition for the running top-quark mass without tadpole contributions has the advantage that electroweak corrections to the relation between the pole and $\overline{\text{MS}}$ mass become small [72]. Using the direct relation between the pole and $\overline{\text{MS}}$ mass without tadpole contributions leads to a result in good agreement with the running top-quark mass obtained from [109] up to an error of $\mathcal{O}(100\,\text{MeV})$ in the $\overline{\text{MS}}$ top-quark mass [120].

Now all couplings can be evolved to an arbitrary decoupling scale μ_{dec} at which the decoupling procedure takes place. The decoupling constants depend on X_t in the mixed scheme, see equations (3.13). Since the top-Yukawa coupling is the most dominant Yukawa coupling, X_t should be computed with one-loop precision. Therefore, in a first step, $m_t^{\overline{\text{DR}}}$ in the MSSM is computed from $m_t^{\overline{\text{MS}}}$ in the SM with the help of the one-loop decoupling coefficient $\zeta_{m_t}^{(1)}$. X_t which appears in $\zeta_{m_t}^{(1)}$ can be approximated by

$$X_t = \frac{1}{2M_t}s_{2\theta_t}(M_{\tilde{t}_1}^2 - M_{\tilde{t}_2}^2) \tag{4.21}$$

and the $\overline{\text{DR}}$ couplings in the MSSM by their corresponding SM $\overline{\text{MS}}$ values. Then, a more precise value for X_t can be computed according to

$$X_t = \frac{\zeta_{m_t}^{(1)}}{2m_t^{\overline{\text{MS}}}}s_{2\theta_t}(M_{\tilde{t}_1}^2 - M_{\tilde{t}_2}^2). \tag{4.22}$$

In a similar manner, $\alpha_{t,b,s}^{\overline{\text{DR}}}$ at one-loop level are computed from $\alpha_{t,b,s}^{\overline{\text{MS}}}$ with their corresponding one-loop decoupling coefficients where MSSM $\overline{\text{DR}}$ couplings are approximated by SM $\overline{\text{MS}}$ ones. Then, $\alpha_{t,b,s}^{\overline{\text{DR}}}$ can be computed at two-loop level, using the corresponding two-loop decoupling coefficients where MSSM $\overline{\text{DR}}$ couplings at one-loop level are used. All other needed parameters are taken from the spectrum generator. The resummation of t_β-enhanced supersymmetric radiative corrections for α_b is done according to [121, 122]. Since $\alpha_{1,2,\tau}^{\overline{\text{DR}}}$ are numerically not as important as $\alpha_{s,t,b}^{\overline{\text{DR}}}$, their values are approximated to be their SM ones.

4.5. Numerical Analysis including Electroweak Interactions

4.5.1. Decoupling-Scale Dependence

In a first numerical analysis, the decoupling-scale dependence of the running top-quark mass is analyzed to estimate the theoretical uncertainty of the result. For this purpose, $m_t^{\overline{\text{DR}}}$ is evaluated at different renormalization and decoupling scales.

In the following plots, M_{SUSY} is defined to be the arithmetic mean of all gluino and squark masses, as defined in equation (4.2), since strong interactions give the most dominant corrections in the running-and-decoupling procedure for which this scale is meaningful. The smallest shown value corresponds to $\mu_{\text{dec}} = M_Z$ and the vertical line to $\mu_{\text{dec}} = M_t$. The notation is analog to the SQCD analysis.

(a) $\tilde{m}_t = 350$ GeV, $\mu_{\text{ren}} = \sqrt{M_{\tilde{t}_1} M_{\tilde{t}_2}}$

(b) $\tilde{m}_t = 350$ GeV, $\mu_{\text{ren}} = 3\sqrt{M_{\tilde{t}_1} M_{\tilde{t}_2}}$

(c) $\tilde{m}_t = 1$ TeV, $\mu_{\text{ren}} = \sqrt{M_{\tilde{t}_1} M_{\tilde{t}_2}}$

(d) $\tilde{m}_t = 350$ GeV, $\mu_{\text{ren}} = M_t$
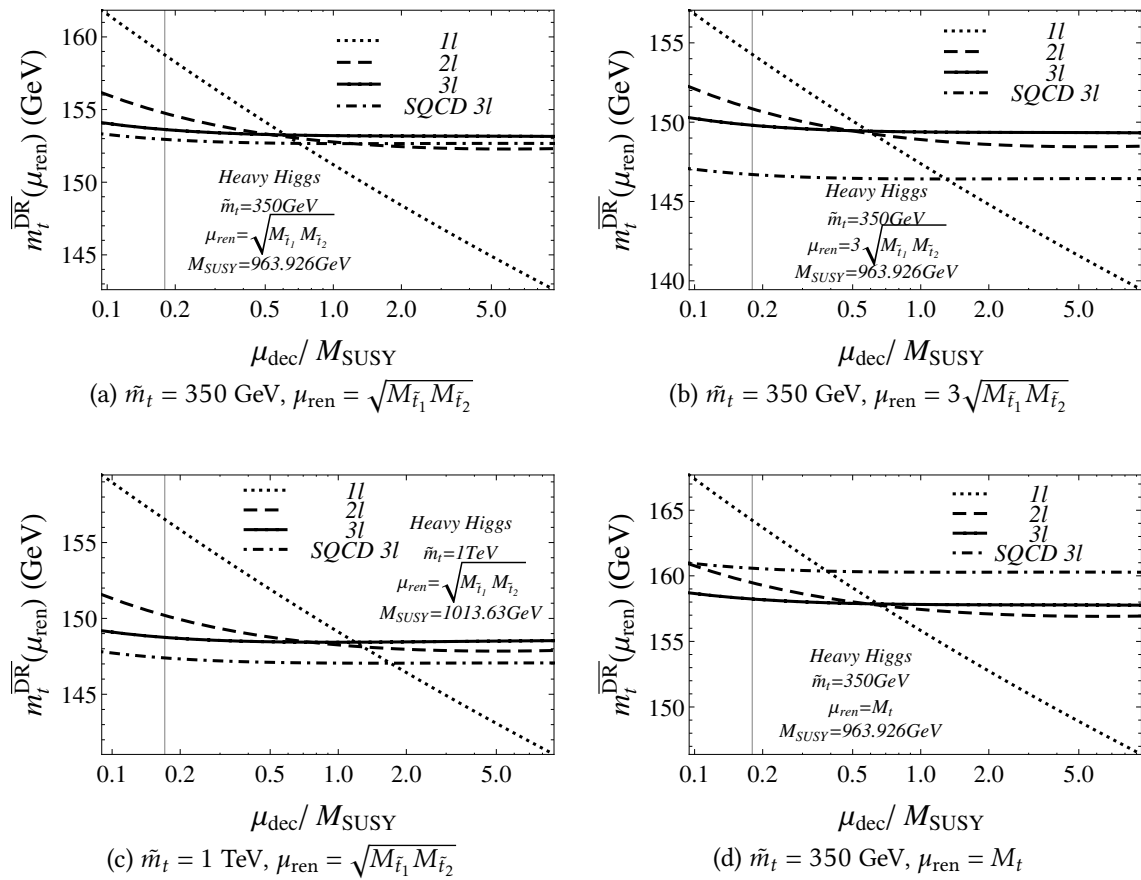
Figure 4.4.: Dependence of the running top-quark mass on the decoupling scale in the Heavy Higgs scenario for four different choices of $\tilde{m}_t$ and μ_{ren}. The result of the one-, two- and three-loop running-and-decoupling analysis including electroweak effects is shown as dotted, dashed and solid curves, respectively. The dashed-dotted curve shows the three-loop result where only SQCD corrections are included in the RGEs and decoupling coefficients.

In Figure 4.4, the decoupling-scale dependence of the running top-quark mass in the Heavy Higgs scenario for four different combinations of $\tilde{m}_t$ and μ_{ren} is shown. In

Figure 4.4 (a), the renormalization scale is chosen to be $\sqrt{M_{\tilde{t}_1} M_{\tilde{t}_2}}$ and the parameter $\tilde{m}_t$ is set to 350 GeV which results in a light stop mass of the same size. As one can see, including radiative corrections at higher orders to the analysis strongly reduces the decoupling-scale dependence of the running top-quark mass, as expected. At the three-loop level, the change in $m_t^{\overline{DR}}$ when varying the decoupling scale in the shown range is comparable in size to the SQCD analysis and amounts to less than 1 GeV. Restricting the decoupling scale to be in the range $0.5M_{\text{SUSY}}$ to $10M_{\text{SUSY}}$ reduces the variation in $m_t^{\overline{DR}}$ to be about 100 MeV. Setting μ_{dec} to low scales like M_t or M_Z is not a good choice regarding convergence behavior. However, in some cases supersymmetric corrections to the running top-quark mass are evaluated at low energy scales, see e.g. [104]. At $\mu_{\text{dec}} = M_Z$, which corresponds to the lowest shown value of μ_{dec}, the difference in $m_t^{\overline{DR}}$ going from the one- to the two-loop analysis is approximately 5.8 GeV and from the two- to the three-loop analysis 2 GeV. Therefore, at this decoupling scale, a three-loop analysis is necessary to compete with the experimental uncertainty of the top pole mass of about 1 GeV. The intersections of the one-, two- and three-loop curves are at $\mu_{\text{dec}} \approx 0.6M_{\text{SUSY}}$. At this scale, higher order corrections are small. For this scenario and at this renormalization scale, this value for μ_{dec} would be the optimal choice regarding the convergence behavior. However, no general statement can be made since it depends on the scenario. The difference to the pure SQCD analysis amounts to less than 0.8 GeV but strongly depends on the chosen renormalization scale. In Figure 4.4 (b), the same curves are shown but with μ_{ren} set to $3\sqrt{M_{\tilde{t}_1} M_{\tilde{t}_2}}$. Here, the difference to the pure SQCD analysis is increased and amounts to approximately 3 GeV which indicates that the renormalization-scale dependence of the running top-quark changes when including electroweak effects in the analysis, this will be discussed below. In Figure 4.4 (c), the parameter $\tilde{m}_t$ is increased to 1 TeV which corresponds to a higher value of the light stop mass of the same size. Compared to the result of Figure 4.4 (a), the three-loop result is decreased by approximately 4.5 GeV while the difference to the pure SQCD analysis is increased by approximately 0.6 GeV. In Figure 4.4 (d), the renormalization scale is set to the top-quark pole mass to investigate the decoupling-scale stability at low renormalization scales. Furthermore, the running top-quark mass at this scale is needed in Chapter 5 in the context of determining the lightest CP even Higgs boson mass. At this renormalization scale, electroweak effects in the running-and-decoupling procedure reduce the value of the running top-quark mass by approximately 2.4 GeV. In all four shown combinations of $\tilde{m}_t$ and μ_{ren}, the three-loop result is stable up to an order of 100 MeV w.r.t. a variation of the decoupling scale in the range $0.5M_{\text{SUSY}} \leq \mu_{\text{dec}} \leq 10M_{\text{SUSY}}$. Since the masses of the neutralinos $M_{\chi_{1,2}^0}$ and the chargino $M_{\chi_1^\pm}$ are below the top-quark mass in the Heavy Higgs scenario, they should have been present in the effective theory, which would complicate this procedure. However, a consistent treatment of light neutralinos and charginos is beyond the scope of this thesis.

So far, the running-and-decoupling procedure including electroweak effects was shown in the Heavy Higgs scenario. To give an insight on the predictions for the running top-quark mass in a different scenario, the following plots show the results of the same analysis done in the Heavy Sfermions scenario for four different combinations of $\tilde{m}_t$ and μ_{ren}.

(a) $\tilde{m}_t = 3$ TeV, $\mu_{\mathrm{ren}} = \sqrt{M_{\tilde{t}_1} M_{\tilde{t}_2}}$

(b) $\tilde{m}_t = 3$ TeV, $\mu_{\mathrm{ren}} = 3\sqrt{M_{\tilde{t}_1} M_{\tilde{t}_2}}$

(c) $\tilde{m}_t = 8$ TeV, $\mu_{\mathrm{ren}} = \sqrt{M_{\tilde{t}_1} M_{\tilde{t}_2}}$

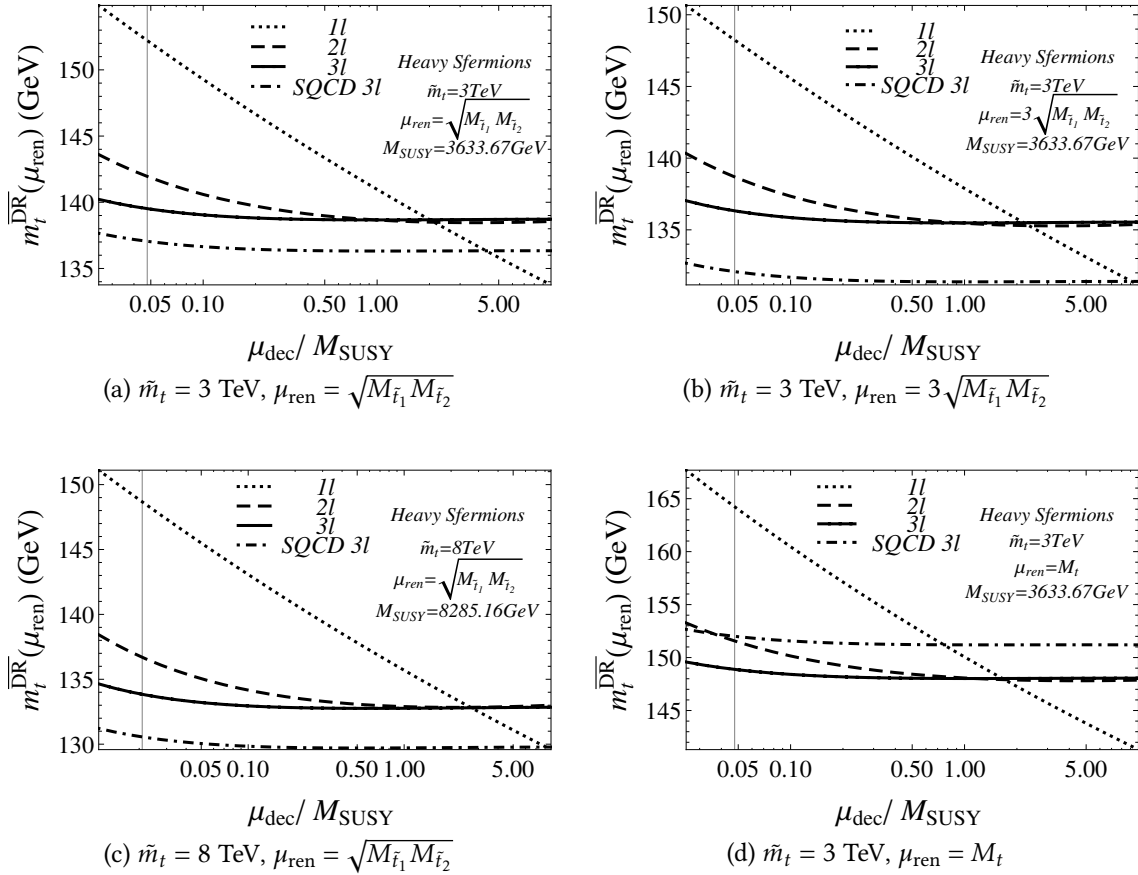(d) $\tilde{m}_t = 3$ TeV, $\mu_{\mathrm{ren}} = M_t$

Figure 4.5.: Dependence of the running top-quark mass on the decoupling scale in the Heavy Sfermions scenario for four different choices of $\tilde{m}_t$ and μ_{ren}. The result of the one-, two- and three-loop running-and-decoupling analysis including electroweak effects is shown as dotted, dashed and solid curves, respectively. The dashed-dotted curve shows the three-loop result where only SQCD corrections are included in the RGEs and decoupling coefficients.

In Figure 4.5 (a), the parameter $\tilde{m}_t$ is set to 3 TeV which corresponds to sfermion masses of the same size. The renormalization scale is set to the geometric mean of both stop masses. Including radiative corrections at higher orders in the analysis reduces the decoupling-scale dependence, as seen in the Heavy Higgs scenario. A variation of μ_{dec} in the shown range results in a change in $m_t^{\overline{\mathrm{DR}}}$ of about 1.3 GeV. However, choosing the decoupling scale to be $\gtrsim M_{\mathrm{SUSY}}$ reduces this scale dependence and the running top-quark mass is stable up to an order of 100 MeV. In this plot, the shift in the top-quark mass regarding electroweak effects amounts to approximately 2.5 GeV. Increasing the renormalization scale to $3\sqrt{M_{\tilde{t}_1} M_{\tilde{t}_2}}$ increases the effect of electroweak interactions to about 4.5 GeV, as can be seen in Figure 4.5 (b). The effect of heavy sfermion masses of about 8 TeV is analyzed in Figure 4.5 (c) where the parameter $\tilde{m}_t$ is set to the mentioned value. In this plot, the running top-quark mass at $\mu_{\mathrm{ren}} = \sqrt{M_{\tilde{t}_1} M_{\tilde{t}_2}}$ is about 133 GeV when including electroweak interactions in the running-and-decoupling procedure and about 3.2 GeV below that value by only considering SQCD contributions. For high values of μ_{dec}, the two- and the three-loop curves are very close and the difference amounts to approximately 100 MeV. To ensure decoupling-scale stability of the

running top-quark mass for small renormalization scales, μ_{ren} is set to M_t in Figure 4.5 (d). In this plot, electroweak effects result in a change in $m_t^{\overline{\text{DR}}}$ of about 3 GeV. In all four shown plots in Figure 4.5, the theoretical error of the running top-quark mass of the three-loop analysis based on a variation of the unphysical decoupling scale in the range $0.5M_{\text{SUSY}} \leq \mu_{\text{dec}} \leq 10M_{\text{SUSY}}$ is of $\mathcal{O}(100 \text{ MeV})$.
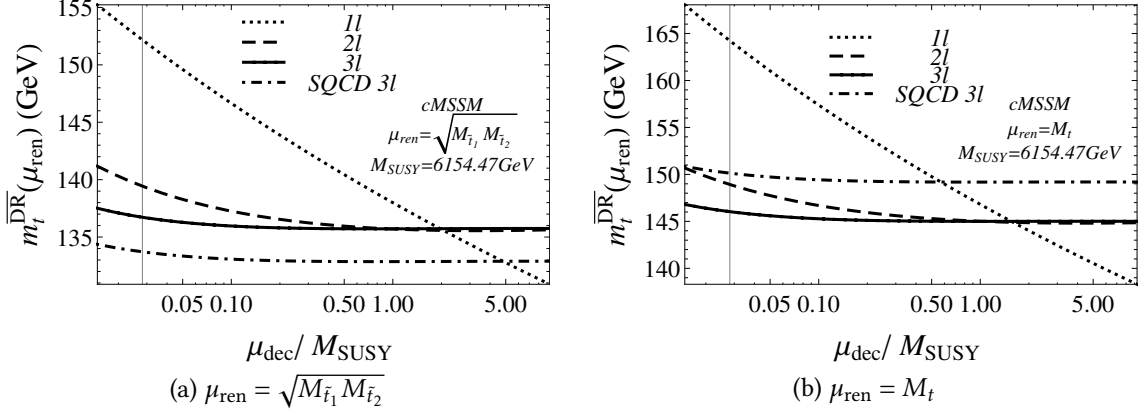

Figure 4.6.: Dependence of the running top-quark mass on the decoupling scale in the cMSSM scenario for two different choices of μ_{ren}. The result of the one-, two- and three-loop running-and-decoupling analysis including electroweak effects is shown as dotted, dashed and solid curves, respectively. The dashed-dotted curve shows the three-loop result where only SQCD corrections are included in the RGEs and decoupling coefficients.

To complete the analysis about decoupling-scale stability of the running top-quark mass, the cMSSM scenario is discussed in Figure 4.6 for two different renormalization scales. In Figure 4.6 (a), μ_{ren} is set to $\sqrt{M_{\tilde{t}_1} M_{\tilde{t}_2}}$. As expected, the inclusion of radiative corrections at higher orders in the analysis reduces the decoupling-scale dependence of $m_t^{\overline{\text{DR}}}$. In the shown range, one observes a variation in the running top-quark mass of about 1.6 GeV. However, restricting μ_{dec} to be between $0.5M_{\text{SUSY}}$ and $10M_{\text{SUSY}}$ reduces this variation to about 100 MeV. The contribution of electroweak corrections in the running-and-decoupling procedure amounts to approximately 3 GeV for the running top-quark mass. In Figure 4.6 (b), the renormalization scale is set to M_t to investigate decoupling-scale stability at small renormalization scales. Compared to Figure 4.6 (a), one observes a shift of the one-, two- and three-loop curves of about 9 GeV. However, the shift of the result of the SQCD analysis amounts to approximately 16 GeV. This indicates a different renormalization-scale behavior of the running top-quark mass which depends on including or not including electroweak effects in the analysis. At this renormalization scale, the effect of electroweak contributions amounts to approximately -4 GeV for the running top-quark mass. In both plots of Figure 4.6, the difference between the two- and the three-loop curve is of $\mathcal{O}(100 \text{ MeV})$ for sufficiently large decoupling scales $\mu_{\text{dec}} \gtrsim M_{\text{SUSY}}$.

It is interesting to know, how the two-loop corrections of $\mathcal{O}(\alpha_s \alpha_{t,b,\tau})$ contribute to the decoupling-scale stability of the running top-quark mass since these are only calculated in the gauge-less limit and in the limit of equal masses.

(a) Heavy Higgs, $\tilde{m}_t = 350$ GeV

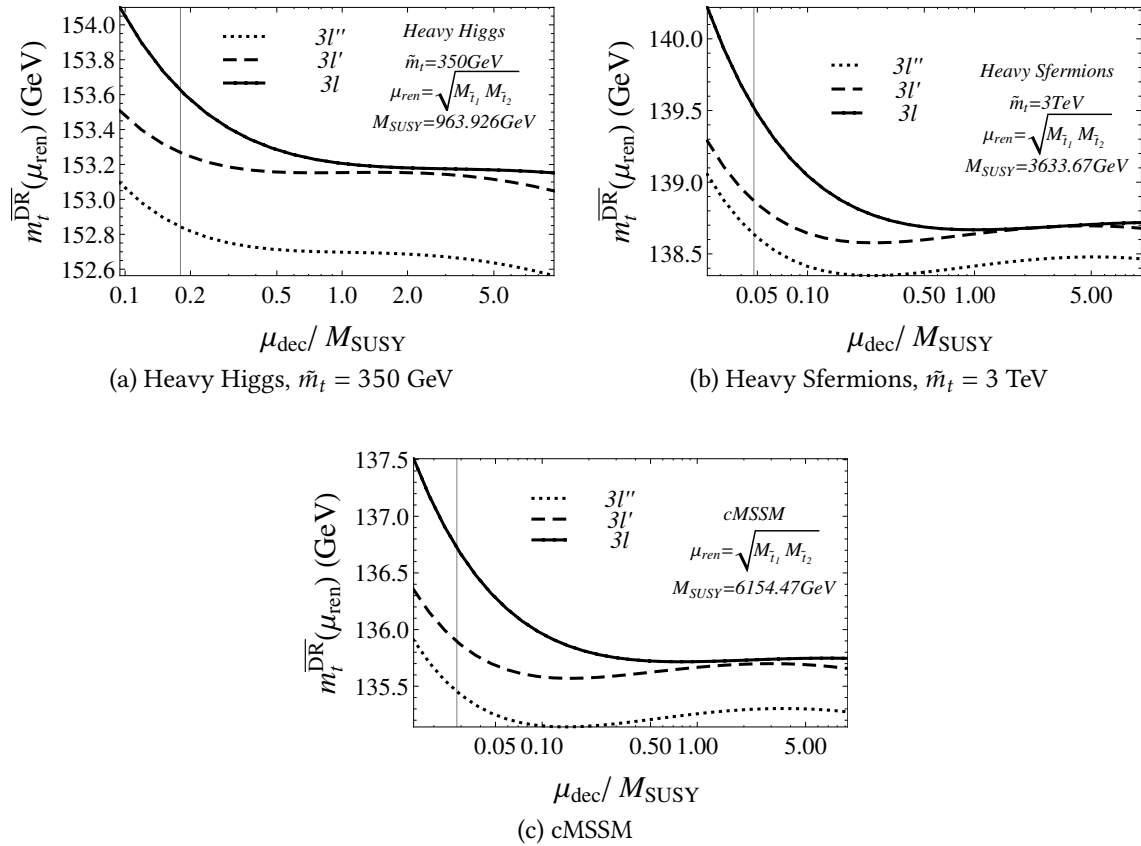(b) Heavy Sfermions, $\tilde{m}_t = 3$ TeV

(c) cMSSM

Figure 4.7.: Dependence of the running top-quark mass on the decoupling scale in the Heavy Higgs, Heavy Sfermions and cMSSM scenario. The renormalization scale is kept fixed at $\sqrt{M_{\tilde{t}_1} M_{\tilde{t}_2}}$. The result of the three-loop running-and-decoupling analysis including electroweak effects is shown as a solid curve. In the dotted and dashed curves, the the two-loop Yukawa corrections are disabled in the decoupling coefficients. In the dotted curve, the assumptions used for the two-loop Yukawa sector are also applied in the one-loop Yukawa part of ζ_{m_t}.

In Figure 4.7, the dependence of the running top-quark mass on the decoupling scale in the Heavy Higgs, Heavy Sfermions and cMSSM scenario is shown. In the solid curve, the result of the three-loop analysis is plotted. The dashed curve represents the result obtained by doing the same analysis but disabling the two-loop Yukawa corrections of $\mathcal{O}(\alpha_s \alpha_{t,b,\tau})$ in the decoupling coefficients. This result is called 3l'. One can see that for high values of the decoupling scale $\mu_{\text{dec}} \gtrsim M_{\text{SUSY}}$, the two-loop Yukawa corrections for the decoupling coefficients reduce the decoupling-scale dependence in all three plots in Figure 4.7. However, for small values of the decoupling scale, the decoupling-scale dependence is increased. In this region, the anomalous dimension of the top-quark mass in the MSSM becomes more relevant for which the three-loop Yukawa part is not included in the analysis[4]. It is assumed that including this part will reduce the decoupling-scale dependence. Nevertheless, to avoid huge scale dependence, one can set the decoupling scale to $\mu_{\text{dec}} \approx M_{\text{SUSY}}$ where the decoupling-scale dependence is very weak. In the range

---

[4]It is not directly available in the literature

$M_{\mathrm{SUSY}} \leq \mu_{\mathrm{dec}} \leq 10 M_{\mathrm{SUSY}}$ including (not including) two-loop Yukawa interactions in the decoupling coefficients results in a change of $m_t^{\overline{\mathrm{DR}}}$ of about 50 MeV (100 MeV) in the Heavy Higgs, 30 MeV (40 MeV) in the Heavy Sfermions and 10 MeV (30 MeV) in the cMSSM scenario, as can be seen in Figure 4.7 (a)-(c).

In the dotted curves, denoted by 3l", the two-loop Yukawa part in the decoupling coefficients is disabled and in addition, the assumptions used for the two-loop Yukawa sector[5] are also applied in the one-loop Yukawa part of ζ_{m_t}. The effect of these assumptions on $m_t^{\overline{\mathrm{DR}}}$ amounts to approximately 0.5 GeV in the Heavy Higgs, 0.25 GeV in the Heavy Sfermions and 0.4 GeV in the cMSSM scenario. Therefore, the effect of the used assumptions in the two-loop Yukawa sector on the running top-quark mass is assumed to be small, compared to remaining uncertainties.

So far, the decoupling-scale stability of the running top-quark mass was analyzed. In the following, the decoupling-scale dependence is investigated for the top Yukawa coupling, as can bee seen in Figure 4.8.

---

[5]The gauge-less limit is applied and all particles share the same mass M_{S} except $\tilde{t}_2$ and $\tilde{b}_2$.

(a) Heavy Higgs, $\tilde{m}_t = 350$ GeV

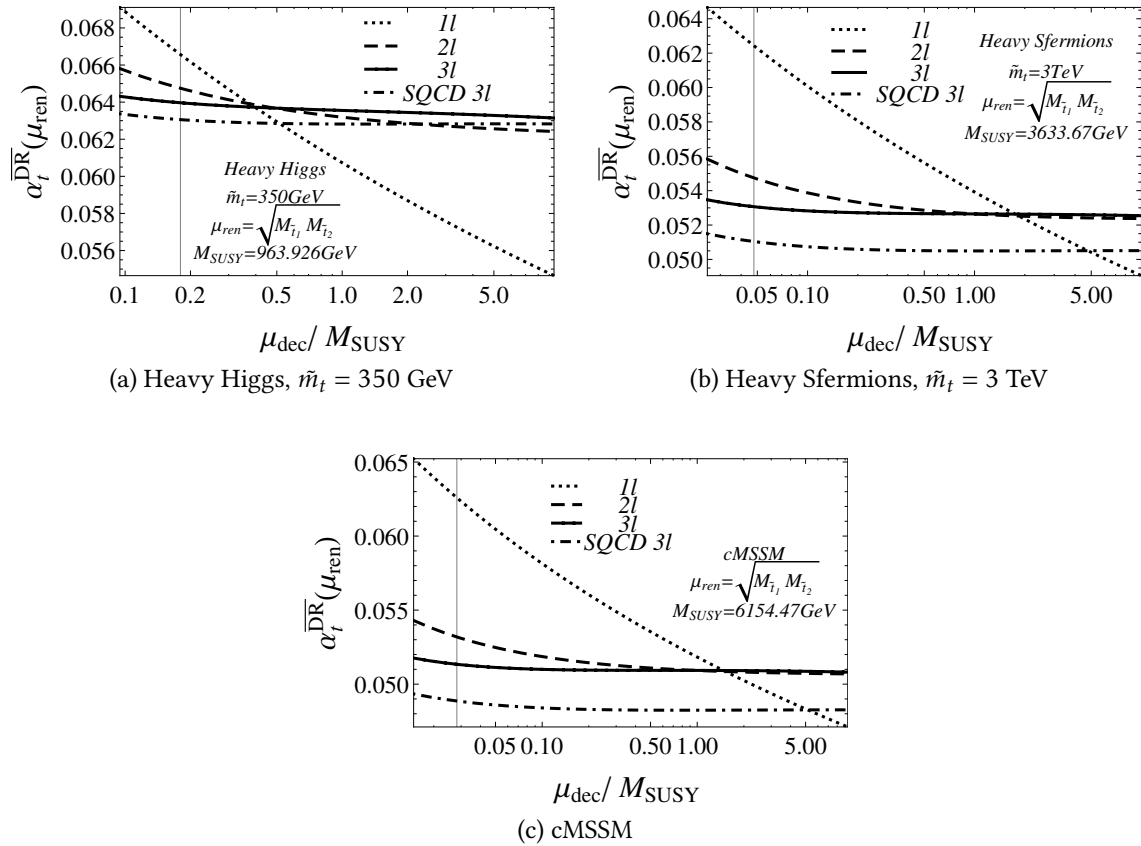(b) Heavy Sfermions, $\tilde{m}_t = 3$ TeV

(c) cMSSM

Figure 4.8.: Dependence of the top Yukawa coupling on the decoupling scale in the Heavy Higgs, Heavy Sfermions and cMSSM scenario. The renormalization scale is kept fixed at $\sqrt{M_{\tilde{t}_1} M_{\tilde{t}_2}}$. The result of the one-, two- and three-loop running-and-decoupling analysis including electroweak effects is shown as dotted, dashed and solid curves, respectively. The dashed-dotted curve shows the three-loop result where only SQCD corrections are included in the RGEs and decoupling coefficients.

In Figure 4.8 (a), the decoupling-scale dependence of the top Yukawa coupling in the Heavy Higgs scenario is shown, where the parameter $\tilde{m}_t$ is set to 350 GeV. As expected, including radiative correction at higher orders in the analysis reduces the decoupling-scale dependence of the top Yukawa coupling. At three-loop level, the variation of $\alpha_t^{\overline{\text{DR}}}$ amounts to approximately 0.0012 when varying μ_{dec} in the shown range. The increase of the value of the top Yukawa coupling due to electroweak effects amounts to approximately 0.001 at $\mu_{\text{dec}} \approx M_{\text{SUSY}}$. The same analysis in the Heavy Sfermions scenario with the parameter $\tilde{m}_t$ set to 3 TeV is shown in Figure 4.8 (b). Here, varying the decoupling scale in the shown range results in a change in $\alpha_t^{\overline{\text{DR}}}$ of about 0.0008 in the three-loop analysis. However, restricting the decoupling scale to be in the range $0.5 M_{\text{SUSY}} \leq \mu_{\text{dec}} \leq 10 M_{\text{SUSY}}$ reduces the variation in $\alpha_t^{\overline{\text{DR}}}$ to about 0.0001. Electroweak effects in the running-and-decoupling analysis lead to an increase of the value of $\alpha_t^{\overline{\text{DR}}}$ of about 0.0022. For high values of μ_{dec} the difference between the two- and three-loop curves is only about 0.0002. In the cMSSM scenario, as shown in Figure 4.8 (c), the results are very similar to the ones in the Heavy Sfermions scenario. A variation of the decoupling scale in the range $0.5 M_{\text{SUSY}} \leq \mu_{\text{dec}} \leq 10 M_{\text{SUSY}}$ leads to a variation in $\alpha_t^{\overline{\text{DR}}}$

of about 0.00015. Electroweak effects lead to an increase in $\alpha_t^{\overline{\text{DR}}}$ of about 0.0025.

(a) Heavy Higgs, $\tilde{m}_t = 350$ GeV

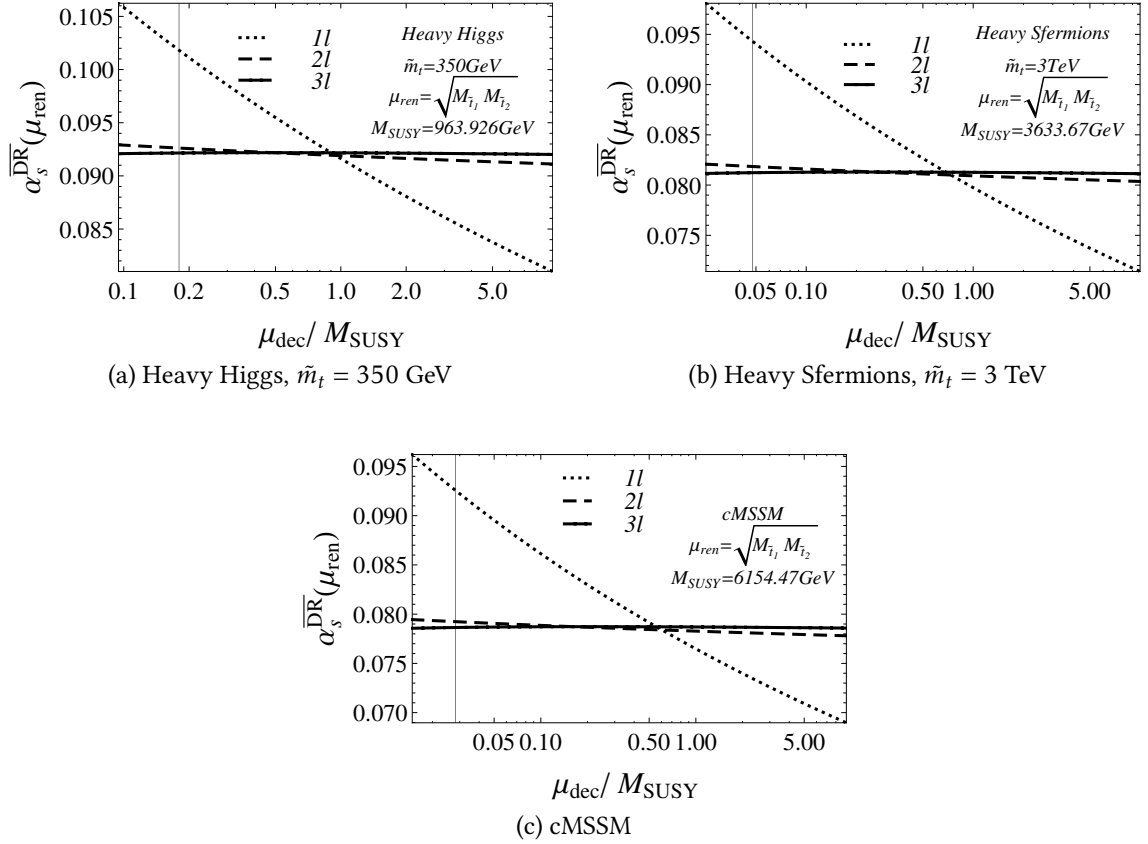(b) Heavy Sfermions, $\tilde{m}_t = 3$ TeV

(c) cMSSM

Figure 4.9.: Dependence of the strong coupling on the decoupling scale in the Heavy Higgs, Heavy Sfermions and cMSSM scenario. The renormalization scale is kept fixed at $\sqrt{M_{\tilde{t}_1} M_{\tilde{t}_2}}$. The result of the one-, two- and three-loop running-and-decoupling analysis including electroweak effects is shown as dotted, dashed and solid curves, respectively.

The decoupling-scale dependence of the strong coupling $\alpha_s^{\overline{\text{DR}}}$ is now discussed. In Figure 4.9, α_s^{DR} is computed for the Heavy Higgs, Heavy Sfermions and cMSSM scenario as a function of the decoupling scale. Since electroweak interactions do not appear at one-loop order in the decoupling coefficient ζ_{α_s}, their contributions to the running-and-decoupling procedure are expected to be small. A numerical analysis could confirm this assumption. The absolute difference in $\alpha_s^{\overline{\text{DR}}}$ between the pure SQCD analysis and the analysis including electroweak interactions is of the order 10^{-7} and therefore negligible. In Figure 4.9 (a), the strong coupling in the Heavy Higgs scenario is shown, where the parameter $\tilde{m}_t$ is set to 350 GeV. There is a strong decrease in the decoupling-scale dependence of $\alpha_s^{\overline{\text{DR}}}$ in the two-loop analysis, compared to the result of the one-loop analysis. In the three-loop analysis of the Heavy Higgs, Heavy Sfermions and cMSSM scenario, the variation of $\alpha_s^{\overline{\text{DR}}}$ when varying the decoupling scale in the shown range amounts to approximately 0.0002.

4.5.2. Renormalization-Scale Dependence

Since the running top-quark mass does not change significantly when varying the decoupling scale in a reasonable range[6], the latter will be kept fixed at $\mu_{\text{dec}} = M_{\text{SUSY}}$ in the following discussion, except stated otherwise.

(a) Heavy Higgs, $\tilde{m}_t = 350$ GeV

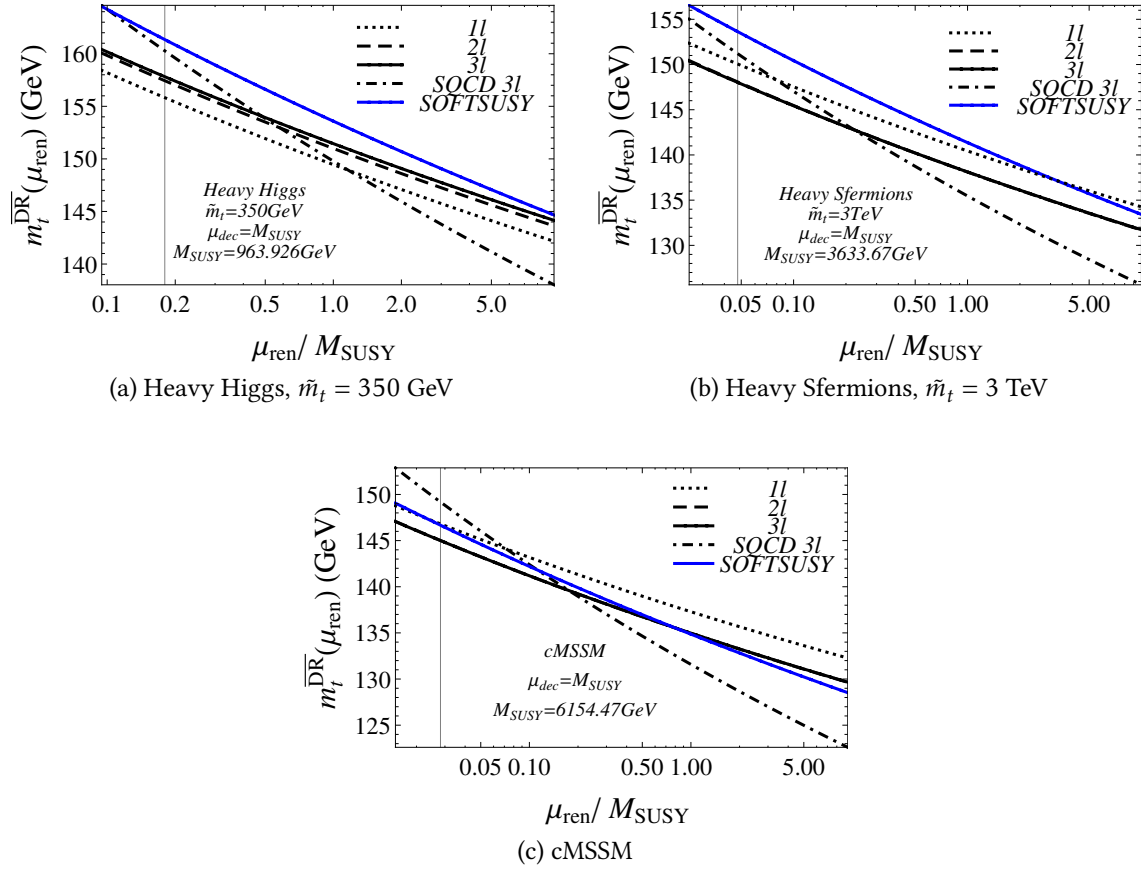(b) Heavy Sfermions, $\tilde{m}_t = 3$ TeV

(c) cMSSM

Figure 4.10.: Dependence of the running top-quark mass on the renormalization scale in the Heavy Higgs, Heavy Sfermions and cMSSM scenario. The decoupling scale is kept fixed at M_{SUSY}. The result of the one-, two- and three-loop running-and-decoupling analysis including electroweak effects is shown as a dotted, dashed and solid black curve, respectively. The dashed-dotted curve shows the three-loop result where only SQCD corrections are included in the RGEs and decoupling coefficients. The blue curve is the result obtained with SOFTSUSY v. 3.6.1.

In Figure 4.10, the dependence of the running top-quark mass on the renormalization scale in the Heavy Higgs, Heavy Sfermions and cMSSM scenario is shown. One can see that enabling electroweak interactions in the running-and-decoupling procedure flattens the curves in all three scenarios. The different dependence on the renormalization scale which depends on including or not including electroweak corrections shows that a consistent analysis must be performed when including $m_t^{\overline{\text{DR}}}(\mu_{\text{ren}})$ in subsequent calculations. This feature will be shown in the context of the determination of the lightest

---

[6]A reasonable range would be $0.5 M_{\text{SUSY}} \leq \mu_{\text{dec}} \leq 2 M_{\text{SUSY}}$.

CP even Higgs boson mass in Chapter 5. In Figure 4.10 (a), the Heavy Higgs scenario with the parameter $\tilde{m}_t$ set to 350 GeV is shown. At $\mu_{\mathrm{ren}} = M_Z$, the SQCD result is about 4 GeV higher than the result of the analysis including electroweak contributions and for $\mu_{\mathrm{ren}} = 10 M_{\mathrm{SUSY}}$ about 6 GeV lower. In Figure 4.10 (b), the Heavy Sfermions scenario with $\tilde{m}_t = 3$ TeV is shown. At $\mu_{\mathrm{ren}} = M_Z$, the SQCD result is about 4.5 GeV higher and at $\mu_{\mathrm{ren}} = 10 M_{\mathrm{SUSY}}$ 6 GeV lower than the result of the electroweak analysis. In the cMSSM scenario, the corresponding numbers are about 6 GeV at $\mu_{\mathrm{ren}} = M_Z$ and 7 GeV at $\mu_{\mathrm{ren}} = M_{\mathrm{SUSY}}$, as shown in Figure 4.10 (c).

In all three scenarios, the convergence behavior when including more loop corrections in the electroweak analysis seems to be the approximately the same for all renormalization scales in the shown range. In the Heavy Higgs scenario, going from the one- to the two-loop analysis leads to an increase of the value of the running top-quark mass of about 1.5 GeV and from the two- to the three-loop analysis of about 0.4 GeV. In the Heavy Sfermions and cMSSM scenario, the difference of $m_t^{\overline{\mathrm{DR}}}$ between the one- and two-loop analysis is about 2.2 GeV and between the two- and three-loop analysis below 100 MeV.

The blue curves show the result obtained with SOFTSUSY v. 3.6.1. Since the $\overline{\mathrm{DR}}$ value of the running top-quark mass can't be retrieved directly from SOFTSUSY, it is calculated by combining the $\overline{\mathrm{DR}}$ vacuum expectation value with the $\overline{\mathrm{DR}}$ top Yukawa coupling, see equation (4.20). The result of SOFTSUSY seems to be too large in the Heavy Higgs and Heavy Sfermions scenario. In the Heavy Higgs scenario, the difference between the result of SOFTSUSY and the running-and-decoupling analysis amounts to approximately 4 GeV for $\mu_{\mathrm{ren}} = M_Z$ and reduces to 0.8 GeV for $\mu_{\mathrm{ren}} = 10 M_{\mathrm{SUSY}}$. In the Heavy Sfermions scenario, the corresponding numbers are 6 GeV for $\mu_{\mathrm{ren}} = M_Z$ and 1.6 GeV for $\mu_{\mathrm{ren}} = 10 M_{\mathrm{SUSY}}$ and in the cMSSM scenario 2 GeV for $\mu_{\mathrm{ren}} = M_Z$ and -1 GeV for $\mu_{\mathrm{ren}} = 10 M_{\mathrm{SUSY}}$.

Care has to be taken regarding the comparison of the running top-quark mass of SOFTSUSY with the result obtained with the running-and-decoupling procedure because of the following reasons. In SOFTSUSY, the running top-quark mass in the MSSM is computed at the scale M_Z using the two-loop QCD and the full one-loop supersymmetric contributions to $m_t^{\overline{\mathrm{DR}}}(M_Z)$ from equations (D.16)-(D.18) of [108], as stated in equation (3.2) of [103]. However, it seems that the high-precision spectrum generation for the Heavy Higgs and Heavy Sfermions scenario does not include three-loop RGE terms and/or 2-loop threshold corrections since the generation process is much faster than the typical runtime of »a minute per parameter point« [104]. Therefore it is assumed that for both the Heavy Higgs and the Heavy Sfermions scenario only a two-loop analysis is performed. For the cMSSM scenario, for which MSUGRA input parameters are used, the stated runtime of a minute per parameter point is confirmed which leads to the assumption that only in this scenario the high-precision calculation is done. A comparison with the running-and-decoupling approach is only reasonable if one sets the decoupling scale to the value $\mu_{\mathrm{dec}} = M_Z$. However, this is not a good choice if only a two-loop analysis is performed, as can be seen in Figures 4.4-4.6. At this decoupling scale, the appearing logarithms involving supersymmetric particles become huge and spoil perturbation theory. The smallest value of μ_{dec} in this Figure corresponds to M_Z. Setting $\mu_{\mathrm{dec}} = M_Z$ instead of $\mu_{\mathrm{dec}} \approx M_{\mathrm{SUSY}}$ will increase the running top-quark mass in the two-loop analysis, which is an effect due to bad convergence behavior of the perturbative series.

(a) Heavy Higgs, $\tilde{m}_t = 350$ GeV

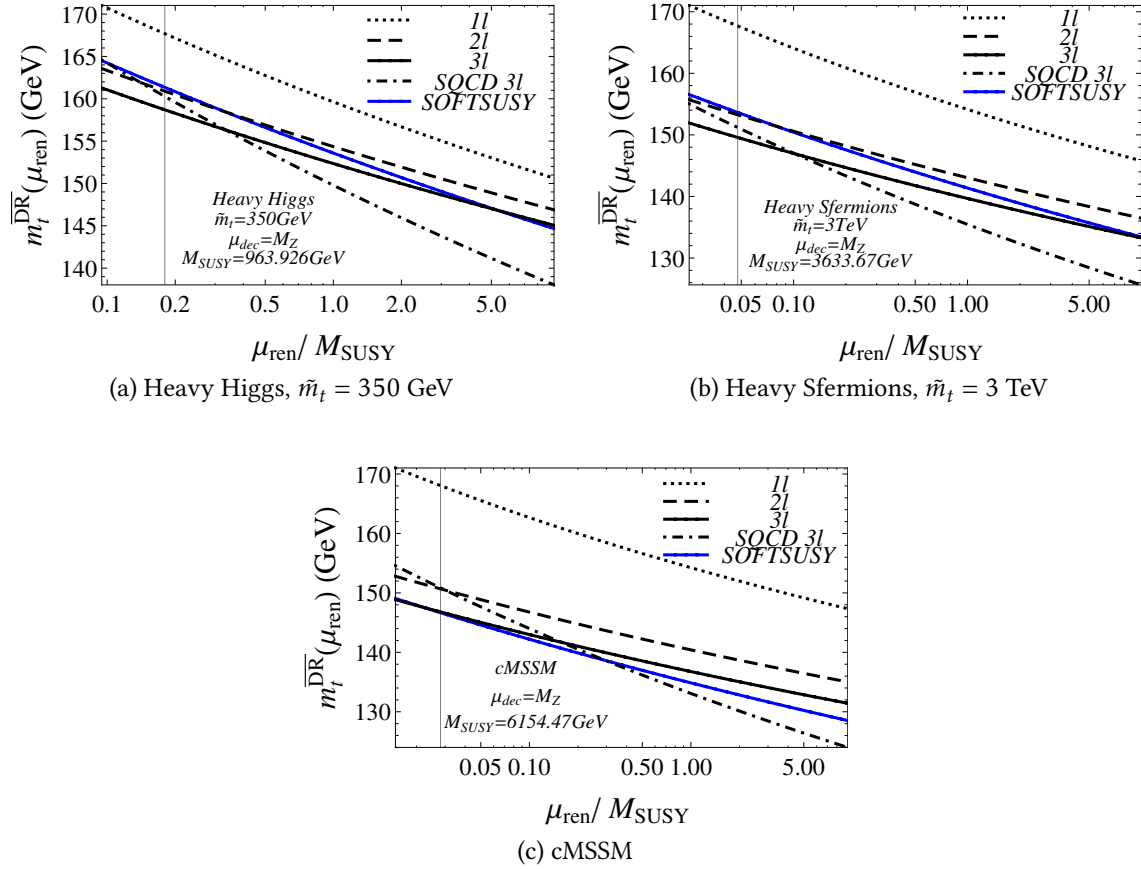(b) Heavy Sfermions, $\tilde{m}_t = 3$ TeV

(c) cMSSM

Figure 4.11.: Dependence of the running top-quark mass on the renormalization scale in the Heavy Higgs, Heavy Sfermions and cMSSM scenario. The decoupling scale is kept fixed at M_Z. The result of the one-, two- and three-loop running-and-decoupling analysis including electroweak effects is shown as a dotted, dashed and solid black curve, respectively. The dashed-dotted curve shows the three-loop result where only SQCD corrections are included in the RGEs and decoupling coefficients. The blue curve is the result obtained with SOFTSUSY v. 3.6.1.

In Figure 4.11, the same curves are displayed as in Figure 4.10 but the decoupling scale has been set to $\mu_{\mathrm{dec}} = M_Z$ to enable a reasonable comparison with the result obtained with SOFTSUSY. As one can see, the convergence in the running-and-decoupling approach for $\mu_{\mathrm{dec}} = M_Z$ is much worse than for $\mu_{\mathrm{dec}} = M_{\mathrm{SUSY}}$. The difference of $m_t^{\overline{\mathrm{DR}}}$ between the two- and the three-loop analysis is increased from 0.4 GeV to about 1 GeV in the Heavy Higgs and from below 100 MeV to almost 4 GeV in the Heavy Sfermions and cMSSM scenario, strongly indicating a bad choice for μ_{dec} regarding convergence behavior. As already mentioned, the results of the Heavy Higgs and Heavy Sfermions scenario obtained with SOFTSUSY are assumed to not include three-loop RGEs and/or two-loop threshold corrections. Therefore one expects the SOFTSUSY results to be near the results of the two-loop running-and-decoupling analysis which can be confirmed in Figure 4.11 (a) and (b) for small renormalization scales. However, the dependence on the renormalization scale of the running-top quark mass obtained with SOFTSUSY is somewhere in between the dependence of the result of the pure SQCD and the full running-and-decoupling analysis which leads to the assumption that SOFTSUSY overestimates

SQCD effects in RGEs. Therefore, one observes a difference for high renormalization scales. At $\mu_{\text{ren}} = 10 M_{\text{SUSY}}$, this difference in $m_t^{\overline{\text{DR}}}$ is about 2 GeV for the Heavy Higgs and 3 GeV for the Heavy Sfermions scenario. In the cMSSM scenario, the value of $m_t^{\overline{\text{DR}}}$ agrees well with the result of the three-loop running-and-decoupling analysis for small renormalization scales. However, for $\mu_{\text{ren}} = 10 M_{\text{SUSY}}$ one observes a difference of about 2 GeV.

In summary, electroweak effects in the running-and-decoupling procedure for the determination of the running top-quark mass and the top Yukawa coupling are in general not negligible. A variation of the unphysical decoupling scale in the range from $1/2 M_{\text{SUSY}}$ to $2 M_{\text{SUSY}}$ does not change the values of the running top-quark mass and the top Yukawa coupling significantly. In all investigated scenarios, electroweak effects soften the renormalization-scale dependence of the running top-quark mass. A comparison with SOFTSUSY is only valid if one sets the decoupling scale to M_Z, which spoils the perturbative series and leads to bad convergence behavior. At this decoupling scale, a three-loop analysis is necessary to reduce the theoretical uncertainty to be of the same size as the experimental error of the top-quark pole mass. If these aspects are incorporated, the result for the running top-quark mass of the running-and-decoupling procedure is in quite good agreement with the SOFTSUSY result for small renormalization scales. The effects of Yukawa interactions in the determination of the strong coupling are of $\mathcal{O}(10^{-7})$ in $\alpha_s^{\overline{\text{DR}}}$ and therefore negligible.

5. Mass of the Lightest CP-Even Higgs Boson in the MSSM

In July of 2012, both CMS and ATLAS discovered the Higgs boson which was a huge milestone in particle physics. The combined uncertainty of the Higgs boson mass of the current measurements is about 0.3%:

$$M_h = 125.09 \pm 0.21 \pm 0.11 \text{ GeV} \qquad \text{ATLAS and CMS [123]} \tag{5.1}$$

In the SM, the mass of the Higgs boson is a free parameter but if one assumes the MSSM as the underlying theory, the masses of the Higgs bosons can be predicted. Here, the lightest CP-even Higgs boson is assumed to be the discovered one. It should be noted that there is also the possibility that a lighter Higgs boson exists which was neither detected by LEP [124] nor by LHC experiments [125]. This possibility is beyond the scope of this thesis and will not be discussed. By doing a high-precision analysis to determine the mass of the lightest Higgs boson one can exclude the MSSM scenarios whose resulting masses do not coincide with the experimental measurements, given in equation (5.1).

The dominant corrections to the CP-even Higgs boson self-energies originate from the top quark/squark sector and are proportional to $\alpha_t m_t^2 \sim m_t^4$, see e.g. [126]. At one-loop order, the corresponding diagrams are shown in Figure 5.1. In the following, the approximation by only taking into account the dominant terms in the electroweak sector $\sim \alpha_t m_t^2$ is denoted by m_t^4 approximation.

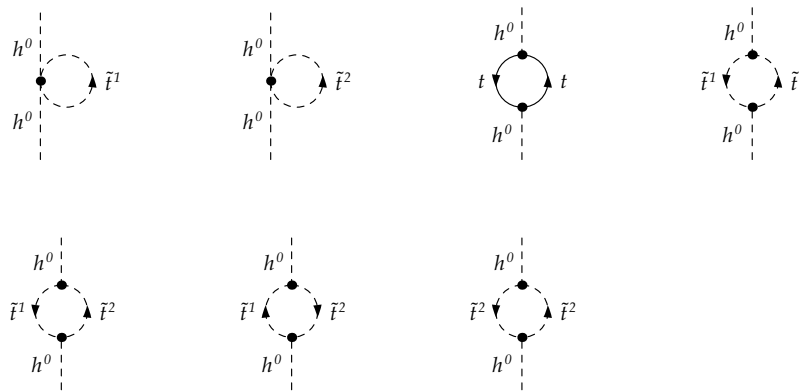Figure 5.1.: Dominant corrections to the Higgs boson mass at one-loop order

Currently, the commonly used computer programs to determine the mass of the lightest CP-even Higgs boson are `FeynHiggs` [127–131] which contains all numerically important two-loop corrections and includes resummations of large logarithms and `CPsuperH` [132,133] which is based on a renormalization group improved diagrammatic calculation.

5. Mass of the Lightest CP-Even Higgs Boson in the MSSM

In 2010, the computer program `H3.m` was released [126, 134, 135] which contains three-loop SQCD corrections to the CP-even Higgs boson self-energies in certain mass hierarchies in the m_t^4 approximation. In the following, these corrections will be simply denoted by $\mathcal{O}(\alpha_s^2 \alpha_t)$ corrections.

They are expressed in terms of $\overline{\text{DR}}$ instead of on-shell parameters for the sake of better convergence of the perturbative series, see Figure 8 of [126]. This was also studied recently in [136].

The basic workflow of `H3.m` is the following:

- `H3.m` makes use of `FeynHiggs` to compute the on-shell two-loop corrections.

- The exact corrections to the self-energies of the CP-even Higgs bosons up to $\mathcal{O}(\alpha_s \alpha_t, \alpha_t)$ in the on-shell scheme are computed by `H3.m` and subtracted from the FeynHiggs result.

- The exact corrections to the self-energies of the CP-even Higgs bosons up to $\mathcal{O}(\alpha_s \alpha_t, \alpha_t)$ and corrections of $\mathcal{O}(\alpha_s^2 \alpha_t)$ with parameters expressed in the $\overline{\text{DR}}$ scheme are computed by `H3.m` and added to the previous result.

Most $\overline{\text{DR}}$ and on-shell parameters can be taken from the output of the spectrum generator which is managed by `H3.m`. However, the mass of the lightest Higgs boson M_h is very sensitive to the value of $m_t^{\overline{\text{DR}}}$ due to the dominant m_t^4 terms. Numerically, a variation of one GeV in $m_t^{\overline{\text{DR}}}$ will result in a variation of approximately one GeV in M_h for SUSY masses of $\mathcal{O}(1\,\text{TeV})$. Therefore a precise determination of $m_t^{\overline{\text{DR}}}$ is crucial for the calculation of M_h. In order to resum large logarithms, the running-and-decoupling procedure for the determination of $m_t^{\overline{\text{DR}}}$ is used, as it is discussed in Chapter 4.

As it is shown in Section 4.4, the dependence of the running top-quark mass and the top Yukawa coupling on the renormalization scale strongly depends whether or not one includes electroweak interactions in the running-and-decoupling procedure. Since the on-shell Higgs boson mass is very sensitive to $m_t^{\overline{\text{DR}}}$ a consistent analysis is important to ensure stability of the on-shell Higgs boson mass regarding a variation of the unphysical renormalization scale. Therefore, if one includes electroweak interactions in the determination of the running top-quark mass and the top Yukawa coupling, one must also include electroweak interactions in the calculation of the on-shell Higgs boson mass to ensure renormalization-scale stability. The parameters $\alpha_s^{\overline{\text{DR}}}$, $\alpha_t^{\overline{\text{DR}}}$ and $m_t^{\overline{\text{DR}}}$ are computed according to the running-and-decoupling approach, discussed in Chapter 4. All other $\overline{\text{DR}}$ parameters are taken from the output of the spectrum generator[1].

In a first approach, `H3.m` is modified to determine the running top-quark mass using the running-and-decoupling procedure in SQCD. This modification among other features is included in the release of `H3.m` version 1.3 [83]. Details on the changelog of this version are given in Appendix D. In the recent version of `H3.m` which is not yet published also electroweak effects regarding the determination of the running top-quark mass $m_t^{\overline{\text{DR}}}$ and the top Yukawa coupling $y_t^{\overline{\text{DR}}}$ are included. To guarantee consistency, the analytic α_t^2 [32] corrections to the Higgs boson self-energies which are expressed through parameters of the $\overline{\text{DR}}$ and on-shell scheme are implemented which give the dominant contribution in the pure electroweak sector. The implementation of bottom and tau Yukawa

---

[1]To be precise, the $\overline{\text{DR}}$ stop masses are computed from the $\overline{\text{DR}}$ stop mass matrix using $m_t^{\overline{\text{DR}}}$ from the running-and-decoupling procedure.

corrections to the on-shell Higgs boson mass are not discussed in this thesis since their contributions are small for not too large values of t_β.

5.1. The Lightest CP-Even Higgs Boson Mass in the m_t^4 Approximation

Corrections to the Higgs boson self-energies in the m_t^4 approximation[2] up to $\mathcal{O}(\alpha_s^2 \alpha_t)$ with parameters expressed in the $\overline{\text{DR}}$ scheme are available in H3.m. The remaining one- and two-loop corrections are not included but can be taken from FeynHiggs.

In a first approach, only the dominant m_t^4 corrections are included in the determination of the lightest CP-even Higgs boson mass, in the following denoted by $M_h^{m_t^4}$. In this approach, the program FeynHiggs is not used[3]. Therefore, the restriction to $\mu_{\text{ren}} = M_t$ is not necessary enabling important checks regarding renormalization-scale stability, as it will be discussed in the following.

To fix the notation, the running top-quark mass and top Yukawa coupling obtained through the running-and-decoupling procedure including electroweak effects are denoted by $m_t^{\overline{\text{DR}}}$ and $y_t^{\overline{\text{DR}}}$, respectively. The corresponding parameters are labeled $m_t^{\overline{\text{DR}},\text{SUSY}}$ and $y_t^{\overline{\text{DR}},\text{SUSY}}$ if only strong interactions are taken into account in the RGEs and decoupling coefficients in the running-and-decoupling procedure. The result of the running top-quark mass obtained from SOFTSUSY is called $m_t^{\overline{\text{DR}},\text{SOFTSUSY}}$.

In Figure 5.2, the dependence of the on-shell Higgs boson mass in the m_t^4 approximation on the renormalization scale[4] is shown. This dependence is unphysical and due to the truncation of perturbative expansions. Hence, it can be used as a measure for theoretical uncertainties of $M_h^{m_t^4}$. The smallest shown value of the renormalization scale corresponds to $\mu_{\text{ren}} = M_Z$ and the vertical line to $\mu_{\text{ren}} = M_t$. The latter is chosen for the combination with the FeynHiggs result, as discussed in Section 5.2.

Varying the renormalization scale from $\mu_{\text{ren}} = 0.1 M_{\text{SUSY}}$ to $\mu_{\text{ren}} = 2 M_{\text{SUSY}}$ leads to a change in the Higgs boson mass of about 1 GeV using $m_t^{\overline{\text{DR}}}$ and $y_t^{\overline{\text{DR}}}$ in the corrections to the Higgs boson self-energies of $\mathcal{O}(\alpha_s^2 \alpha_t, \alpha_s \alpha_t, \alpha_t^2, \alpha_t)$, as shown in the solid black curve. Using $m_t^{\overline{\text{DR}},\text{SQCD}}$ and $y_t^{\overline{\text{DR}},\text{SQCD}}$ in the corrections to the Higgs boson self-energies of $\mathcal{O}(\alpha_s^2 \alpha_t, \alpha_s \alpha_t, \alpha_t)$ leads to a similar variation in $M_h^{m_t^4}$, as shown in the dashed-dotted black curve. However, using $m_t^{\overline{\text{DR}}}$ and $y_t^{\overline{\text{DR}}}$ in the corrections to the on-shell Higgs boson mass without $\mathcal{O}(\alpha_t^2)$ terms in the Higgs boson self-energies, increases the renormalization-scale dependence which leads to a change in $M_h^{m_t^4}$ of approximately 5 GeV in the shown range, displayed in the solid red curve. On the other hand, using $m_t^{\overline{\text{DR}},\text{SQCD}}$ and $y_t^{\overline{\text{DR}},\text{SQCD}}$ in the corrections to the Higgs boson self-energies including terms of $\mathcal{O}(\alpha_t^2)$ leads to a renormalization-scale dependence which is comparable in size

---

[2]regarding the one- and three-loop corrections to the self-energies, the two-loop results are directly taken from [?, 32]

[3]in contrast to the approach discussed in Section 5.2

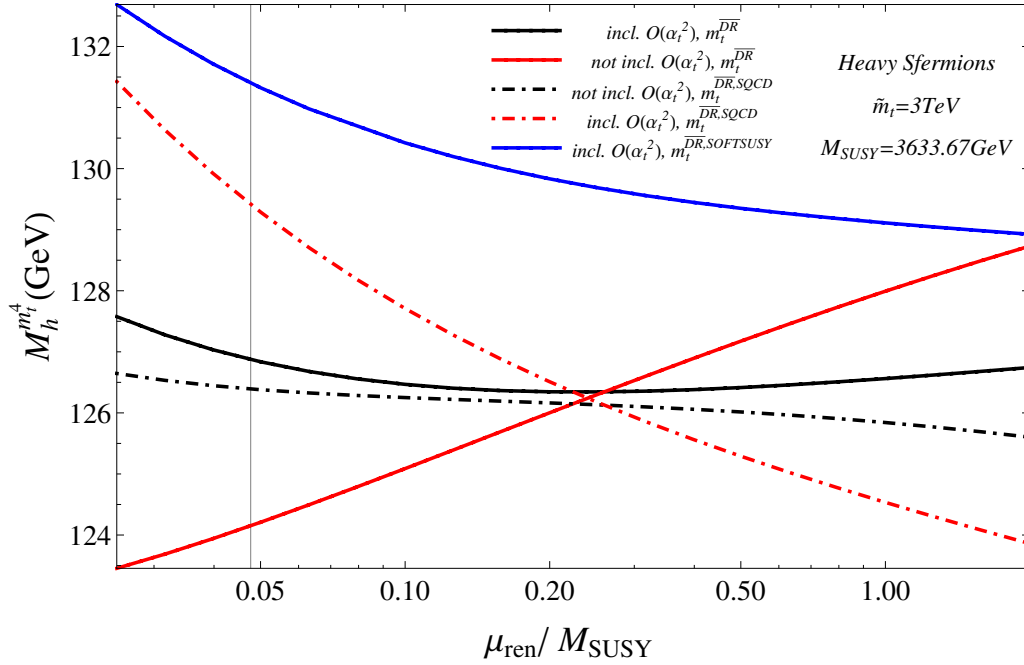[4]normalized to M_{SUSY} as defined in equation (4.2)

Figure 5.2.: Dependence of the on-shell Higgs boson mass on the renormalization scale in the Heavy Sfermions scenario. In the solid (dashed-dotted) curves $\alpha_t^{\overline{DR}}$ and $m_t^{\overline{DR}}$ are calculated with the running-and-decoupling procedure including (not including) electroweak effects. In the dashed-dotted red (black) curve α_t^2 corrections to the Higgs boson self-energies are (not) included. In the solid black (red) curve α_t^2 corrections to the Higgs boson self-energies are (not) included. The blue curve represents the result where the top-quark mass is obtained with SOFTSUSY and $\mathcal{O}(\alpha_t^2)$ corrections to the Higgs boson self-energies are included.

but with a different sign, as shown in the dashed-dotted red curve. Thus, the effects on the renormalization-scale dependence of electroweak corrections in the running-and-decoupling procedure for the determination of the running top-quark mass and top Yukawa coupling mainly compensate the effects on the renormalization-scale dependence of corrections to the on-shell Higgs boson self-energies of $\mathcal{O}(\alpha_t^2)$. For small renormalization scales, a naive[5] inclusion of $\mathcal{O}(\alpha_t^2)$ corrections appears to have a strong effect. The difference to the result without $\mathcal{O}(\alpha_t^2)$ corrections is approximately 3 GeV for $\mu_{\mathrm{ren}} = M_t$ and using $m_t^{\overline{DR},SQCD}$ and $y_t^{\overline{DR},SQCD}$, as can be seen by comparing the dashed-dotted black and red curves. However, due to the huge renormalization-scale dependence, a precise quantization of pure $\mathcal{O}(\alpha_t^2)$ effects is not possible. The effects of electroweak corrections to the running-and-decoupling analysis for the determination of the running top-quark mass and top Yukawa coupling together with the effects of $\mathcal{O}(\alpha_t^2)$ corrections to the Higgs boson self-energies amount to a change in $M_h^{m_t^4}$ of less than 1.2 GeV in the shown range, as can be seen by comparing the solid and dashed-dotted black curves. The renormalization-scale dependence of $M_h^{m_t^4}$ when using $m_t^{\overline{DR},SOFTSUSY}$ is strong and amounts to a change in the Higgs boson mass of about 3.7 GeV when

---

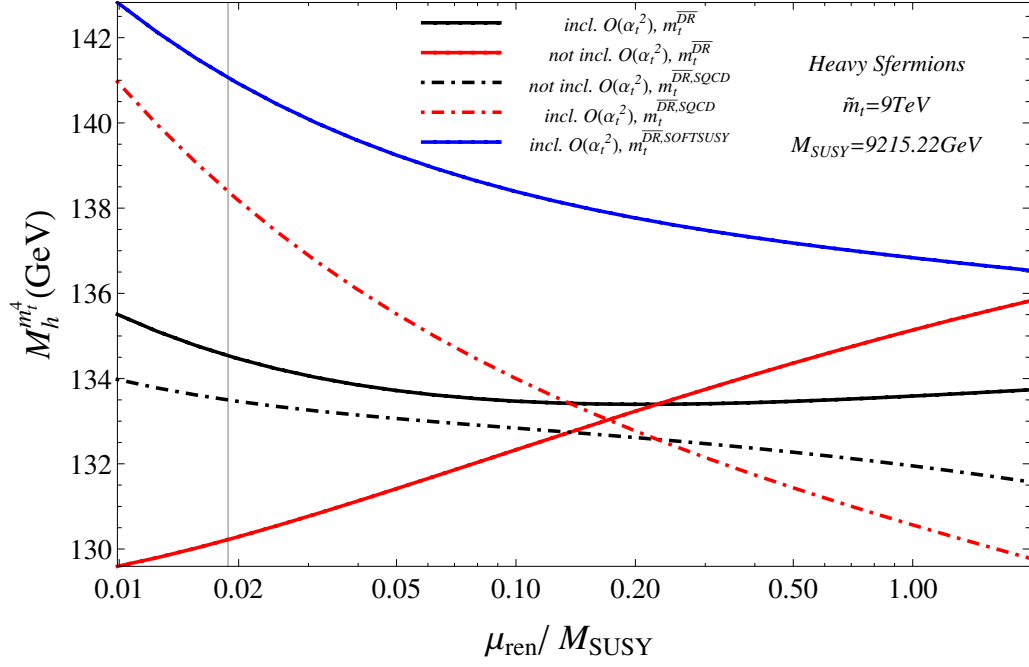[5]i.e. not using $m_t^{\overline{DR}}$

Figure 5.3.: Dependence of the on-shell Higgs boson mass on the renormalization scale in the Heavy Sfermions scenario. In the solid (dashed-dotted) curves $m_t^{\overline{\text{DR}}}$ is calculated with the running-and-decoupling procedure including (not including) electroweak effects. In the dashed-dotted red (black) curve α_t^2 corrections to the Higgs boson self-energies are (not) included. In the solid black (red) curve α_t^2 corrections to the Higgs boson self-energies are (not) included. The blue curve represents the result where the top-quark mass and top Yukawa coupling are obtained with SOFTSUSY and $\mathcal{O}(\alpha_t^2)$ corrections to the Higgs boson self-energies are included.

varying the renormalization scale in the same range, as can be seen in the blue curve. In Figure 5.3, the same curves as in the previous plot are shown but with $\tilde{m}_t = 9$ TeV. Qualitatively, the behavior of the different results w.r.t. a variation of the renormalization scale is very similar to the ones in Figure 5.2. However, the scale dependence of the dashed-dotted black curve is slightly worse. The change in $M_h^{m_t^4}$ when varying the renormalization scale in the shown range amounts to approximately 2.5 GeV. Regarding the solid black curve, the change in $M_h^{m_t^4}$ amounts to approximately 1.8 GeV. As expected, the red curves have a strong renormalization-scale dependence due to the inconsistent treatment of the running top-quark mass and top Yukawa coupling w.r.t. evaluating the Higgs boson self-energies. The change in $M_h^{m_t^4}$ is about 6 GeV for the solid and 11.5 GeV for the dashed-dotted red curve. Again, the scale-dependence of $M_h^{m_t^4}$ using $m_t^{\overline{\text{DR}},\text{SOFTSUSY}}$ is strong and leads to a change in $M_h^{m_t^4}$ of about 6.2 GeV for a variation of μ_{ren} in the shown range.

In Figure 5.4, the same curves as in Figure 5.2 and 5.3 are shown for the Heavy Higgs scenario. Including $\mathcal{O}(\alpha_t^2)$ corrections in the Higgs boson self-energies and electroweak interactions in the running-and-decoupling procedure leads to a change in $M_h^{m_t^4}$ of ap-
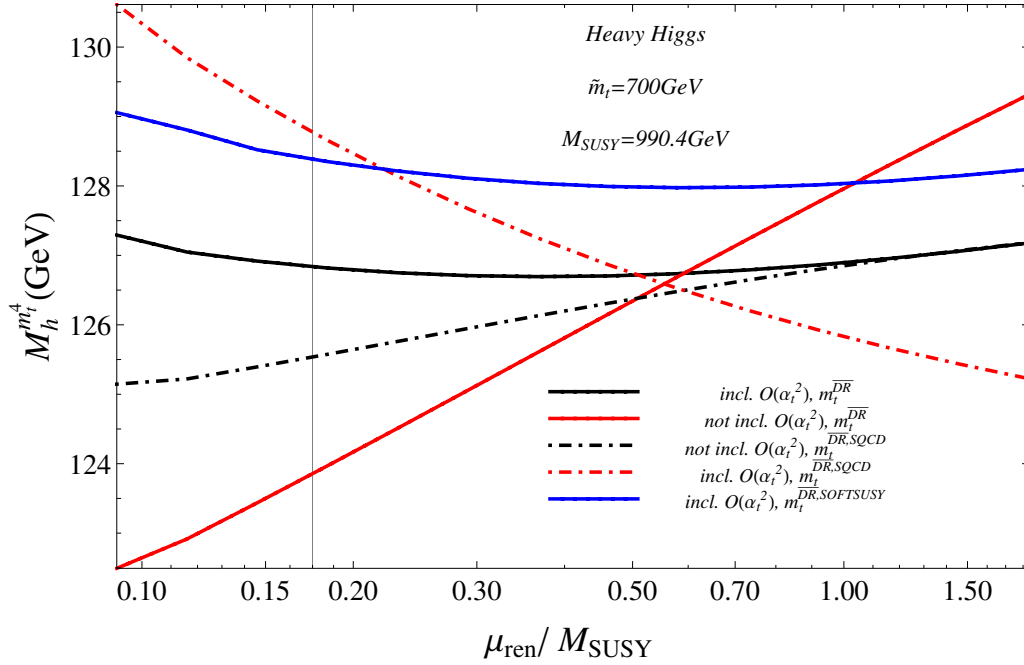
Figure 5.4.: Dependence of the on-shell Higgs boson mass on the renormalization scale in the Heavy Higgs scenario. In the solid (dashed-dotted) curves $m_t^{\overline{\text{DR}}}$ is calculated with the running-and-decoupling procedure including (not including) electroweak effects. In the dashed-dotted red (black) curve α_t^2 corrections to the Higgs boson self-energies are (not) included. In the solid black (red) curve α_t^2 corrections to the Higgs boson self-energies are (not) included. The blue curve represents the result where the top-quark mass and top Yukawa coupling are obtained with SOFTSUSY and $\mathcal{O}(\alpha_t^2)$ corrections to the Higgs boson self-energies are included.

proximately 0.5 GeV when varying μ_{ren} in the shown range, as can be seen in the solid black curve. Not including the $\mathcal{O}(\alpha_t^2)$ terms in the Higgs boson self-energy corrections and electroweak effects in the running-and-decoupling analysis will result in a change in $M_h^{m_t^4}$ of about 2 GeV in the given range, shown in the dashed-dotted black curve. As expected, the inconsistent analysis leads to a huge scale-dependence and the change in $M_h^{m_t^4}$ amounts to approximately 6.8 GeV for the solid and 5.5 GeV for the dashed-dotted red curve.

To complete the analysis regarding renormalization-scale stability of $M_h^{m_t^4}$, the cMSSM scenario is investigated in the following.
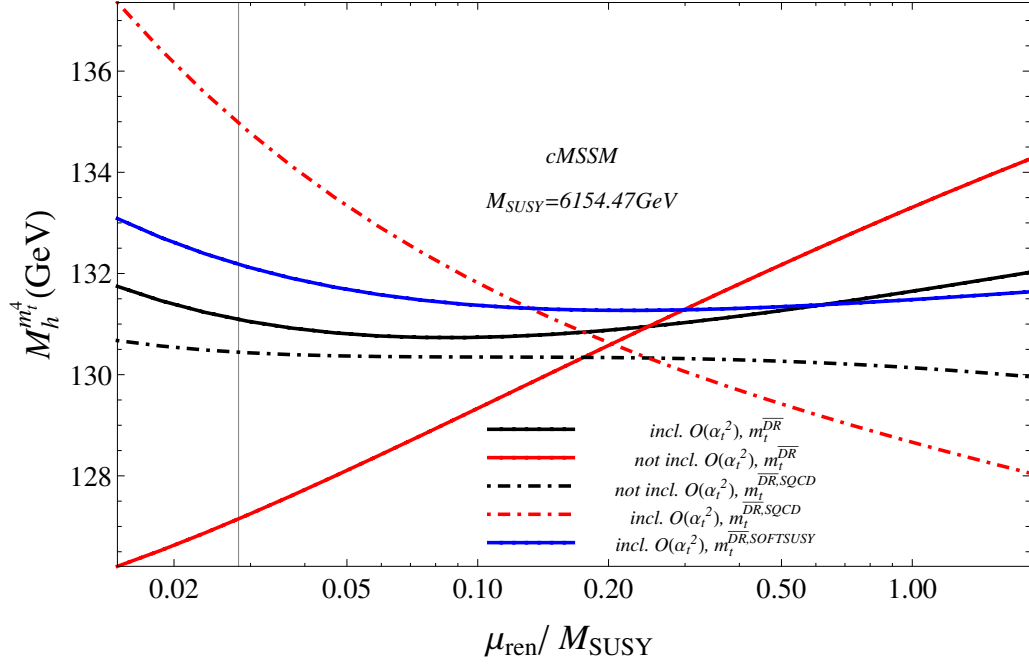
Figure 5.5.: Dependence of the on-shell Higgs boson mass on the renormalization scale in the cMSSM scenario. In the solid (dashed-dotted) curves $m_t^{\overline{\text{DR}}}$ is calculated with the running-and-decoupling procedure including (not including) electroweak effects. In the dashed-dotted red (black) curve α_t^2 corrections to the Higgs boson self-energies are (not) included. In the solid black (red) curve α_t^2 corrections to the Higgs boson self-energies are (not) included. The blue curve represents the result where the top-quark mass and top Yukawa coupling are obtained with SOFTSUSY and $\mathcal{O}(\alpha_t^2)$ corrections to the Higgs boson self-energies are included.

In Figure 5.5, the dependence of the on-shell Higgs boson mass on the renormalization scale in the cMSSM scenario is shown. The different curves in the plot have a similar behavior as the ones in Figure 5.2-5.4. However, since the result of the top-quark mass obtained with SOFTSUSY is assumed to also include three-loop RGEs and/or two-loop threshold corrections for this scenario, the resulting Higgs boson mass is expected to be near the result of the running-and-decoupling analysis, which is confirmed. Both the results with $m_t^{\overline{\text{DR}},\text{SOFTSUSY}}$ and with $m_t^{\overline{\text{DR}}}$ are stable up to difference of about 1.2 GeV in $M_h^{m_t^4}$ when varying the renormalization scale in the shown range, as can be seen in the blue and the solid black curve. The difference in $M_h^{m_t^4}$ for both results is smaller than 1.2 GeV and declines when increasing μ_{ren} up to about $\mu_{\text{ren}} = 0.6 M_{\text{SUSY}}$. The dashed-dotted black curve has a very weak dependence on μ_{ren} and the change in $M_h^{m_t^4}$ is about 0.7 GeV in the shown range. Again, a consistent analysis is crucial for a precise determination of the on-shell Higgs boson mass, as can be seen in the huge scale dependence of the red curves. The change in $M_h^{m_t^4}$ when varying the renormalization scale in the shown range amounts to approximately 8 GeV for the solid and 9.5 GeV for the dashed-dotted red curve.

In summary, the renormalization-scale dependence of the lightest CP-even Higgs boson mass in the m_t^4 approximation is stable up to a variation in $M_h^{m_t^4}$ of less than 2 GeV in the range $M_Z \leq \mu_\mathrm{ren} \leq 2M_\mathrm{SUSY}$ for all investigated scenarios. However, this is only the case, if a consistent analysis is done, i.e. (not) including electroweak corrections in the running-and-decoupling procedure for the determination of the running top-quark mass and top Yukawa coupling and (not) including the $\mathcal{O}(\alpha_t^2)$ corrections to the self-energies of the Higgs bosons.

5.2. The Lightest CP-Even Higgs Boson Mass

So far, only corrections of $\mathcal{O}(\alpha_s^2\alpha_t, \alpha_s\alpha_t, \alpha_t^2, \alpha_t)$ have been discussed. However, the complete set of one-loop corrections and the dominant two-loop corrections are available in `FeynHiggs`. To get a more precise value for the Higgs boson mass, one also has to include these corrections.

To accomplish this, the on-shell corrections of $\mathcal{O}(\alpha_s\alpha_t, \alpha_t)$ as well as corrections of $\mathcal{O}(\alpha_t^2)$ are subtracted from the full `FeynHiggs` on-shell self-energies. Then, corrections of the same order are added back where the parameters are expressed in the $\overline{\mathrm{DR}}$ scheme.

The renormalization scale of the `FeynHiggs` result must be set to $\mu_\mathrm{ren} = M_t$ [137] where $\overline{\mathrm{DR}}$ parameters appearing in the corrections to the self-energies have to be evaluated. Therefore, a variation of μ_ren for checks regarding renormalization-scale stability is not possible anymore. However, the previous analysis shows that at least corrections of $\mathcal{O}(\alpha_s^2\alpha_t, \alpha_s\alpha_t, \alpha_t^2, \alpha_t)$ are stable up to a difference in the Higgs boson mass of $\mathcal{O}(1\ \mathrm{GeV})$ for a very wide range of μ_ren when doing a consistent analysis, see Figures 5.2 - 5.5.

In Figure 5.6, the result of the Higgs boson mass including the remaining one- and two-loop self-energy corrections from `FeynHiggs` is shown in the Heavy Sfermions scenario. The black (orange) curves represent the three-loop (two-loop) results for which the respective remainder of the corrections to the self-energies at one- and two-loop level, denoted by FH_rem, is taken from `FeynHiggs 2.11.0`. In the red curves, the three-loop $M_h^{m_t^4}$ results are shown for which the remaining corrections from `FeynHiggs` are not included. For consistency, electroweak corrections in the determination of the running top-quark mass and top Yukawa coupling via the running-and-decoupling analysis are only included in the solid curves, where $\mathcal{O}(\alpha_t^2)$ corrections to the self-energies of the Higgs bosons are included. For comparison, the stand-alone results of `FeynHiggs` are displayed. In the dotted (dashed) green curve, the two-loop `FeynHiggs` result is shown where the top-quark mass is expressed in the on-shell ($\overline{\mathrm{MS}}$) scheme. In the solid green curve, the `FeynHiggs` flag `looplevel` is set to 3 which corresponds to an all-order resummation of the leading and subleading contributions from the stop sector. A resummation of large logarithms is also accomplished by calculating the running top-quark mass and top Yukawa coupling via the running-and-decoupling method which enables a reasonable comparison. The blue curve represents the result for the Higgs boson mass which is directly computed by `SOFTSUSY`. The gray band represents the measured Higgs boson mass, as shown in equation (5.1).

One can see that the resummed `FeynHiggs` result, shown in the solid green curve, is very close to the two-loop result where the parameters in the $\mathcal{O}(\alpha_s\alpha_t, \alpha_t)$ corrections are cal-
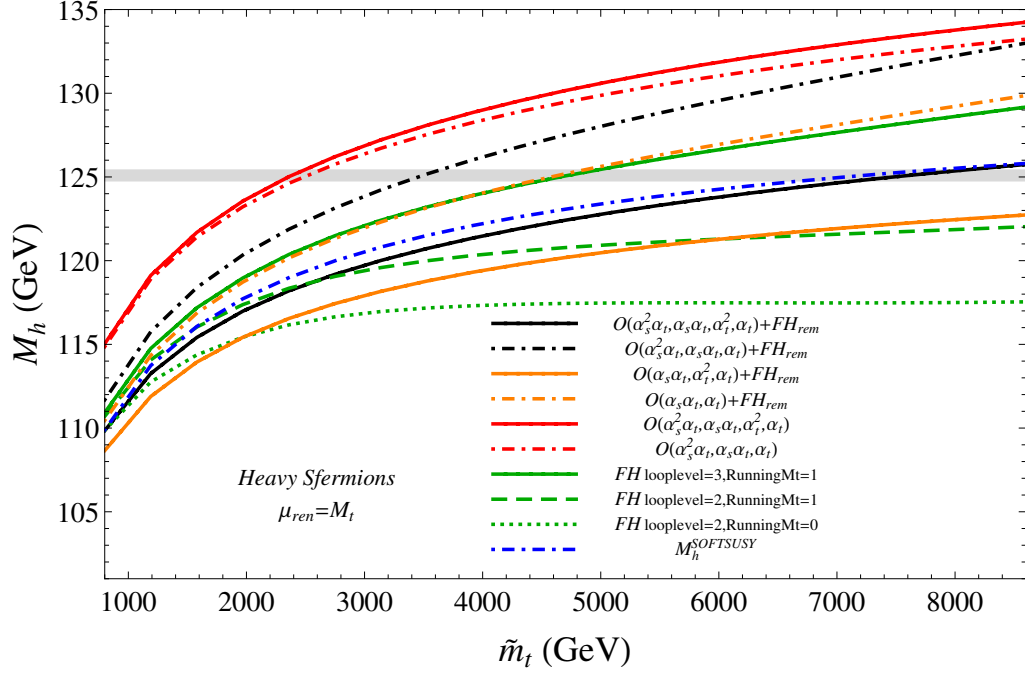
Figure 5.6.: Dependence of the on-shell Higgs boson mass on the parameter $\tilde{m}_t$ in the Heavy Sfermions scenario. The black (orange) curves represent the three-loop (two-loop) results for which the respective remainder of the corrections to the self-energies at two-loop level is taken from `FeynHiggs 2.11.0`. In the red curves, the three-loop results are shown for which the missing corrections from `FeynHiggs` are not included. In the dotted-dashed black and red curves, the Yukawa interactions are not included in the running-and-decoupling procedure for the determination of $m_t^{\overline{\text{DR}}}$ and $\mathcal{O}(\alpha_t^2)$ corrections to the Higgs boson self-energies are not expressed in terms of $\overline{\text{DR}}$ parameters. In the dotted (dashed) green curve, the two-loop `FeynHiggs` result is shown where the top-quark mass is expressed in the on-shell ($\overline{\text{MS}}$) scheme. In the solid green curve, the `FeynHiggs` flag `looplevel` is set to 3. The blue curve shows the result by `SOFTSUSY`. The gray band represents the measured Higgs boson mass.

culated in the $\overline{\text{DR}}$ scheme with the running top-quark mass and top Yukawa coupling obtained with the SQCD running-and-decoupling analysis, as shown in the dashed-dotted orange curve. The difference amounts to less than 1 GeV for the shown range of $\tilde{m}_t$.

However, for high values of $\tilde{m}_t$ there is a difference of about 6 GeV to the resummed `FeynHiggs` result when using the $\overline{\text{DR}}$ scheme for the parameters also for the $\mathcal{O}(\alpha_t^2)$ corrections and electroweak effects in the running-and-decoupling analysis for the determination of the running top-quark mass and top Yukawa coupling, as shown in the orange solid curve.

It is unclear how this discrepancy occurs. The running-and-decoupling approach for resumming large logarithms is different from the method which is implemented in `FeynHiggs` and therefore, a step-by-step comparison is not possible. Different sources of errors have been investigated. Complications can either arise in the subtraction proce-

dure of on-shell corrections of $\mathcal{O}(\alpha_t^2)$ to the self-energies of the `FeynHiggs` result[6] or in the calculation and implementation of corrections of the same order expressed through $\overline{\text{DR}}$ parameters. In the subtraction procedure of the $\mathcal{O}(\alpha_t^2)$ terms of the self-energies, the same parameters are used as in `FeynHiggs`[7]. The $\mathcal{O}(\alpha_t^2)$ corrections to the self-energies in the on-shell scheme are directly taken from [32, 138]. Regarding the $\overline{\text{DR}}$ corrections of $\mathcal{O}(\alpha_t^2)$, renormalization-scale stability with variations of the Higgs boson mass below 2 GeV indicates consistency with the determination of the running top-quark mass and top Yukawa coupling through the running-and-decoupling procedure which is an important check. Also, the implementation of $\mathcal{O}(\alpha_t^2)$ corrections in `H3.m` leads to a result which is in agreement with the right plot of Figure (2) in [32], when using the same[8] input numbers as the authors.

Regarding the determination of the running top-quark mass for the Higgs boson self-energies, the philosophy of the running-and-decoupling approach at three-loop order clearly differs from the `FeynHiggs` approach. In the latter, only a one-loop conversion from the top-quark pole mass to the $\overline{\text{MS}}$ mass is done [136] which is in principle compatible with the required two-loop precision of the Higgs boson self-energies. However, higher order corrections in the relation between the top-quark pole and $\overline{\text{MS}}$ mass are important and are of $\mathcal{O}(\text{GeV})$, see e.g. [88]. Therefore, it is advisable to use a more precise value of $m_t^{\overline{\text{DR}}}$. However, the analysis must be consistent regarding renormalization-scale stability of the on-shell Higgs boson mass. In the running-and-decoupling approach for the determination of the running top-quark mass for the Higgs boson self-energies, this requirement is not spoiled.

In `SOFTSUSY`, the leading two-loop corrections are implemented in the calculation of the CP-even Higgs boson masses. The small difference of $\lesssim 1$ GeV between the three-loop analysis and the `SOFTSUSY` result is therefore assumed to be accidental, as can be seen by comparing the solid black and dashed-dotted blue curve.

Adding the three-loop corrections to the self-energies, displayed by changing the color of the curves from orange to black, will result in a positive shift of the Higgs boson mass up to approximately 3 GeV for high values of $\tilde{m}_t$ in the given range.

The shift of the `FeynHiggs` result w.r.t. changing the renormalization scheme of the top-quark mass[9] amounts to about 4.5 GeV for $\tilde{m}_t = 8600$ GeV and demonstrates the sensitivity of the Higgs boson mass on m_t, as can be seen by comparing the dotted and dashed green curve.

The values of $\tilde{m}_t$ for which the experimental value of the measured Higgs boson mass of approximately 125 GeV is reached, strongly depends on the analysis. In the case where $\mathcal{O}(\alpha_s^2\alpha_t, \alpha_s\alpha_t, \alpha_t^2, \alpha_t)$ corrections are expressed in $\overline{\text{DR}}$ parameters and the running top-quark mass and top Yukawa coupling are obtained via the running-and-decoupling procedure including electroweak effects, $\tilde{m}_t$ must be $\gtrsim 7$ TeV, as can be seen by the

---

[6]Thanks goes to T. Hahn for fixing an important bug in the function `FHAddSelf`. This fix is included in `FeynHiggs` $\geq$`2.11.0`.

[7]It turns out that not all parameters are given in the on-shell scheme. The gluino mass, extracted by the function `FHGetPara`, is the $\overline{\text{DR}}$ mass and the stop masses slightly differ from the ones of the output of `SOFTSUSY`. However, it is unlikely that slightly different parameters are the reason for the big discrepancy in M_h.

[8]A precise comparison is not possible since the exact value of $\alpha_s^{\overline{\text{DR}}}$ is not given in [32].

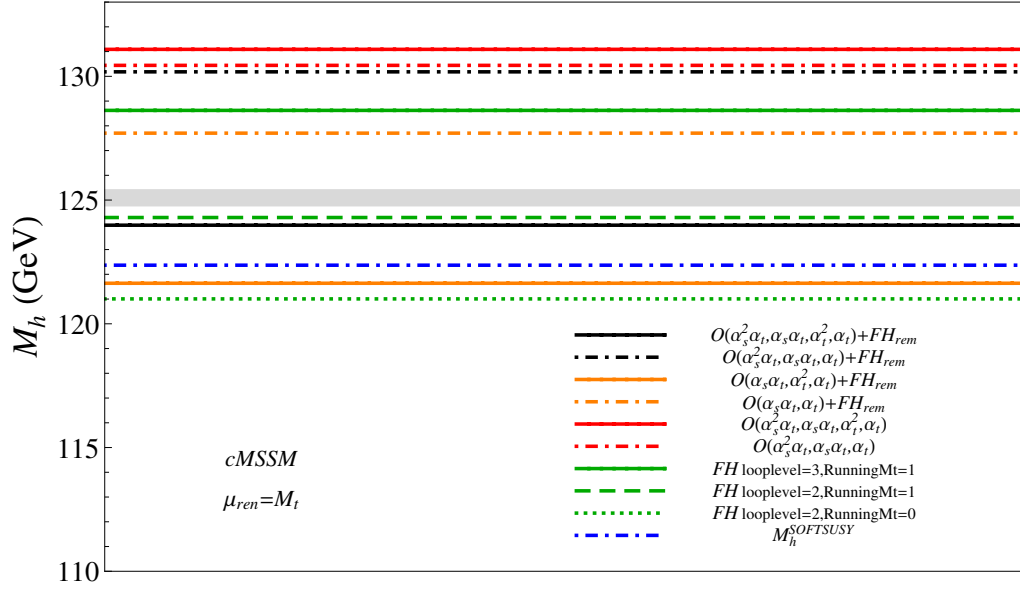[9]from on-shell to $\overline{\text{MS}}$

Figure 5.7.: The value of the on-shell Higgs boson mass in the cMSSM scenario. The black (orange) lines represent the three-loop (two-loop) results for which the respective remainder of the corrections to the self-energies at two-loop level is taken from `FeynHiggs 2.11.0`. In the red lines, the three-loop results are shown for which the missing corrections from `FeynHiggs` are not included. In the dotted (dashed) green line, the two-loop `FeynHiggs` result is shown where the top-quark mass is expressed in the on-shell ($\overline{\text{MS}}$) scheme. In the dotted-dashed black and red line, the Yukawa interactions are not included in the running-and-decoupling procedure for the determination of $m_t^{\overline{\text{DR}}}$ and $\mathcal{O}(\alpha_t^2)$ corrections to the Higgs boson self-energies are not expressed in terms of $\overline{\text{DR}}$ parameters. In the solid green line, the `FeynHiggs` flag `looplevel` is set to 3. The blue line shows the result by `SOFTSUSY`. The gray band represents the measured Higgs boson mass.

intersection of the black solid curve with the gray band. Without expressing the parameters of the $\mathcal{O}(\alpha_t^2)$ corrections in the $\overline{\text{DR}}$ scheme and using the SQCD values for the running top-quark mass and Yukawa coupling, the experimental value can be reached for $\tilde{m}_t \approx 3500 - 4500$ GeV, as can be seen by the intersections of the dashed-dotted black curve with the gray band.

In Figure 5.7, the same analysis is done for the cMSSM scenario. For the reader's convenience, the plotting style was adapted from the previous figure.

Qualitatively, the results are very similar to the ones of the Heavy Sfermions scenario. The difference between the two-loop analysis, where the parameters in the corrections of $\mathcal{O}(\alpha_s\alpha_t, \alpha_t)$ to the Higgs boson self-energies are expressed with $\overline{\text{DR}}$ parameters taking into account the running top-quark mass and top Yukawa coupling of the SQCD running-and-decoupling procedure and the resummed `FeynHiggs` result amounts to approximately 1 GeV, as can be seen by comparing the solid green and the dashed-dotted orange curve. Again, including corrections of $\mathcal{O}(\alpha_t^2)$ with the parameters expressed in the $\overline{\text{DR}}$ instead of the on-shell scheme and taking into account electroweak interactions in the running-and-decoupling procedure leads to a reduction of the value of the Higgs

boson mass of about 6 GeV, as can be seen by comparing the dashed-dotted with the solid black and orange curves. The three-loop result of this analysis is compatible with the experimental value, if theoretical errors of at least ± 1 GeV are taken into account. The difference between the `FeynHiggs` result when using the $\overline{\text{MS}}$ instead of the on-shell top-quark mass, amounts to approximately 3 GeV, by comparing the dotted with the dashed green curve. The result of the Higgs boson mass of `SOFTSUSY`, shown as the dashed-dotted blue curve, is only about 1 GeV higher than the solid orange curve.

In summary, the result of the lightest CP-even Higgs boson mass is calculated based on using the one- and two-loop on-shell self-energy corrections from `FeynHiggs` except corrections of $\mathcal{O}(\alpha_s^2 \alpha_t, \alpha_s \alpha_t, \alpha_t^2, \alpha_t)$ which are calculated in terms of $\overline{\text{DR}}$ parameters whereas the improved result for the running top-quark mass through the running-and-decoupling procedure is used. In this way, large logarithms are resummed which enables a comparison with the resummed `FeynHiggs` result. One observes a significant difference whose origin is not yet known. However, if only SQCD corrections are included in the running-and-decoupling procedure for the determination of $m_t^{\overline{\text{DR}}}$ and $\mathcal{O}(\alpha_t^2)$ corrections to the Higgs boson self-energies are expressed through on-shell parameters, the difference to the resummed `FeynHiggs` result is within the theoretical error.

6. Summary

The decoupling coefficients ζ_{g_s}, $\zeta_{y_{t,b}}$ and $\zeta_{m_{t,b}}$ w.r.t. the SM as the effective theory and the MSSM as the full theory were computed in the decoupling limit up to $\mathcal{O}(\alpha_s^2, \alpha_s \alpha_{t,b,\tau}, \alpha_{s,t,b,\tau,1,2})$. At $\mathcal{O}(\alpha_s^2, \alpha_{s,t,b,\tau,1,2})$, the full mass dependence was taken into account and at $\mathcal{O}(\alpha_s \alpha_{t,b,\tau})$, the gauge-less limit was applied and a common SUSY mass scale was chosen.

The relevant decoupling coefficients ζ_{m_t}, ζ_{y_t} and ζ_{g_s} were used to determine the $\overline{\text{DR}}$ top-quark mass, top Yukawa coupling and strong coupling in the MSSM, based on experimental values of SM parameters and certain choices of MSSM spectra.

In order to resum large logarithms, RGEs of the SM were used to evolve the masses and couplings to an arbitrary decoupling scale at which the decoupling takes place. Then, MSSM RGEs were used to run the parameters to the desired renormalization scale.

For the numerical analysis of this procedure, three different MSSM scenarios were investigated. An estimation of the theoretical error was done by varying the unphysical decoupling scale. In all analyzed scenarios, three-loop RGEs and two-loop decoupling coefficients reduced the scale dependence of the top-quark mass to about 100 MeV, which is is sufficiently precise w.r.t. the experimental error on the on-shell top-quark mass of $\mathcal{O}(1 \text{ GeV})$.

As an example, the mass of the lightest CP-even Higgs boson was calculated by modifying the existing computer program `H3.m` to take into account the improved determination of the running top-quark mass and the top Yukawa coupling.

Consistency regarding the different renormalization-scale dependence of the running top-quark mass and top Yukawa coupling whether or not one includes electroweak corrections in the running-and-decoupling analysis was observed by investigating the unphysical renormalization-scale dependence of the on-shell Higgs boson mass at $\mathcal{O}(\alpha_s^2 \alpha_t, \alpha_s \alpha_t, \alpha_t^2, \alpha_t)$ and $\mathcal{O}(\alpha_s^2 \alpha_t, \alpha_s \alpha_t, \alpha_t)$, respectively.

Since not all known corrections to the Higgs boson self-energies are available, the missing one- and two-loop corrections were taken from `FeynHiggs`. In a first approach, the on-shell self-energy corrections of order $\mathcal{O}(\alpha_s^2 \alpha_t, \alpha_s \alpha_t, \alpha_t)$ were subtracted from the `FeynHiggs` result and added back again but with parameters expressed in the $\overline{\text{DR}}$ scheme. For the $\overline{\text{DR}}$ top-quark mass, the result from the SQCD running-and-decoupling procedure was used. At two-loop order, agreement with the resumed `FeynHiggs` result was observed. The relevant changes, among other features, were included in version 1.3 of `H3.m`. In a second approach, electroweak corrections in the running-and-decoupling analysis for the determination of the top-quark mass were included. To be consistent, also the corrections to the Higgs boson self-energies of $\mathcal{O}(\alpha_t^2)$ were subtracted from the on-shell `FeynHiggs` result and added back but with parameters expressed in the $\overline{\text{DR}}$ scheme. A significant difference to the resummed `FeynHiggs` result was found, whose origin is yet unclear.

Acknowledgments

First of all, I want to thank Matthias Steinhauser and Luminita Mihaila for supervising my PhD thesis and many helpful discussions from which I profited in countless ways.

Secondly, I would like to thank Philipp Kant for the possibility to maintain and improve `H3.m` which proved to be a good application for the running top-quark mass and the top Yukawa coupling in the MSSM.

I want to thank Nikolai Zerf for many useful programs and his support regarding the development of `H3.m`.

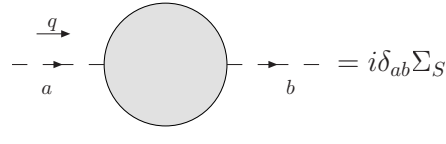I would like to thank my colleagues for the good atmosphere.

Last but not least, special thanks goes to my loved ones for supporting me.

A. Lorentz Structure of Self-Energies

In the following, the decompositions of one-particle-irreducible diagrams (shown as gray circles) are listed. The external momentum is denoted by q, color charges by a and b.
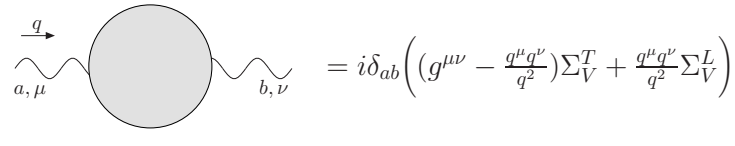
A.1. Scalars

Scalar particles do not have a Lorentz structure. Thus, only a factor i and the color structure δ_{ab} are extracted.

$$- \xrightarrow{q} \bigcirc \xrightarrow{} - = i\delta_{ab}\Sigma_S$$

$$\text{(A.1)}$$

A.2. Vector Bosons
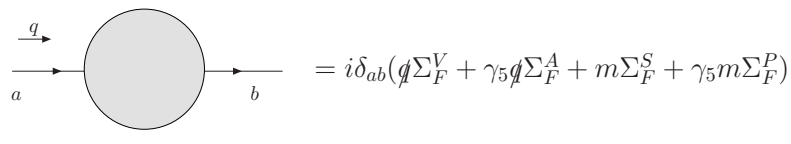
The self-energies of vector bosons Σ_V can be decomposed into a transversal part Σ_V^T and a longitudinal part Σ_V^L.

$$\xrightarrow{q} \bigcirc = i\delta_{ab}\left((g^{\mu\nu} - \tfrac{q^\mu q^\nu}{q^2})\Sigma_V^T + \tfrac{q^\mu q^\nu}{q^2}\Sigma_V^L\right)$$

$$\text{(A.2)}$$

A.3. Fermions
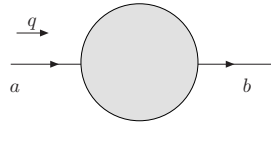
The self-energy of a fermion F with mass m can be decomposed into a scalar part Σ_F^S, a vector part Σ_F^V, an axial part Σ_F^A and a pseudoscalar part Σ_F^P.

$$\xrightarrow{q} \bigcirc \xrightarrow{} = i\delta_{ab}(\slashed{q}\Sigma_F^V + \gamma_5\slashed{q}\Sigma_F^A + m\Sigma_F^S + \gamma_5 m\Sigma_F^P)$$

$$\text{(A.3)}$$

In an alternative way, one can decompose the fermion self-energy into a left/right handed scalar and vector part.

A. Lorentz Structure of Self-Energies

$$= i\delta_{ab}(mP_L\Sigma_F^{LS} + mP_R\Sigma_F^{RS} + \slashed{q}P_L\Sigma_F^{LV} + \slashed{q}P_R\Sigma_F^{RV})$$

(A.4)

B. Example of `QGRAF.dat`

This example file generates diagrams for the $h^0 \bar{t} t$ vertex of $\mathcal{O}(\alpha_s^2, \alpha_s \alpha)$ only taking into account one-particle-irreducible diagrams with at least one heavy internal particle.

B.1. `QGRAF.dat`

```
output = 'outfile' ;
style = 'q2enew.sty' ;
model = 'MSSM.lag' ;
in = ft ,h0 ,fT   ;
out =   ;
loops = 2 ;
loop_momentum = k ;
options =   ;

* vevs from gauge bosons and epsilon scalars vanish
true = sbridge[gamma, Z0t, Z0l, Wminust, Wminusl, g,
es, esgamma, esZ0, esWminus, 0, 0] ;

* include at least one heavy particle
false = iprop[fchi01, fchi02, fchi03, fchi04,
fchi1, fchi2, fg, H0, A0, Hminus,
snuel, snumu, snutau, sel1, sel2, smu1, smu2, stau1, stau2,
su1, su2, sc1, sc2, st1, st2, esgamma, esZ0, es, esWminus,
sd1, sd2, ss1, ss2, sb1, sb2, 0, 0] ;

* diagram must be proportional to the strong coupling,
* vertices have to be defined in MSSM.lag
* according to e.g.
* [H0, sc2, Sc2; gpow = '0']
* or
* [St1, st1, Sb1, sb1; gpow = '2']
true = vsum[gpow, 2, 8];

* only include 1 PI diagrams
true = bridge[g, gamma, Z0t, Z0l, Wminust, Wminusl,
es, esgamma, esZ0, esWminus,
c, cgamma, cz, cplus, cminus, fchi01, fchi02, fchi03, fchi04,
fchi1, fchi2, fg, h0, H0, A0, Hminus, G0, Gminus,
snuel, snumu, snutau, sel1, sel2, smu1, smu2, stau1, stau2,
fnuel, fnumu, fnutau, fel, fmu, ftau,
su1, su2, sc1, sc2, st1, st2, fu, fc, ft,
sd1, sd2, ss1, ss2, sb1, sb2, fd, fs, fb, 0, 0];
```

C. MSSM Scenarios

In the following, the mass spectra of the scenarios used for the numerical analysis in Chapter 4 and Chapter 5 are shown. The MSSM models are defined in Section 4.2. The values are given in units of GeV.

C.1. 'Heavy Higgs'

$$
\begin{aligned}
&M_{\tilde{g}} = 876.65, &&M_{\tilde{t}_1} = 331.00, &&M_{\tilde{b}_1} = 1012.88, &&M_{\tilde{c}_l} = 1028.88, \\
&M_{\tilde{c}_r} = 1028.91, &&M_{\tilde{s}_l} = 1031.70, &&M_{\tilde{s}_r} = 1029.46, &&M_{\tilde{u}_l} = 1028.88, \\
&M_{\tilde{u}_r} = 1028.91, &&M_{\tilde{d}_l} = 1031.70, &&M_{\tilde{d}_r} = 1029.46, &&M_A = 1000.00, \\
&M_{H^\pm} = 1003.57, &&M_{H^0} = 1000.05, &&M_{\chi_1^0} = 86.72, &&M_{\chi_2^0} = 158.41, \\
&M_{\chi_3^0} = 211.13, &&M_{\chi_4^0} = 271.12, &&M_{\chi_1^\pm} = 154.30, &&M_{\chi_2^\pm} = 270.33, \\
&M_{\tilde{\nu}_e} = 999.24, &&M_{\tilde{\nu}_\mu} = 999.24, &&M_{\tilde{\nu}_\tau} = 998.40, &&M_{\tilde{e}_1} = 1002.63, \\
&M_{\tilde{e}_2} = 1001.51, &&M_{\tilde{\mu}_1} = 1002.63, &&M_{\tilde{\mu}_2} = 1001.51, &&M_{\tilde{\tau}_1} = 999.66, \\
&M_{\tilde{\tau}_2} = 1001.92, &&M_{\tilde{t}_2} = 1045.29, &&M_{\tilde{b}_2} = 1027.31, &&\tilde{m}_t = 350.00
\end{aligned}
$$

C.2. 'Heavy Sfermions'

$$
\begin{aligned}
&M_{\tilde{g}} = 1762.43, &&M_{\tilde{t}_1} = 3008.54, &&M_{\tilde{b}_1} = 3030.91, &&M_{\tilde{c}_l} = 4049.37, \\
&M_{\tilde{c}_r} = 4042.41, &&M_{\tilde{s}_l} = 4050.03, &&M_{\tilde{s}_r} = 4041.94, &&M_{\tilde{u}_l} = 4049.37, \\
&M_{\tilde{u}_r} = 4042.41, &&M_{\tilde{d}_l} = 4050.03, &&M_{\tilde{d}_r} = 4041.94, &&M_A = 1000.00, \\
&M_{H^\pm} = 1003.48, &&M_{H^0} = 1000.06, &&M_{\chi_1^0} = 202.93, &&M_{\chi_2^0} = 208.35, \\
&M_{\chi_3^0} = 1495.94, &&M_{\chi_4^0} = 1556.03, &&M_{\chi_1^\pm} = 205.62, &&M_{\chi_2^\pm} = 1556.05, \\
&M_{\tilde{\nu}_e} = 4008.29, &&M_{\tilde{\nu}_\mu} = 4008.29, &&M_{\tilde{\nu}_\tau} = 4006.59, &&M_{\tilde{e}_1} = 4009.42, \\
&M_{\tilde{e}_2} = 4004.71, &&M_{\tilde{\mu}_1} = 4009.42, &&M_{\tilde{\mu}_2} = 4004.71, &&M_{\tilde{\tau}_1} = 4001.28, \\
&M_{\tilde{\tau}_2} = 4007.75, &&M_{\tilde{t}_2} = 3034.18, &&M_{\tilde{b}_2} = 4034.17, &&\tilde{m}_t = 3000.00
\end{aligned}
$$

C.3. 'cMSSM'

$$
\begin{array}{llll}
M_{\tilde{g}} = 1964.83, & M_{\tilde{t}_1} = 4304.76, & M_{\tilde{b}_1} = 4899.72, & M_{\tilde{c}_l} = 7315.54, \\
M_{\tilde{c}_r} = 7315.14, & M_{\tilde{s}_l} = 7315.85, & M_{\tilde{s}_r} = 7314.77, & M_{\tilde{u}_l} = 7316.02, \\
M_{\tilde{u}_r} = 7315.18, & M_{\tilde{d}_l} = 7316.33, & M_{\tilde{d}_r} = 7315.70, & M_A = 1695.80, \\
M_{H^\pm} = 1697.93, & M_{H^0} = 1695.75, & M_{\chi_1^0} = 355.85, & M_{\chi_2^0} = 487.93, \\
M_{\chi_3^0} = 498.28, & M_{\chi_4^0} = 722.37, & M_{\chi_1^\pm} = 483.14, & M_{\chi_2^\pm} = 722.50, \\
M_{\tilde{\nu}_e} = 7240.27, & M_{\tilde{\nu}_\mu} = 7237.12, & M_{\tilde{\nu}_\tau} = 6265.69, & M_{\tilde{e}_1} = 7241.05, \\
M_{\tilde{e}_2} = 7239.89, & M_{\tilde{\mu}_1} = 7237.90, & M_{\tilde{\mu}_2} = 7233.57, & M_{\tilde{\tau}_1} = 5098.68, \\
M_{\tilde{\tau}_2} = 6266.55, & M_{\tilde{t}_2} = 4905.19, & M_{\tilde{b}_2} = 5409.09 &
\end{array}
$$

D. `H3.m` Version 1.3

D.1. Introduction

`H3.m` [126] is a `Mathematica` package for evaluating the mass of the lightest CP-even Higgs boson within the MSSM to three loop accuracy. In 2014, version 1.3 of `H3.m` was published [83]. Its new features including details on the internal structure are described in the following.

D.2. Functions that Set Up or Retrieve Parameters

To define various parameters used in the calculation it is a common practice to make use of the SUSY Les Houches Accord (SLHA) interface [101, 102]. It includes a unique set of conventions for supersymmetric extensions of the Standard Model together with generic file structures. Since most spectrum generators (e.g. `SOFTSUSY` [103]) handle their input variables according to the SLHA interface, it is feasible to include a robust SLHA interface into `H3.m`.

In previous versions of `H3.m` a self-written routine handled the reading and writing of SLHA files. Since conventions of the SLHA structure might change in future versions, it is easier to rely on an external program which is specialized to handle those files. The `MATHEMATICA` package `SLAM` [139] proves to be a more robust way to take care of this requirement. In `H3.m` version 1.3, `SLAM` is used per default. To enable backward compatibility the old routine was not removed and remains as an optional choice. An additional feature of `SLAM` is the possibility to create a spectrum SLHA file out of built-in scenarios (e.g. msugra) for which the user can directly specify its input parameters. Also the user can create a spectrum SLHA file by defining a complete model.

The SLHA spectrum file should contain at least the following data:

Block	Required Entries
SMINPUTS	2, 3, 4, 5, 6
GAUGE	1, 2, 3
HMIX	1, 2, 3
MSOFT	3, 41 - 49
AU	(3, 3)
YU	(3, 3)
MASS	36, 1000021,
	1000001-1000006,
	2000001-2000006
STOPMIX	(1, 1)
STOPMIX	(1, 2)
STOPMIX	(2, 1)
STOPMIX	(2, 2)

In order to properly determine the mixing angle, all four STOPMIX entries have to be given. For more information see Section D.2.1.2.

D.2.1. H3GetSLHA

The function H3GetSLHA parses an SLHA spectrum file and sets the parameters for the calculation accordingly. Then, it passes the file to FeynHiggs. If the SLHA path is set to "Null" or the path doesn't lead to a file, SLAM is used to generate an SLHA file. Additionally, the $\overline{\text{DR}}$ top-quark mass and the strong coupling constant are calculated within SQCD.

D.2.1.1. Options

- **useSLAM**: If True, use SLAM to take care of the SLHA service.

- **SpectrumGenerator**: Set spectrum generator, e.g. "softsusy"

- **calcmt**: Define which methods are used to calculate the top-quark mass, e.g. {"Mtdec"} or {"Mtdec", "MtTSIL"}. Possible strings in braces are "Mtdec" (decoupling method), "MtTSIL" (fixed order calculation using TSIL, not recommended), "Mtspect" (out of spectrum generator, not recommended).

- **usemt**: Define which method for the top-quark mass is used for H3m[]. Possible strings are "Mtdec", "MtTSIL" or "Mtspect".

D.2.1.2. Internal Structure

The inner workings of SLAM are documented in the official documentation. Here I review the main aspects.

First, one defines an input request list where one can store the values of the needed parameters into local variables. If no file is given, SLAM creates a spectrum via SLAM'ObtainLesHouchesSpectrum.

Otherwise `SLAM` will read the SLHA file with the function
`SLAM'ReadLesHouchesSpectrumFile`.
One has to include an extra block ("EXTPAR") in the SLHA file for it to be properly read by `FeynHiggs`. It contains information about the renormalization scale at which the parameters (and later the Higgs boson mass) are calculated.

With the obtained parameters one can compute the quantities needed in the calculation, e.g. the mixing angle out of the squark rotation matrix. For this purpose a new routine `WriteRotationMatrix`
was written. First one creates a rotation matrix which fulfills certain conventions: The Eigenvectors have to be orderd by ascending Eigenvalues in order to make sure that the mass of the first mass Eigenstate is lower than the second. This is done with the function `SortEigenVectors`.
Also, if the determinant is not equal to one, the second Eigenvector will be multiplied by -1 to ensure that it is a proper rotation matrix and not a reflexion matrix. Then the mixing angle can be determined. All the models which are included in `SLAM` can be used to generate a spectrum.

D.2.2. `H3SetSLHA` (Obsolete)

The function `H3SetSLHA` was substituted by `H3GetSLHA` but still remains in `H3.m` to enable backward compatibility. The information on how to use this function including optional arguments is included in the official documentation.

D.3. Running-and-Decoupling Procedure

In version 1.3 of `H3.m` a new implementation of the running-and-decoupling method is included. For this purpose, the decoupling coefficient ζ_{m_t} which relates the top-quark mass of the SM with the one of the MSSM was calculated up to $\mathcal{O}(\alpha_s^2)$. In addition, for the top-quark mass the fixed-order calculation which evaluates the two-loop on-shell integrals numerically with the program `TSIL` [82] is included again for consistency checks.

D.3.1. Internal Structure

The whole running-and-decoupling procedure is included in the package `/MtopAlphasDR/MtopAlphasDR.m` and invoked with the function
`MtopAlphasDR`
which returns the strong coupling constant α_s and the top-quark mass m_t in the MSSM. Its arguments are (in this order):
$\alpha_s(M_Z)$, M_Z, M_t^{OS}, M_{bot}^{OS}, θ_t^{OS}, M_{gl}^{OS}, $M_{\tilde{u}_1}$, $M_{\tilde{u}_2}$, $M_{\tilde{d}_1}$, $M_{\tilde{d}_2}$, $M_{\tilde{c}_1}$, $M_{\tilde{c}_2}$, $M_{\tilde{s}_1}$, $M_{\tilde{s}_2}$, $M_{\tilde{t}_1}$, $M_{\tilde{t}_2}$, $M_{\tilde{b}_1}$, $M_{\tilde{b}_2}$.
Also, it has the following optional arguments:
Loop order (default: 4),
decoupling scale (default: -1 which sets the decoupling scale to the mean of all squark and gluino masses),
decoupling loop order (default: -1 which uses the same order as the loop order)

D.4. Installation and Usage Example

D.4.1. Download

`H3.m` version 1.3 can be downloaded from:
`https://www.ttp.kit.edu/Progdata/ttp14/ttp14-025/h3m.tar.gz`

D.4.2. Installation

In version 1.3 of `H3.m` the installation procedure changes a bit. All the required steps are documented in the new manual. Here, I point out the difference to the old version.

`SLAM` has to be installed as an additional package. For this, a link to `SLAM` has to be in the directory where `H3.m` is installed. This is done with the command
`ln -s /path/to/SLAM-directory /path/you/want/to/install/to/H3/SLAM`.
The rest of the installation procedure is unchanged.

D.4.3. Usage Example

To make it easy for new users, an example file is provided in the installation directory.

E. One-Loop Decoupling Coefficients ζ_ξ, ζ_{g_s} and $\zeta_{m_{t,b}}^{\text{SQCD}}$

In the following, the one-loop decoupling coefficients ζ_ξ, ζ_{g_s} and $\zeta_{m_{t,b}}^{\text{SQCD}}$ up to $\mathcal{O}(\epsilon)$ are given. Here, all supersymmetric particles share the same mass M_S except $\tilde{t}_2$ and $\tilde{b}_2$, whose masses are $M_{\tilde{t}_2}$ and $M_{\tilde{b}_2}$, respectively.

$$
\begin{aligned}
\zeta_\xi = 1 + \frac{a_s}{12}\Big\{ &C_A + 2C_A L_{M_S} + T\Big(10L_{M_S} + L_{M_{\tilde{t}_2}} + L_{M_{\tilde{b}_2}}\Big) \\
&+ \frac{\epsilon}{2}\Big[2C_A\Big(L_{M_S} + L_{M_S}^2 + \zeta(2)\Big) + T\Big(10L_{M_S}^2 + L_{M_{\tilde{t}_2}}^2 + L_{M_{\tilde{b}_2}}^2 + 12\zeta(2)\Big)\Big]\Big\}, \quad \text{(E.1)}
\end{aligned}
$$

$$
\begin{aligned}
\zeta_{g_s} = 1 + \frac{a_s}{24}\Big\{ &-C_A\Big(1 + 2L_{M_S}\Big) - T\Big(10L_{M_S} + L_{M_{\tilde{t}_2}} + L_{M_{\tilde{b}_2}}\Big) \\
&+ \frac{\epsilon}{2}\Big[-2C_A\Big(L_{M_S} + L_{M_S}^2 + \zeta(2)\Big) - T\Big(10L_{M_S}^2 + L_{M_{\tilde{t}_2}}^2 + L_{M_{\tilde{b}_2}}^2 + 12\zeta(2)\Big)\Big]\Big\}, \quad \text{(E.2)}
\end{aligned}
$$

$$
\begin{aligned}
\zeta_{m_t}^{\text{SQCD}} = 1 + C_F \frac{a_s}{16(M_S^2 - M_{\tilde{t}_2}^2)^2}\Big\{ &\Big(1 - 4L_{M_S}\Big)M_S^4 + 4\Big(-1 + L_{M_S} + L_{M_{\tilde{t}_2}}\Big)M_S^2 M_{\tilde{t}_2}^2 \\
&+ \Big(3 - 2L_{M_S} - 2L_{M_{\tilde{t}_2}}\Big)M_{\tilde{t}_2}^4 - 8M_S^3 X_t + 8\Big(1 - L_{M_S} + L_{M_{\tilde{t}_2}}\Big)M_S M_{\tilde{t}_2}^2 X_t \\
&+ \frac{\epsilon}{2}\Big[-16\Big(1 + L_{M_S}\Big)M_S^3 X_t + 8\Big(2 - L_{M_S}^2 + L_{M_{\tilde{t}_2}}(2 + L_{M_{\tilde{t}_2}})\Big)M_S M_{\tilde{t}_2}^2 X_t \\
&+ M_S^4\Big(5 + 2L_{M_S} - 4L_{M_S}^2 - 4\zeta(2)\Big) \\
&+ 4M_S^2 M_{\tilde{t}_2}^2\Big(-4 + (-4 + L_{M_S})L_{M_S} + 2L_{M_{\tilde{t}_2}} + L_{M_{\tilde{t}_2}}^2 + 2\zeta(2)\Big) \\
&- M_{\tilde{t}_2}^4\Big(-11 + 2(-4 + L_{M_S})L_{M_S} + 2L_{M_{\tilde{t}_2}}(1 + L_{M_{\tilde{t}_2}}) + 4\zeta(2)\Big)\Big]\Big\} \quad \text{(E.3)}
\end{aligned}
$$

The decoupling coefficient $\zeta_{m_b}^{\text{SQCD}}$ can be derived from $\zeta_{m_t}^{\text{SQCD}}$ by applying the substitutions (3.21). ζ_{g_s} and $\zeta_{m_b}^{\text{SQCD}}$ are in full agreement with the literature [34, 46, 48].

Bibliography

[1] F. Englert and R. Brout, "Broken symmetry and the mass of gauge vector mesons", *Phys. Rev. Lett.* **13** (Aug, 1964) 321–323. http://link.aps.org/doi/10.1103/PhysRevLett.13.321.

[2] R. Brout and F. Englert, "Spontaneous symmetry breaking in gauge theories: A Historical survey", arXiv:hep-th/9802142 [hep-th].

[3] P. W. Higgs, "Broken symmetries and the masses of gauge bosons", *Phys. Rev. Lett.* **13** (Oct, 1964) 508–509. http://link.aps.org/doi/10.1103/PhysRevLett.13.508.

[4] G. S. Guralnik, C. R. Hagen, and T. W. B. Kibble, "Global conservation laws and massless particles", *Phys. Rev. Lett.* **13** (Nov, 1964) 585–587. http://link.aps.org/doi/10.1103/PhysRevLett.13.585.

[5] G. S. Guralnik, "The history of the guralnik, hagen and kibble development of the theory of spontaneous symmetry breaking and gauge particles", *International Journal of Modern Physics A* **24** no. 14, (2009) 2601–2627, http://www.worldscientific.com/doi/pdf/10.1142/S0217751X09045431. http://www.worldscientific.com/doi/abs/10.1142/S0217751X09045431.

[6] The Royal Swedish Academy of Sciences, Press release, 2013.

[7] **ATLAS, CMS** Collaboration, M. Flechl, "Higgs physics: Review of recent results and prospects from ATLAS and CMS", arXiv:1503.00632 [hep-ex].

[8] **Super-Kamiokande** Collaboration, Y. Fukuda *et al.*, "Evidence for oscillation of atmospheric neutrinos", *Phys.Rev.Lett.* **81** (1998) 1562–1567, arXiv:hep-ex/9807003 [hep-ex].

[9] E. W. Kolb and M. S. Turner, "The Early Universe", *Front.Phys.* **69** (1990) 1–547.

[10] G. Bertone, D. Hooper, and J. Silk, "Particle dark matter: Evidence, candidates and constraints", *Phys.Rept.* **405** (2005) 279–390, arXiv:hep-ph/0404175 [hep-ph].

[11] E. Komatsu, K. M. Smith, J. Dunkley, C. L. Bennett, B. Gold, G. Hinshaw, N. Jarosik, D. Larson, M. R. Nolta, L. Page, D. N. Spergel, M. Halpern, R. S. Hill, A. Kogut, M. Limon, S. S. Meyer, N. Odegard, G. S. Tucker, J. L. Weiland, E. Wollack, and E. L. Wright, "Seven-year wilkinson microwave anisotropy probe (wmap) observations: Cosmological interpretation", *The Astrophysical Journal Supplement Series* **192** no. 2, (2011) 18. http://stacks.iop.org/0067-0049/192/i=2/a=18.

[12] S. P. Martin, "A Supersymmetry Primer", arXiv:hep-ph/9709356v6.

[13] J. Wess and B. Zumino, "Supergauge transformations in four dimensions", *Nuclear Physics B* **70** no. 1, (1974) 39 − 50.

[14] N. Craig, "The State of Supersymmetry after Run I of the LHC", arXiv:1309.0528 [hep-ph].

[15] M. Mühlleitner, "Higgs Couplings and their Implications for New Physics Scales", arXiv:1506.03070 [hep-ph].

[16] C. Englert, A. Freitas, M. Mühlleitner, T. Plehn, M. Rauch, *et al.*, "Precision Measurements of Higgs Couplings: Implications for New Physics Scales", *J.Phys.* **G41** (2014) 113001, arXiv:1403.7191 [hep-ph].

[17] K. Yagyu, "Higgs boson couplings as a probe of new physics", arXiv:1505.06886 [hep-ph].

[18] G. 't Hooft and M. Veltman, "Regularization and renormalization of gauge fields", *Nuclear Physics B* **44** no. 1, (1972) 189 − 213.

[19] C. Bollini and J. Giambiagi, "Dimensional Renormalization: The Number of Dimensions as a Regularizing Parameter", *Nuovo Cim.* **B12** (1972) 20−25.

[20] W. A. Bardeen, A. J. Buras, D. W. Duke, and T. Muta, "Deep Inelastic Scattering Beyond the Leading Order in Asymptotically Free Gauge Theories", *Phys. Rev.* **D18** (1978) 3998.

[21] T. Appelquist and J. Carazzone, "Infrared singularities and massive fields", *Phys. Rev. D* **11** (May, 1975) 2856−2861. http://link.aps.org/doi/10.1103/PhysRevD.11.2856.

[22] K. Chetyrkin, B. Kniehl, and M. Steinhauser, "Decoupling Relations to $\mathcal{O}(\alpha_s^3)$ and their Connection to Low-Energy Theorems", *Nucl.Phys. B510 (1998) 61-87* (1997) , arXiv:hep-ph/9708255v2.

[23] H. Georgi, "Effective-Field Theory", *Annual Review of Nuclear and Particle Science* **43** (1993) 209−252.

[24] **CMS** Collaboration, S. Chatrchyan *et al.*, "Observation of a new boson at a mass of 125 GeV with the CMS experiment at the LHC", *Phys.Lett.* **B716** (2012) 30−61, arXiv:1207.7235 [hep-ex].

[25] **ATLAS** Collaboration, G. Aad *et al.*, "Observation of a new particle in the search for the Standard Model Higgs boson with the ATLAS detector at the LHC", *Phys.Lett.* **B716** (2012) 1−29, arXiv:1207.7214 [hep-ex].

[26] H. E. Haber and Y. Nir, "Multi-scalar models with a high-energy scale", *Nuclear Physics B* **335** no. 2, (1990) 363 − 394.

[27] H. E. Haber, "The Higgs data and the Decoupling Limit", arXiv:1401.0152 [hep-ph].

[28] H. E. Haber, "Nonminimal Higgs sectors: The Decoupling limit and its phenomenological implications", arXiv:hep-ph/9501320 [hep-ph].

[29] M. Carena, H. E. Haber, I. Low, N. R. Shah, and C. E. M. Wagner, "Complementarity between nonstandard Higgs boson searches and precision Higgs boson measurements in the MSSM", *Phys.Rev.* **D91** no. 3, (2015) 035003, arXiv:1410.4969 [hep-ph].

[30] N. Baro and F. Boudjema, "Automatized full one-loop renormalization of the mssm. ii. the chargino-neutralino sector, the sfermion sector, and some applications", *Phys. Rev. D* **80** (Oct, 2009) 076010. http://link.aps.org/doi/10.1103/PhysRevD.80.076010.

[31] N. Baro, F. Boudjema, and A. Semenov, "Automatized full one-loop renormalization of the MSSM: The Higgs sector, the issue of $\tan\beta$ and gauge invariance", *Phys. Rev. D* **78** (Dez., 2008) 115003, arXiv:0807.4668v2 [hep-ph]. http://link.aps.org/doi/10.1103/PhysRevD.78.115003.

[32] A. Brignole, G. Degrassi, P. Slavich, and F. Zwirner, "On the O(alpha(t)**2) two loop corrections to the neutral Higgs boson masses in the MSSM", *Nucl.Phys.* **B631** (2002) 195–218, arXiv:hep-ph/0112177 [hep-ph].

[33] J. Haestier, S. Heinemeyer, D. Stockinger, and G. Weiglein, "Electroweak precision observables: Two-loop Yukawa corrections of supersymmetric particles", *JHEP* **0512** (2005) 027, arXiv:hep-ph/0508139 [hep-ph].

[34] A. Bauer, L. Mihaila, and J. Salomon, "Matching coefficients for alpha(s) and m(b) to O(alpha**2(s)) in the MSSM", *JHEP* **0902** (2009) 037, arXiv:0810.5101 [hep-ph].

[35] Kunz, D. A., "Elektroschwache Korrekturen zu Entkopplungskoeffizienten im Minimalen Supersymmetrischen Standardmodell", diploma thesis, KIT, 2012.

[36] Rzehak, H. A., "Zwei-Schleifen-Beiträge im supersymmetrischen Higgs-Sektor", PhD thesis, Technische Universität München, 2005.

[37] D. Binosi and L. Theussl, "JaxoDraw: A graphical user interface for drawing Feynman diagrams", *Comput.Phys.Commun.* **161:76-86,2004** (Comput.Phys.Commun.161:76-86,2004) , hep-ph/0309015.

[38] W. Siegel, "Supersymmetric dimensional regularization via dimensional reduction", *Physics Letters B* **84** no. 2, (1979) 193 – 196.

[39] W. Siegel, "Inconsistency of supersymmetric dimensional regularization", *Physics Letters B* **94** no. 1, (1980) 37 – 40.

[40] M. Steinhauser, "Higgs decay into gluons up to $\mathcal{O}(\alpha(s)^3 G(F) m(t)^2)$", *Phys. Rev.* **D59** (1999) 054005, arXiv:hep-ph/9809507.

[41] W. Bernreuther and W. Wetzel, "Decoupling of heavy quarks in the minimal subtraction scheme", *Nuclear Physics B* **197** no. 2, (1982) 228 – 236.

[42] S. Larin, T. van Ritbergen, and J. Vermaseren, "The Large quark mass expansion of Gamma (Z0 —> hadrons) and Gamma (tau- —> tau-neutrino + hadrons) in the order alpha-s**3", *Nucl.Phys.* **B438** (1995) 278–306, arXiv:hep-ph/9411260 [hep-ph].

[43] Y. Schroder and M. Steinhauser, "Four-loop decoupling relations for the strong coupling", *JHEP* **0601** (2006) 051, arXiv:hep-ph/0512058 [hep-ph].

[44] K. Chetyrkin, J. H. Kühn, and C. Sturm, "QCD decoupling at four loops", *Nucl.Phys.* **B744** (2006) 121–135, arXiv:hep-ph/0512060 [hep-ph].

[45] A. G. Grozin, J. Hoff, M. Steinhauser, M. Höschele, *et al.*, "Simultaneous decoupling of bottom and charm quarks", *JHEP* **1109** (2011) 066, `arXiv:1107.5970 [hep-ph]`.

[46] R. Harlander, L. Mihaila, and M. Steinhauser, "Two-loop matching coefficients for the strong coupling in the MSSM", *Phys.Rev.* **D72** (2005) 095009, `arXiv:hep-ph/0509048 [hep-ph]`.

[47] R. Harlander, L. Mihaila, and M. Steinhauser, "Running of alpha(s) and m(b) in the MSSM", *Phys.Rev.* **D76** (2007) 055002, `arXiv:0706.2953 [hep-ph]`.

[48] A. Kurz, M. Steinhauser, and N. Zerf, "Decoupling Constant for α_s and the Effective Gluon-Higgs Coupling to Three Loops in Supersymmetric QCD", *JHEP* **1207** (2012) 138, `arXiv:1206.6675 [hep-ph]`.

[49] J. C. Ward, "An identity in quantum electrodynamics", *Phys. Rev.* **78** (Apr, 1950) 182–182. `http://link.aps.org/doi/10.1103/PhysRev.78.182`.

[50] I. Jack, D. Jones, and A. Kord, "Snowmass benchmark points and three-loop running", *Annals Phys.* **316** (2005) 213–233, `arXiv:hep-ph/0408128 [hep-ph]`.

[51] P. Nogueira, "Automatic Feynman Graph Generation", *Journal of Computational Physics* **105** no. 2, (1993) 279 – 289.

[52] A. Denner, H. Eck, O. Hahn, and J. Kueblbeck, "Feynman rules for fermion-number-violating interactions", *Nuclear Physics B* **387** no. 2, (1992) 467 – 481.

[53] R. Harlander, Priv. communication.

[54] R. V. Harlander, L. Mihaila, and M. Steinhauser, "The SUSY-QCD beta function to three loops", *Eur.Phys.J.* **C63** (2009) 383–390, `arXiv:arXiv:0905.4807v2 [hep-ph] [hep-ph]`.

[55] T. Seidensticker, "Automatic application of successive asymptotic expansions of Feynman diagrams", *TTP99-22* (1999) , `hep-ph/9905298v1`.

[56] R. Harlander, T. Seidensticker, and M. Steinhauser, "Complete Corrections of $\mathcal{O}(\alpha\alpha_s)$ to the Decay of the Z Boson into Bottom Quarks", *Phys.Lett. B426 (1998) 125-132* (1997) , `arXiv:hep-ph/9712228v2`.

[57] T. Hahn, "Generating Feynman diagrams and amplitudes with FeynArts 3", *Computer Physics Communications* **140** no. 3, (2001) 418 – 431, `arXiv:hep-ph/0012260v2`.

[58] Salomon, J. E., "Das Laufen und die Vereinigung der Eichkopplungen des Standardmodells zur Drei-Schleifen-Ordnung", PhD thesis, Karlsruher Institut für Technologie, 2012.

[59] J. Salomon, Priv. communication.

[60] M. Steinhauser, "MATAD: a program package for the computation of MAssive TADpoles", *Comput.Phys.Commun.* **134:335-364** (2001) , `hep-ph/0009029`.

[61] S. Larin, F. Tkachov, and J. Vermaseren, "The FORM version of MINCER", `NIKHEF-H-91-18`.

[62] J. A. M. Vermaseren, "New features of FORM", `math-ph/0010025`.

[63] M. Steinhauser, T. Ueda, and J. A. M. Vermaseren, "Parallel versions of FORM and more", *Nucl.Part.Phys.Proc.* **261-262** (2015) 45–57, `arXiv:1501.07119 [hep-ph]`.

[64] T. Ueda and J. Vermaseren, "Recent developments on FORM", *J.Phys.Conf.Ser.* **523** (2014) 012047.

[65] J. Kuipers, T. Ueda, J. Vermaseren, and J. Vollinga, "FORM version 4.0", *Comput.Phys.Commun.* **184** (2013) 1453–1467, `arXiv:1203.6543 [cs.SC]`.

[66] G. Passarino and M. Veltman, "One Loop Corrections for e+ e- Annihilation Into mu+ mu- in the Weinberg Model", *Nucl.Phys.* **B160** (1979) 151.

[67] V. A. Smirnov, "Asymptotic expansions in limits of large momenta and masses", *Commun.Math.Phys.* **134** (1990) 109–137.

[68] A. V. Bednyakov, "Running Mass of the b-Quark in QCD and SUSY QCD", *International Journal of Modern Physics A* **22** (2007) , `arXiv:0707.0650v2 [hep-ph]`.

[69] S. Coleman and S. L. Glashow, "Departures from the eightfold way: Theory of strong interaction symmetry breakdown", *Phys. Rev.* **134** (May, 1964) B671–B681. `http://link.aps.org/doi/10.1103/PhysRev.134.B671`.

[70] R. Hempfling and B. A. Kniehl, "On the relation between the fermion pole mass and MS Yukawa coupling in the standard model", *Phys.Rev.* **D51** (1995) 1386–1394, `arXiv:hep-ph/9408313 [hep-ph]`.

[71] B. A. Kniehl, J. H. Piclum, and M. Steinhauser, "Relation between bottom-quark MS-bar Yukawa coupling and pole mass", *Nucl.Phys.* **B695** (2004) 199–216, `arXiv:hep-ph/0406254 [hep-ph]`.

[72] M. Faisst, J. H. Kühn, and O. Veretin, "Pole versus MS mass definitions in the electroweak theory", *Phys.Lett.* **B589** (2004) 35–38, `arXiv:hep-ph/0403026 [hep-ph]`.

[73] M. Faisst, J. Kühn, T. Seidensticker, and O. Veretin, "Three loop top quark contributions to the rho parameter", *Nuclear Physics B* **665** no. 0, (2003) 649 – 662.

[74] J. Guasch, J. Sola, and W. Hollik, "Yukawa coupling corrections to scalar quark decays", *Phys.Lett.* **B437** (1998) 88–99, `arXiv:hep-ph/9802329 [hep-ph]`.

[75] S. Heinemeyer, W. Hollik, H. Rzehak, and G. Weiglein, "High-precision predictions for the MSSM Higgs sector at O(alpha(b) alpha(s))", *Eur.Phys.J.* **C39** (2005) 465–481, `arXiv:hep-ph/0411114 [hep-ph]`.

[76] A. Denner, "Techniques for calculation of electroweak radiative corrections at the one loop level and results for W physics at LEP-200", *Fortsch.Phys.* **41** (1993) 307–420, `arXiv:0709.1075 [hep-ph]`.

[77] S. P. Martin, "Three-loop corrections to the lightest Higgs scalar boson mass in supersymmetry", *Phys.Rev.* **D75** (2007) 055005, `arXiv:hep-ph/0701051 [hep-ph]`.

[78] N. Arkani-Hamed and S. Dimopoulos, "Supersymmetric unification without low energy supersymmetry and signatures for fine-tuning at the LHC", *JHEP* **0506** (2005) 073, `arXiv:hep-th/0405159` `[hep-th]`.

[79] G. Giudice and A. Romanino, "Split supersymmetry", *Nucl.Phys.* **B699** (2004) 65–89, `arXiv:hep-ph/0406088` `[hep-ph]`.

[80] N. Arkani-Hamed, S. Dimopoulos, G. Giudice, and A. Romanino, "Aspects of split supersymmetry", *Nucl.Phys.* **B709** (2005) 3–46, `arXiv:hep-ph/0409232` `[hep-ph]`.

[81] S. P. Martin, "Fermion self-energies and pole masses at two-loop order in a general renormalizable theory with massless gauge bosons", *Phys.Rev.* **D72** (2005) 096008, `arXiv:hep-ph/0509115` `[hep-ph]`.

[82] S. P. Martin and D. G. Robertson, "TSIL: A Program for the calculation of two-loop self-energy integrals", *Comput.Phys.Commun.* **174** (2006) 133–151, `arXiv:hep-ph/0501132` `[hep-ph]`.

[83] D. Kunz, L. Mihaila, and N. Zerf, "$\mathcal{O}(\alpha_s^2)$ corrections to the running top-Yukawa coupling and the mass of the lightest Higgs boson in the MSSM", *JHEP* **1412** (2014) 136, `arXiv:1409.2297` `[hep-ph]`.

[84] K. Chetyrkin and M. Steinhauser, "Short distance mass of a heavy quark at order α_s^3", *Phys.Rev.Lett.* **83** (1999) 4001–4004, `arXiv:hep-ph/9907509` `[hep-ph]`.

[85] K. Chetyrkin and M. Steinhauser, "The Relation between the MS-bar and the on-shell quark mass at order alpha(s)**3", *Nucl.Phys.* **B573** (2000) 617–651, `arXiv:hep-ph/9911434` `[hep-ph]`.

[86] K. Melnikov and T. v. Ritbergen, "The Three loop relation between the MS-bar and the pole quark masses", *Phys.Lett.* **B482** (2000) 99–108, `arXiv:hep-ph/9912391` `[hep-ph]`.

[87] P. Marquard, L. Mihaila, J. Piclum, and M. Steinhauser, "Relation between the pole and the minimally subtracted mass in dimensional regularization and dimensional reduction to three-loop order", *Nucl.Phys.* **B773** (2007) 1–18, `arXiv:hep-ph/0702185` `[hep-ph]`.

[88] P. Marquard, A. V. Smirnov, V. A. Smirnov, and M. Steinhauser, "Quark Mass Relations to Four-Loop Order in Perturbative QCD", *Phys.Rev.Lett.* **114** no. 14, (2015) 142002, `arXiv:1502.01030` `[hep-ph]`.

[89] R. Tarrach, "The pole mass in perturbative qcd", *Nuclear Physics B* **183** no. 3, (1981) 384 – 396.

[90] O. Tarasov, "Anomalous Dimensions Of Quark Masses In Three Loop Approximation", `JINR-P2-82-900 ETC.`

[91] S. Larin, "The Renormalization of the axial anomaly in dimensional regularization", *Phys.Lett.* **B303** (1993) 113–118, `arXiv:hep-ph/9302240` `[hep-ph]`.

[92] K. Chetyrkin and M. Zoller, "Three-loop beta-functions for top-Yukawa and the Higgs self-interaction in the Standard Model", *JHEP* **1206** (2012) 033, `arXiv:1205.2892` `[hep-ph]`.

[93] A. Bednyakov, A. Pikelner, and V. Velizhanin, "Yukawa coupling beta-functions in the Standard Model at three loops", *Phys.Lett.* **B722** (2013) 336–340, `arXiv:1212.6829`.

[94] K. Chetyrkin, "Quark mass anomalous dimension to O (alpha-s**4)", *Phys.Lett.* **B404** (1997) 161–165, `arXiv:hep-ph/9703278 [hep-ph]`.

[95] P. Baikov, K. Chetyrkin, and J. Kühn, "Quark Mass and Field Anomalous Dimensions to $\mathcal{O}(\alpha_s^5)$", *JHEP* **1410** (2014) 76, `arXiv:1402.6611 [hep-ph]`.

[96] L. Hall, "Grand unification of effective gauge theories", *Nuclear Physics B* **178** no. 1, (1981) 75 – 124.

[97] P. Ferreira, I. Jack, and D. Jones, "The Three loop SSM beta functions", *Phys.Lett.* **B387** (1996) 80–86, `arXiv:hep-ph/9605440 [hep-ph]`.

[98] J. B. et al (PDG), "Review of particle physics", *Phys. Rev. D* **86** (Jul, 2012) 010001. `http://link.aps.org/doi/10.1103/PhysRevD.86.010001`.

[99] **ATLAS, CDF, CMS, D0** Collaboration, "First combination of Tevatron and LHC measurements of the top-quark mass", `arXiv:1403.4427 [hep-ex]`.

[100] M. Carena, S. Heinemeyer, O. Stål, C. Wagner, and G. Weiglein, "MSSM Higgs Boson Searches at the LHC: Benchmark Scenarios after the Discovery of a Higgs-like Particle", *Eur.Phys.J.* **C73** no. 9, (2013) 2552, `arXiv:1302.7033 [hep-ph]`.

[101] P. Z. Skands, B. Allanach, H. Baer, C. Balazs, G. Belanger, *et al.*, "SUSY Les Houches accord: Interfacing SUSY spectrum calculators, decay packages, and event generators", *JHEP* **0407** (2004) 036, `arXiv:hep-ph/0311123 [hep-ph]`.

[102] B. Allanach, C. Balazs, G. Belanger, M. Bernhardt, F. Boudjema, *et al.*, "SUSY Les Houches Accord 2", *Comput.Phys.Commun.* **180** (2009) 8–25, `arXiv:0801.0045 [hep-ph]`.

[103] B. Allanach, "SOFTSUSY: a program for calculating supersymmetric spectra", *Comput.Phys.Commun.* **143** (2002) 305–331, `arXiv:hep-ph/0104145 [hep-ph]`.

[104] B. Allanach, A. Bednyakov, and R. Ruiz de Austri, "Higher order corrections and unification in the minimal supersymmetric standard model: SOFTSUSY3.5", *Comput.Phys.Commun.* **189** (2015) 192–206, `arXiv:1407.6130 [hep-ph]`.

[105] **ILC** Collaboration, G. Aarons *et al.*, "International Linear Collider Reference Design Report Volume 2: Physics at the ILC", `arXiv:0709.1893 [hep-ph]`.

[106] W. Martens, L. Mihaila, J. Salomon, and M. Steinhauser, "Minimal Supersymmetric SU(5) and Gauge Coupling Unification at Three Loops", *Phys.Rev.* **D82** (2010) 095013, `arXiv:1008.3070 [hep-ph]`.

[107] K. Chetyrkin, J. H. Kühn, and M. Steinhauser, "RunDec: A Mathematica package for running and decoupling of the strong coupling and quark masses", *Comput.Phys.Commun.* **133** (2000) 43–65, `arXiv:hep-ph/0004189 [hep-ph]`.

[108] D. M. Pierce, J. A. Bagger, K. T. Matchev, and R.-j. Zhang, "Precision corrections in the minimal supersymmetric standard model", *Nucl.Phys.* **B491** (1997) 3–67, `arXiv:hep-ph/9606211 [hep-ph]`.

Bibliography

[109] D. Buttazzo, G. Degrassi, P. P. Giardino, G. F. Giudice, F. Sala, *et al.*, "Investigating the near-criticality of the Higgs boson", *JHEP* **1312** (2013) 089, `arXiv:1307.3536 [hep-ph]`.

[110] K. Chetyrkin, J. Kühn, A. Maier, P. Maierhofer, P. Marquard, *et al.*, "Charm and Bottom Quark Masses: An Update", *Phys.Rev.* **D80** (2009) 074010, `arXiv:0907.2110 [hep-ph]`.

[111] K. Chetyrkin and M. Zoller, "Three-loop beta-functions for top-Yukawa and the Higgs self-interaction in the Standard Model", *JHEP* **1206** (2012) 033, `arXiv:1205.2892 [hep-ph]`.

[112] L. Mihaila, J. Salomon, and M. Steinhauser, "Gauge coupling beta functions in the Standard Model", *PoS* **LL2012** (2012) 043, `arXiv:1209.5497 [hep-ph]`.

[113] L. N. Mihaila, J. Salomon, and M. Steinhauser, "Renormalization constants and beta functions for the gauge couplings of the Standard Model to three-loop order", *Phys.Rev.* **D86** (2012) 096008, `arXiv:1208.3357 [hep-ph]`.

[114] S. Larin and J. Vermaseren, "The Three loop QCD Beta function and anomalous dimensions", *Phys.Lett.* **B303** (1993) 334–336, `arXiv:hep-ph/9302208 [hep-ph]`.

[115] A. Bednyakov, A. Pikelner, and V. Velizhanin, "Yukawa coupling beta-functions in the Standard Model at three loops", *Phys.Lett.* **B722** (2013) 336–340, `arXiv:1212.6829`.

[116] A. Bednyakov, A. Pikelner, and V. Velizhanin, "Higgs self-coupling beta-function in the Standard Model at three loops", *Nucl.Phys.* **B875** (2013) 552–565, `arXiv:1303.4364`.

[117] R. V. Harlander, L. Mihaila, and M. Steinhauser, "The SUSY-QCD beta function to three loops", *Eur.Phys.J.* **C63** (2009) 383–390, `arXiv:0905.4807 [hep-ph]`.

[118] F. Jegerlehner and M. Kalmykov, "O(alpha alpha(s)) relation between pole- and MS-bar mass of the t quark", *Acta Phys.Polon.* **B34** (2003) 5335–5344, `arXiv:hep-ph/0310361 [hep-ph]`.

[119] D. Eiras and M. Steinhauser, "Two-loop O(alpha alpha(s)) corrections to the on-shell fermion propagator in the standard model", *JHEP* **0602** (2006) 010, `arXiv:hep-ph/0512099 [hep-ph]`.

[120] L. Mihaila, Priv. communication.

[121] L. Hofer, U. Nierste, and D. Scherer, "Resummation of tan-beta-enhanced supersymmetric loop corrections beyond the decoupling limit", *JHEP* **0910** (2009) 081, `arXiv:0907.5408 [hep-ph]`.

[122] M. Carena, D. Garcia, U. Nierste, and C. E. Wagner, "Effective Lagrangian for the $\bar{t}bH^+$ interaction in the MSSM and charged Higgs phenomenology", *Nucl.Phys.* **B577** (2000) 88–120, `arXiv:hep-ph/9912516 [hep-ph]`.

[123] **ATLAS, CMS** Collaboration, G. Aad *et al.*, "Combined Measurement of the Higgs Boson Mass in pp Collisions at $\sqrt{s} = 7$ and 8 TeV with the ATLAS and CMS Experiments", *Phys.Rev.Lett.* **114** (2015) 191803, `arXiv:1503.07589 [hep-ex]`.

[124] **LEP Working Group for Higgs boson searches, ALEPH, DELPHI, L3, OPAL** Collaboration, R. Barate *et al.*, "Search for the standard model Higgs boson at LEP", *Phys.Lett.* **B565** (2003) 61–75, `arXiv:hep-ex/0306033 [hep-ex]`.

[125] G. Cacciapaglia, A. Deandrea, G. Drieu La Rochelle, and J.-B. Flament, "Searching for a lighter higgs boson: Parametrization and sample tests", *Phys. Rev. D* **91** (Jan, 2015) 015012. `http://link.aps.org/doi/10.1103/PhysRevD.91.015012`.

[126] P. Kant, R. Harlander, L. Mihaila, and M. Steinhauser, "Light MSSM Higgs boson mass to three-loop accuracy", *JHEP* **1008** (2010) 104, `arXiv:1005.5709 [hep-ph]`.

[127] T. Hahn, S. Heinemeyer, W. Hollik, H. Rzehak, and G. Weiglein, "High-Precision Predictions for the Light CP -Even Higgs Boson Mass of the Minimal Supersymmetric Standard Model", *Phys.Rev.Lett.* **112** no. 14, (2014) 141801, `arXiv:1312.4937 [hep-ph]`.

[128] M. Frank, T. Hahn, S. Heinemeyer, W. Hollik, H. Rzehak, *et al.*, "The Higgs Boson Masses and Mixings of the Complex MSSM in the Feynman-Diagrammatic Approach", *JHEP* **0702** (2007) 047, `arXiv:hep-ph/0611326 [hep-ph]`.

[129] G. Degrassi, S. Heinemeyer, W. Hollik, P. Slavich, and G. Weiglein, "Towards high precision predictions for the MSSM Higgs sector", *Eur.Phys.J.* **C28** (2003) 133–143, `arXiv:hep-ph/0212020 [hep-ph]`.

[130] S. Heinemeyer, W. Hollik, and G. Weiglein, "The Masses of the neutral CP - even Higgs bosons in the MSSM: Accurate analysis at the two loop level", *Eur.Phys.J.* **C9** (1999) 343–366, `arXiv:hep-ph/9812472 [hep-ph]`.

[131] S. Heinemeyer, W. Hollik, and G. Weiglein, "FeynHiggs: A Program for the calculation of the masses of the neutral CP even Higgs bosons in the MSSM", *Comput.Phys.Commun.* **124** (2000) 76–89, `arXiv:hep-ph/9812320 [hep-ph]`.

[132] J. Lee, A. Pilaftsis, M. Carena, S. Choi, M. Drees, *et al.*, "CPsuperH: A Computational tool for Higgs phenomenology in the minimal supersymmetric standard model with explicit CP violation", *Comput.Phys.Commun.* **156** (2004) 283–317, `arXiv:hep-ph/0307377 [hep-ph]`.

[133] J. Lee, M. Carena, J. Ellis, A. Pilaftsis, and C. Wagner, "CPsuperH2.0: an Improved Computational Tool for Higgs Phenomenology in the MSSM with Explicit CP Violation", *Comput.Phys.Commun.* **180** (2009) 312–331, `arXiv:0712.2360 [hep-ph]`.

[134] R. Harlander, P. Kant, L. Mihaila, and M. Steinhauser, "Higgs boson mass in supersymmetry to three loops", *Phys.Rev.Lett.* **100** (2008) 191602, `arXiv:0803.0672 [hep-ph]`.

[135] J. L. Feng, P. Kant, S. Profumo, and D. Sanford, "Three-loop corrections to the higgs boson mass and implications for supersymmetry at the lhc", *Phys. Rev. Lett.* **111** (Sep, 2013) 131802. `http://link.aps.org/doi/10.1103/PhysRevLett.111.131802`.

[136] S. Borowka, T. Hahn, S. Heinemeyer, G. Heinrich, and W. Hollik, "Renormalization scheme dependence of the two-loop QCD corrections to the neutral Higgs-boson masses in the MSSM", `arXiv:1505.03133 [hep-ph]`.

Bibliography

[137] S. Heinemeyer, Priv. communication.

[138] P. Slavich, Priv. communication.

[139] P. Marquard and N. Zerf, "SLAM, a Mathematica interface for SUSY spectrum generators", *Comput.Phys.Commun.* **185** (2014) 1153–1171, `arXiv:1309.1731` `[hep-ph]`.